

Summer 2009

Micro, nano encapsulation methods for sustained release drug formulations and biomimetic applications

Shantanu Balkundi
Louisiana Tech University

Follow this and additional works at: <https://digitalcommons.latech.edu/dissertations>



Part of the [Biochemistry Commons](#), and the [Biomedical Engineering and Bioengineering Commons](#)

Recommended Citation

Balkundi, Shantanu, "" (2009). *Dissertation*. 434.
<https://digitalcommons.latech.edu/dissertations/434>

This Dissertation is brought to you for free and open access by the Graduate School at Louisiana Tech Digital Commons. It has been accepted for inclusion in Doctoral Dissertations by an authorized administrator of Louisiana Tech Digital Commons. For more information, please contact digitalcommons@latech.edu.

**MICRO, NANO ENCAPSULATION METHODS FOR
SUSTAINED RELEASE DRUG FORMULATIONS
AND BIOMIMETIC APPLICATIONS**

by

Shantanu Balkundi, B.S., M.S.

A Dissertation Presented in Partial Fulfillment
of the Requirements for the Degree
Doctor of Philosophy

COLLEGE OF ENGINEERING AND SCIENCE
LOUISIANA TECH UNIVERSITY

August 2009

UMI Number: 3374696

INFORMATION TO USERS

The quality of this reproduction is dependent upon the quality of the copy submitted. Broken or indistinct print, colored or poor quality illustrations and photographs, print bleed-through, substandard margins, and improper alignment can adversely affect reproduction.

In the unlikely event that the author did not send a complete manuscript and there are missing pages, these will be noted. Also, if unauthorized copyright material had to be removed, a note will indicate the deletion.

UMI[®]

UMI Microform 3374696
Copyright 2009 by ProQuest LLC
All rights reserved. This microform edition is protected against
unauthorized copying under Title 17, United States Code.

ProQuest LLC
789 East Eisenhower Parkway
P.O. Box 1346
Ann Arbor, MI 48106-1346

LOUISIANA TECH UNIVERSITY

THE GRADUATE SCHOOL

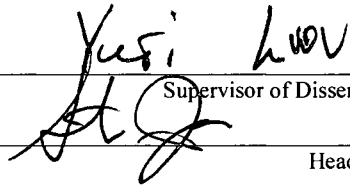
July 7, 2009

Date

We hereby recommend that the dissertation prepared under our supervision
by SHANTANU SHRIKANT BALKUNDI

entitled MICRO, NANO ENCAPSULATION METHODS FOR SUSTAINED RELEASE DRUG FORMULATIONS AND BIOMIMETIC APPLICATIONS

be accepted in partial fulfillment of the requirements for the Degree of
DOCTOR OF PHILOSOPHY



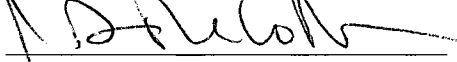
Supervisor of Dissertation Research

Head of Department

BIOMEDICAL ENGINEERING

Department

Recommendation concurred in:



David Mills

 Advisory Committee

June Feung

Approved:


Director of Graduate Studies

Approved:


Dean of the Graduate School


Dean of the College

ABSTRACT

Complex natural polyphenolic compounds are of great interest as substances possessing a high spectrum of biological activity. High antioxidant, antibacterial, antiviral, and other activities have been proven for a wide range of plant extracts and polymeric tannins including their isolated individual compounds (procyanidin B, tannic acid (TA), theaflavin (TF), thearubigins, etc.) [1-3]. The Layer-by-Layer (LbL) assembly technique was used to obtain a new type of protein/polyphenol microcapsule based on naturally occurring polyphenol (-)-epigallocatechin gallate (EGCG) and gelatin, type A. The dependence of permeability on the molecular weight of permeating substances was studied and compared with commonly used polyallylamine/polystyrene sulfonate capsules. A quartz crystal microbalance was used to monitor the regularities of EGCG adsorption in alternation with type A and B Gelatins and electrophoretic mobility measurements were used that indicated that the nature of assembly was dependent on Gelatin properties. It was shown that EGCG retains its antioxidant activity in the LbL assemblies. It was established that the kinetics of the reaction of 2, 2'-azinobis (3-ethylbenzothiazoline-6-sulfonic acid) diammonium salt (ABTS) cation-radicals, with films consisting of 1-10 Gelatin/EGCG bilayers, is affected by film structure. The protein/polyphenols films had EGCG content as high as 30 % w/w. LbL assembly used for encapsulation of EGCG via its alternated adsorption with Gelatins can be a novel technique for new formulations containing polyphenol for drug delivery applications.

Natural polyphenols, with previously demonstrated anti-cancer potential, EGCG, tannic acid, curcumin, and theaflavin, were encased in gelatin-based 200-nm nanoparticles consisting of a soft gel-like interior with or without a surrounding LbL-shell of polyelectrolytes (polystyrene sulfonate/polyallylamine hydrochloride, polyglutamic acid/poly-L-lysine, dextran sulfate/protamine sulfate, carboxymethyl cellulose/Gelatin, type A) assembled using the LbL technique. The characteristics of polyphenol loading and the factors affecting their release from the nanocapsules were investigated. Nanoparticle-encapsulated EGCG retained its biological activity and blocked hepatocyte growth factor (HGF) induced intracellular signaling in the breast cancer cell-line MBA-MD-231 as potently as free EGCG.

Since electrostatic LbL nano-assembly is proven to be a suitable method for surface modifications on charged templates, we also used this technique for nano-coating of the phototrophic purple sulfur bacterium *Allochromatium Vinosum* with different synthetic and biocompatible polyelectrolyte combinations in order to investigate its biomimetic applications as related to drug delivery. The contact mechanisms between the cell surface and the insoluble elemental sulfur was investigated and studied because this step is essential for elemental sulfur uptake. Furthermore, modified uptake of sulfide by the encapsulated cells was also investigated. Growth experiments, after coating of the cells, showed that the surface charge of the bacteria neither affected the uptake of sulfide nor the contact formation between the cells and elemental sulfur. However, an increasing number of layers assembled on the cells slowed or inhibited the uptake of sulfide and elemental sulfur depending on the polymer combination used for coating. This indicated

that LbL self-assembly makes it a suitable method for investigation of cell-surface related aspects in microbiology.

After using LbL assembly successfully for coating microbes, we coated microbial spores in a sheath of functionalized nanofilms. Bacterial spores were encapsulated in organized ultrathin shells using LbL assembly in order to assess the biomaterial as a suitable core and determine the physiological effects of the coating. The shells were constructed on *Bacillus Subtilis* spores using various biocompatible polymers: polyglutamic acid, polylysine, albumin, lysozyme, GelA, protamine sulfate and chondroitin sulphate. The assembly process was monitored by measuring the electrical surface potential (zeta-potential) of the particles at each stage of assembly. Fluorescent laser confocal microscopy and scanning electron microscopy confirmed the formation of uniform coatings on the spores. The surface charge and coating thickness (20-100 nm) could be selectively tuned by using appropriate polymers and number of assembled bilayers. The effect of each coating type on germination was assessed and compared to native spores. The coated spores were viable but the kinetics and extent of germination were changed from control spores in all instances. The results and insight gained from the experiments may be used to design various bioinspired systems. The spores can be made dormant for a desired amount of time using LbL encapsulation technique and can be made active when desired. In this work with LbL nanoassembly, we performed polyphenol based formulations and also modified the bacterial surface to study the effects of encapsulation on the uptake of various compounds.

APPROVAL FOR SCHOLARLY DISSEMINATION

The author grants to the Prescott Memorial Library of Louisiana Tech University the right to reproduce, by appropriate methods, upon request, any or all portions of this Dissertation. It is understood that "proper request" consists of the agreement, on the part of the requesting party, that said reproduction is for his personal use and that subsequent reproduction will not occur without written approval of the author of this Dissertation. Further, any portions of the Dissertation used in books, papers, and other works must be appropriately referenced to this Dissertation.

Finally, the author of this Dissertation reserves the right to publish freely, in the literature, at any time, any or all portions of this Dissertation.

Author



Date

07/27/2009

DEDICATION

To

My father Shrikant Balkundi,
mother Meena Balkundi and
sister Ashwini Balkundi.

TABLE OF CONTENTS

ABSTRACT.....	iii
LIST OF TABLES.....	xii
LIST OF FIGURES	xiii
ACKNOWLEDGEMENTS.....	xvi
CHAPTER 1 NANOORGANIZED POLYELECTROLYTE SHELLS USING LAYER-BY-LAYER ASSEMBLY	1
Overview of Dissertation.....	1
Formation of Nanoshells using Electrostatic Layer-by-Layer Assembly	2
Preparation of LbL Nanoshells	3
Step by Step Description of LbL Process	4
Our Approach- Drug Formulations and Biomimetic	6
CHAPTER 2 EPIGALLOCATECHIN GALLATE / GELATIN LAYER-BY-LAYER ASSEMBLED FILMS AND MICROCAPSULES.....	9
Overview	9
Materials and Methods	12
Film Fabrication	12
(Gelatin/EGCG) ₄ Shell Preparation.....	13
Capsule Permeability Test.....	15
ABTS ⁺ Assay	15
Results and Discussion	16
Layer-by-Layer Assembly on QCM Resonators.....	16

Influence of Gelatin on EGCG Determination with the ABTS ⁺ Assay	19
Interaction of ABTS ⁺ with EGCG in Solution.....	19
Interaction of ABTS ⁺ with Gelatin/EGCG Multilayers.....	22
Gelatin/EGCG Assembly on Cores.....	25
(Gela/EGCG) ₄ Capsules.....	27
CHAPTER 3 LAYER-BY-LAYER COATED GELATIN NANOPARTICLES AS A VEHICLE FOR DELIVERY OF NATURAL POLYPHENOLS	
Overview	31
Materials and Methods	34
Nanoparticles Preparation	34
LbL Shell Assembly on Gelatin Nanoparticles.....	35
Discoloration of ABTS ⁺ by Polyphenols in Solution	36
Discoloration of ABTS ⁺ by Gelatin Nanoparticles Containing Polyphenols	37
Loading of EGCG and other Polyphenols into Gelatin Nanoparticles	37
EGCG Release from Gelatin Particles	38
Western Blotting	39
Characterization of Nanoparticles.....	40
Results and Discussion.....	41
Nanoparticles Preparation	41
Characterization of Gelatin Nanoparticles	43
LbL Assembly of Polyelectrolytes on Gelatin Nanoparticles.....	44
Polyphenol Adsorption into Nanoparticles	47
EGCG Release from Nanoparticles	50
Sustained Release of EGCG from LbL Coated Nanoparticles	54
Biological Activities of LbL coated Nanoparticles Containing EGCG	55

CHAPTER 4 LBL NANOENCAPSULATION OF MICROBES FOR CELL SURFACE MODIFICATION AND INVESTIGATION OF CELLULAR UPTAKE	57
Overview	57
Materials and Methods	59
Polyelectrolytes for Bacteria Encapsulation	60
LbL Shell Assembly on Microbes.....	60
Confocal Microscopy	61
Scanning Electron Microscopy	61
Intracellular Sulfur, Protein and Sulfate Determination in the Cultures.....	61
Results and Discussion	61
Electrochemical Changes of the Cell Surface.....	63
Physical Barrier by Nanoshell.....	69
CHAPTER 5 ENCAPSULATION OF BACTERIAL SPORES IN NANOORGANIZED POLYELECTROLYTE SHELLS	76
Overview	76
Methods and Materials	79
Spore Preparation and Isolation	80
Shell LbL Assembly.....	80
Zeta Potentiometer Measurements	81
Confocal Microscopy	81
Scanning Electron Microscopy	82
Spore Germination Kinetic Assays	82
Fluorimetry.....	83
Results and Discussion	84
The Effect of Coatings on Spore Viability and Germination.....	90

CHAPTER 6 CONCLUSION AND FUTURE WORK 92

REFERENCES 95

LIST OF TABLES

Table 3.1 Kd as a function of pH and nanoparticles coating [62].	53
Table 4.1 Encapsulation and growth conditions for <i>Alc. Vinosum</i> [86].	63

LIST OF FIGURES

Figure 1.1 Electrostatic LbL 2-D substrates and 3-D micro/ nanotemplates.....	3
Figure 2.1 Scheme of GelA/EGCG hollow capsule preparation [23, 52].	11
Figure 2.2 QCM assembly of GelA (a) and GelB (b) in alternation with EGCG. The results of independent experiments are presented.....	17
Figure 2.3 Thickness of GelA/EGCG (a) and GelB/EGCG bilayers (b) as a function of bilayer number, $n=3$	18
Figure 2.4 A734 nm changes after addition of EGCG to an ABTS+• solution. Concentration of EGCG 10^6 , M: 1-0, 2-1.1, and 3-2.2, 4-6.4.	20
Figure 2.5 RSA parameter of EGCG in time in the presence of different amounts of gelatin A. $C_{EGCG}=0.5$ mg/ml.....	21
Figure 2.6 RSA/RSA ₀ as a function of gelatin concentration. $C_{EGCG}=0.5$ mg/mL. Time: 20 min (◦) and 24 h (■).	22
Figure 2.7 a) Kinetic curves of ABTS cation-radical decay on GelA/EGCG films with different number of bilayers (1-6), b) initial rate of ABTS ^{+•} consumption over the time period of 30 s as a function of number of bilayers, $n=3$	23
Figure 2.8 AFM image of the surface of a dried (GelA/EGCG) _{8.5} film (a) and magnified surface image (b).	24
Figure 2.9 ζ -potential changes during the LbL assembly of GelA (1), GelA- FITC (2), or GelB (3) and EGCG on MnCO ₃ cores at pH 6.5, $n=2$	25
Figure 2.10 (GelA-FITC/EGCG) ₄ (a) and (GelB-TRITC/EGCG) ₄ (b) shells on MnCO ₃ cores.	26
Figure 2.11 Confocal image of (GelA/EGCG) ₄ capsules (a) and intensity profile (b) along the indicated cross-section.	27
Figure 2.12 SEM (a) and AFM (b) images of dried (GelA/EGCG) ₄ capsules. The graph presents the AFM height profile along the indicated cross-section.	29

Figure 2.13 Permeability of (Gela/EGCG) ₄ (shaded) and (Gela-FITC/EGCG) ₄ (grey) capsules for FITC- labeled dextrans of different molecular weights at pH 6.5, time=10 min, n=3.....	30
Figure 3.1 Schematic presentation of preparation of LbL-coated Gelatin nanoparticles containing EGCG and their effect on cancer cells [62].	33
Figure 3.2 Gelatin A nanoparticles diameter and polydispersity as a function of pH on the second desolvation stage, n=2.	42
Figure 3.3 AFM images of 120 nm Gelatin B (a, sample from 75 % acetone) and 300 nm Gelatin A (b - e, from water) uncoated (b, d) and coated with (PGA/PLL) ₂ (c) and (PGA/PLL) ₄ (e) shells. The corresponding profiles show sample elevation across the indicated lines.	44
Figure 3.4 Surface charge of Gelatin nanoparticles as functions of a) pH (1- Gela, 2-GelB) and b) outermost polyelectrolyte layer (Gela, pH 6.0), n=2.	45
Figure 3.5 SEM images of 200 nm (a) and 300 nm (b-d) Gela nanoparticles: a) uncoated, b) coated with (PGA/PLL) ₂ shells, c) one nanoparticle coated with (DexS/PtS) ₂ SiO ₂ shell, and d) uncoated nanoparticles after loading EGCG.....	46
Figure 3.6 Total C _{polyphenol} in suspension after loading theaflavins (1), tannic acid (2), EGCG (3), and curcumin (4) in 200 nm Gela particles, n=3.	48
Figure 3.7 Concentration of EGCG in uncoated Gela nanoparticles of different diameters, n=5.	49
Figure 3.8 Concentration of EGCG in nanoparticles coated with different number of PGA/PLL bilayers, dark and shaded bars indicate independent data, n=3 for each.....	50
Figure 3.9 Three-stage release of EGCG from gelatin nanoparticles at pH 6.0.	51
Figure 3.10 C/C _∞ as a function of nanoparticles concentration. a) uncoated nanoparticles, b) PGA/PLL coated nanoparticles. The insert in a) shows the curves in C _∞ /C -1 vs. C _{NP} coordinates.....	52
Figure 3.11 EGCG release from 275 nm Gela nanoparticles coated with PSS/PAH shells. CNP = 0.22 g/L. pH of loading 6.8, pH of release 3.0. Time of loading is 48 h, n=3.....	54
Figure 3.12 Western Blot Analysis to measure c-Met activation, 1 and 5 indicate concentration of EGCG (μm) [62].	56

Figure 4.1	Zeta potentiometer readings during the encapsulation of <i>Alc. Vinosum</i> with PDDA/PGA (a) and PAH/PAA (b) with 3 and 4 layers, respectively, and PAH/PSS (c) with 5 and 6 layers.....	64
Figure 4.2	Formation of intracellular sulfur (a), sulfate (b) and protein concentration (c) with 3 and 4 layers encapsulated <i>Alc. Vinosum</i> during cell growth with sulphide [86].	68
Figure 4.3	Protein concentration (a), formation of sulfate (b) with 3 and 4 layers encapsulated <i>Alc. Vinosum</i> during cell growth with elemental sulphur [86].	69
Figure 4.4	Confocal microscopy image of <i>Alc. Vinosum</i> encapsulated with PAH/PAA cells during growth with elemental sulfur.....	70
Figure 4.5	FE-SEM image of <i>Alc. Vinosum</i> encapsulated with PAH/PAA during growth with elemental sulfur.....	70
Figure 4.6	Formation of intracellular sulfur (a), sulfate (b) and protein concentration (c) with 5 and 6 layers encapsulated <i>Alc. Vinosum</i> during cell growth with sulphide [86].	72
Figure 4.7	Protein concentration (a) and formation of sulfate (b) with 5 and 6 layers encapsulated <i>Alc. Vinosum</i> during cell growth with elemental sulphur [86].	73
Figure 5.1	Scheme for coating bacterial spores with polyelectrolyte multilayers and nanoparticles using LbL [107].....	79
Figure 5.2	ζ -potential of <i>B. Subtilis</i> spore in DI water at pH 6.8, n=2.	84
Figure 5.3	SEM images of <i>B. Subtilis</i> spores (a- control) and of (b) <i>B. Subtilis</i> coated with (PLL/PGA) ₄ + PLL + 22 nm silica nanoparticles.....	87
Figure 5.4	SEM images of <i>B. Subtilis</i> spores coated with (PLL/PGA) ₄ + PLL + 72 nm silica nanoparticles (a and b are two different spores).	87
Figure 5.5	Confocal image of <i>B. Subtilis</i> with shell of (PLL/PGA) ₄ labeled with PLL-RITC, immediately after the shell assembly (first day).	88
Figure 5.6	Confocal image of <i>B. Subtilis</i> with shell of (PLL/PGA) ₄ - Gelatin labeled with PLL-RITC (fifteenth day).	90
Figure 5.7	(a-b) Kinetics of apparent spore germination monitored by release of dipicolinic acid (DPA), n=3.	91

ACKNOWLEDGEMENTS

I owe my sincere gratitude to my mentor and advisor Dr. Yuri Lvov for all his guidance and support for my entire graduate stay at Louisiana Tech University. This work would not have been possible without his insight and advice. Working with him has been a wonderful learning experience. I am also thankful to Dr. David Mills for his insightful comments, encouragement and practical advice. I am grateful to Dr. Mark DeCoster for mentoring me and guiding me at various stages of my graduate study. He was a big source of motivation and inspiration that pushed me to get better at every step of my research. I thank him for all his valuable discussions and encouragement. I would also like to acknowledge Dr. Sidney Sit for commenting on my views and also for his constructive criticism. My sincere thanks also go to Dr. June Feng for her willingness to help and all her support. I would like to acknowledge Dr. Glenn Johnson, who helped me to receive a pre-doctoral fellowship that was administered by the Oak Ridge Institute of Science and Engineering. I have been very fortunate to have worked with Dr. Tatsiana Shutova. I am indebted to her for all that she has taught me over the years. I would also like to thank Dr. Patrick O'Neal, Pranitha Vangala and Bettina Franz for all their help. I am grateful to Dr. Pradeep Chowriappa for all his support. I would like to acknowledge all the staff at IFM for their support. Finally, all my work would not have been possible without the love and support of my family.

CHAPTER 1

NANOORGANIZED POLYELECTROLYTE SHELLS USING LAYER-BY-LAYER ASSEMBLY

Overview of Dissertation

Electrostatic Layer-by-Layer (LBL) assembly can be used for sequential deposition of oppositely charged polyelectrolytes, particles or enzymes on surfaces of variable shape to obtain nanoorganized shells [4]. The nanoshells have an empty or filled core that is encapsulated in a sheath of polyelectrolytes used for various applications. These nanoshells play an important role in the field of nanomedicine, where they are widely being researched for drug delivery. The LBL technique has been used in our research for two independent applications. Chapters 2 and 3 describe the process for forming nanoshells using naturally occurring polyphenols and proteins for drug formulations. In Chapters 4 and 5 we extended the LBL approach to encapsulate microbes and microbial spores to explore microbiological applications. LBL technique is based on the assembly of organized multilayers through alternate adsorption of oppositely charged linear polyions and proteins that involves resaturation of the polymers used for the process. The resaturation of the polyion adsorption is responsible for the reversal of the surface charge of the fabricated film after each step of adsorption. The thickness of the film can be monitored precisely in nanometers. The composition of the wall thickness can be varied for specific applications, thus making it possible to control

the release of the drug that is encapsulated in the polymeric sheath. Polymeric layers of desired nanothickness can either be deposited on a core that will further be loaded with the drug of interest using a concentration gradient of drug crystals, that can be considered to be the core, in which case there is no step of core desolvation. The drug molecules are intact since there is no covalent bonding involved in the shell formation. No covalent binding is involved in the shell formation, which allows drug macromolecules to remain intact, thus helping in achieving a continuous drug release profile [4]. Various parameters like pH, temperature, or magnetic field can be used to control the release of the loaded microcapsule depending on the nature of the polymers and nanoparticles used in the assembly.

LbL can be applied to nanomedicine by using nanoemulsions, polymer conjugates of proteins or drugs or a matrix that has a combination of drugs, proteins and target molecules that help in the detection of the delivered compound in vitro or in vivo. This technique can be useful to exploit numerous applications involving biomimetic or bioresponsive systems. We have demonstrated the use of biocompatible polymers and polyphenols for drug formulation that can further be used with bioresponsive systems for drug delivery. The use of natural polymers provides greater safety and biocompatibility and a promising goal of manufacturing safe medicines.

Formation of Nanoshells using Electrostatic Layer-by-Layer Assembly

A nanoshell can be formed by encapsulation of a core as a template, which is typically stable and permeable, allowing the release of the core material through the shell. The study in Chapter 2 demonstrates the use of a passive core template, where manganese carbonate particles are dissolved after encapsulation using various

polyphenols and gelatins. The data in Chapter 3 shows the use of an active core template, in which gelatin nanoparticles are used as core templates to load various polyphenols. This indicates that electrostatic (LbL) assembly has a great potential to use a wide variety of substances as shell constituents as well as core material. Although this technique has been used for over a decade, it still has to be further developed to acquire an in depth knowledge [5-10].

Preparation of LbL Nanoshells

Iler has reported sequential adsorption of oppositely charged colloids in 1966 [11]. Electrostatic LbL, that involves sequential adsorption, was further developed in the early 1990s [12-15]. This technique is based on resaturation of polyion adsorption that results in the reversal of the terminal surface charge of the film after each adsorption step. [10-12]. Figure 1.1 shows the procedure of electrostatic LbL on 2-D substrates and 3-D micro/ nanotemplates.

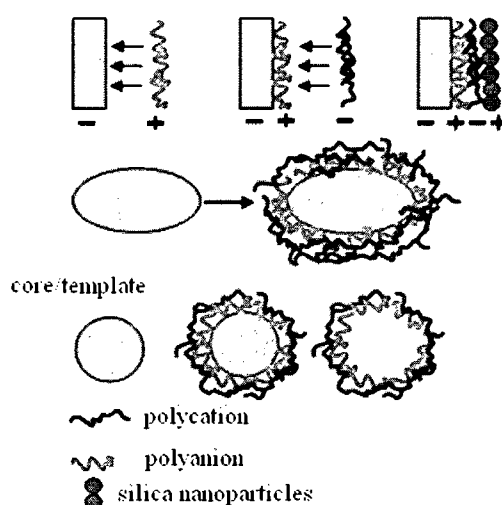


Figure 1.1 Electrostatic LbL 2-D substrates and 3-D micro/ nanotemplates.

The procedure of electrostatic LbL self-assembly can be started on a positively or a negatively charged substrate [4]. The above figure shows various 2-D substrates and 3-D micro / nanotemplates that have been considered to be negative for explanation purposes. For our experiments, we used quartz slides, quartz resonators, manganese carbonate micro cores, and microbial cells that were all negatively charged. Particles with negative surface charge are coated with a layer of polycation in the first step. After an adsorption step, the surface charge is reversed and a thin film is formed making the total surface charge positive. An anionic polyelectrolyte is deposited in the second step making the surface charge negative. The substrate is coated with the desired number of layers and thicknesses [10-12].

Step by Step Description of LbL Process

Electrostatic LbL film fabrication uses the following steps [12, 14, 16]:

1. Make aqueous solutions of polyion, nanoparticles or protein at a concentration of 0.1 - 3 mg/mL and adjust the pH to make the components oppositely charged.
2. Select a substrate carrying a surface charge to be used as a template (e.g. A quartz slide, resonator).
3. Immerse the substrate in the oppositely charged polyion solutions for 10 min. This is the adsorption time.
4. Rinse the substrate for 1 min in water. Adjust the pH of the rinsing solution to keep the polyions in the ionized state.
5. Dry the sample under a stream of nitrogen and then immerse the substrate in the polyion solution that is oppositely charged. This completes the formation of one bilayer on the substrate.

6. Repeat the process for the desired number of layers.

If the charged substrate is in a solution, then it follows the same method for adsorption of polyions, but there is no drying step involved in the process. The samples are centrifuged and the supernatant is replaced with the polyion of the opposite charge. Water is used as the supernatant in the rinsing step. This technique can be used for designing ultrathin multilayer films with a precision better than one nanometer of defined molecular composition. This method has been successfully demonstrated with more than 50 different charged macromolecules. The commonly used synthetic polyelectrolytes are poly(allylamine) (PAH), poly(dimethyldiallylammonium chloride) (PDDA), poly(ethylenimine) (PEI), poly(styrenesulfonate) (PSS), poly(vinylsulfate), and poly(acrylic acid) (PAA) [4]. The commonly used biocompatible polyelectrolytes are polylysine (PLL), chitosan, polyglutamic acid (PLGA), gelatin, chondroitin sulphate, and DNA. We have also used charged inorganic silica nanoparticles along with some of the polymers mentioned above to provide multifunctional armored shells for microbial spores. Some other examples would be to use enzymes, antibodies, and viruses to obtain different functionalities. Different properties like thickness, biocompatibility, controlled permeability, and targeting can be attributed to the films by designing the architecture of these shells as desired.

Various characterization techniques are available to detect the formation of the nanofilms that have been described in following chapters. It has been demonstrated that more than 1000 polyelectrolyte multilayers (PEMs) can be fabricated as thin films [17]. A substrate of any shape or size can be used for the film formation as long as it is charged. Various proteins and nucleic acid have been used in multilayer films to explore

the possibility of using them as biosensors [18-20]. Applications can also be found in the fabrication of scaffolds to study the nature of cell communication [4]. We have made an attempt to efficiently use the multilayer coating in our research by investigating the respective properties of the polyions for different applications. It is complicated to study the nature of the multilayer films in case of solid substrates. We focused our research on studying the multilayer films, which were fabricated on colloidal cores, could be dissolved. The derived hollow capsules allowed us to study polyelectrolyte multilayers at the liquid–liquid interface that is not possible with solid templates [13, 21].

Research on nanoshell formation has been published since 1992 [5-7], and studies on structural characterization and functionality of the nanoshells has been of great interest to many research groups [8, 12, 20]. Caruso and Lvov showed that the pore openings in the polyion multilayers can be used for loading various enzymes [8]. Nanotechnology that uses LbL has been demonstrated to be successful and to have great prospects in medical research. However, many practical clinical applications in nanomedicine, especially nanopharmaceutics, remain to be studied and developed.

Our Approach- Drug Formulations and Biomimetic

Drug formulations: we used LbL to make nanoshells that could be used in the field of drug formulations by fabricating protein/polyphenol microcapsules on using naturally occurring polyphenol (-)-epigallocatechin gallate (EGCG) and gelatins. It was shown that EGCG retains its antioxidant activity in the LbL assemblies. These were designed as carrier systems of submicron dimension that can be used to load various bioactive materials. The elaboration of such systems is challenging for applications that require a sustained release of the bioactive materials that are loaded in them [14]. We

used (-)-epigallocatechin gallate because of its anticancer and antioxidant properties [1]. Gelatins that contain many glycine, proline and 4-hydroxyproline residues [22] as proteins were used as the components of the assemblies. The assemblies had strong antioxidant properties, since polyphenols also protect against free radical species in an oxidizing medium [23, 24]. This was useful in prolonging the life-time of the polyphenols and overall helped in enhancing the effectiveness of the encapsulated substances. Using the LbL technique, we further encapsulated EGCG into gelatin-based 200-300 nm sized particles and coated the loaded gelatin particles with polyelectrolyte shells using various synthetic and biocompatible polyelectrolytes. We characterized the gelatin particles that were loaded with EGCG and optimized the conditions for loading and release of EGCG from the particles. We also showed that the particle-encapsulated EGCG was biologically active as both particles containing EGCG and free EGCG blocked HGF-induced intracellular signaling in the breast cancer cell-line MBA-MD-231.

Biomimetic approach: LbL can be used to fabricate shells on biological cells that act as a non-biological replica allowing the exploration of some of the organizational features of the cells [4]. Hua, et al. [25] has demonstrated that blood platelets can be coated using the LbL technique. LbL was used in our approach for answering some questions in microbiology by modifying the cell surfaces by making them either more hydrophilic or hydrophobic. The encapsulation of the cells was also useful in giving them more colloidal stability. We used the LbL technique to investigate the uptake and release of substrates and products in bacteria viz. *Alc. Vinosum*, using two different approaches; one was by studying the changes in the electrochemical potential of the cell surface and the other was by monitoring the influence of building a physical barrier around the cell.

We showed that the LbL technique offers a great deal of flexibility for surface modifications using *Alc. Vinosum*. We further studied the modification of bacterial spores viz. *Bacillus Subtilis* by reproducing some of the spore shell features using in vitro self-assembly methods. We coated individual bacterial spores using various polyelectrolytes and were also able to coat the cells with an inorganic layer of silica nanoparticles. We showed that the spores were viable after encapsulation using germination assays. It was shown that the coatings affected the diffusion rates of germinant influx into and possibly actual endospore germination. Biocompatible polymers were effective in coating the spores and thus offer the use of these assemblies in applications, such as agricultural pesticides that have a sustained release effect by varying the rate of germination.

CHAPTER 2

EPIGALLOCATECHIN GALLATE / GELATIN LAYER-BY-LAYER ASSEMBLED FILMS AND MICROCAPSULES

Overview

This chapter is based on my contribution to the publication titled ‘Epigallocatechin gallate/gelatin LbL assembled films and microcapsules,’ *J. Colloid Interface Science*, 2009 [26]. Polyphenols having a high spectrum of biological activity are of great interest to researchers for their antioxidant, antibacterial, antiviral, and other properties. Polyphenol compounds originating from plants possess all these biological activities. Polyphenols loaded in nanoscale vehicles instead of free compounds can be used to improve bioavailability and half-life of the compound in vivo and in vitro, optimize routes of their administration, and achieve site specific or targeted drug delivery combined with controlled release profiles [27-29]. Plant polyphenols have been encapsulated in micelles and liposomes [30], protein-lipid emulsions [31], chitosan microspheres [32], other pre-formed materials, such as yeast cell-based material [33], cyclodextrins [34], mesoporous silica [35].

Although numerous studies have been done to study the factors influencing stability, solubility and other characteristics of protein/polyphenol complexes [1, 36-42], there is a vast scope for the application of polyphenols/protein systems that have not completely explored the behavior of nanocomposite biomaterials. Techniques like direct

complexation using gelatin/tannic acid and casein/(-)-epigallocatechin gallate nanoparticles have been studied [40-42]. An LbL technique, with a different approach than ours, has been used to fabricate polyelectrolyte shells around inorganic cores and to also obtain thin wall capsules containing tannic acid that are free-standing in solution [21, 43].

The LbL technique allows multilayers to be constructed with nanometer precision and predetermined layer composition via sequentially saturating adsorption of a layer of each component on a template surface [21, 43-49]. Various species, including polyelectrolytes, nanoparticles, DNA, and enzymes as well as several low molecular weight substances, such as porphyrins, can be used for LbL assembly [44]. In order to study pH-controllable solubility for sustain release formulations, various potential materials used for LbL-constructed multilayers on the basis of tannic acid (TA), or pentagalloyl glucose, with typical artificial polyelectrolytes poly(allylamine hydrochloride), polydiallyldimethylammonium chloride [21], 90% quaternized poly(N-vinylpyridine) [49], naturally derived polyelectrolyte chitosan [44], as well as several uncharged polymers, such as poly(N-vinylcaprolactam), poly(N-vinylpyrrolidone), poly(ethylene oxide), poly(N-isopropyl acrylamide) [50], have been investigated. Quartz crystal microbalance techniques have been used to study the kinetics of the adsorption of EGCG, tannic acid, tearubigins (pigments of black tea) on an immobilized layer of bovine serum albumin [50-52].

In order to get an in-depth understanding of polyphenols and proline-rich proteins using LbL assembly, we used EGCG (Figure 2.1) as one of the components of the assembly because of its well-known health benefits, anticancer and antioxidant activity

[1]. EGCG comes from a family of flavonoids, specifically, flavan-3-ols [26]. It is highly soluble in aqueous solutions and most organic solvents, making it even more challenging for encapsulation. Its molar mass is 458.37 g/mol.

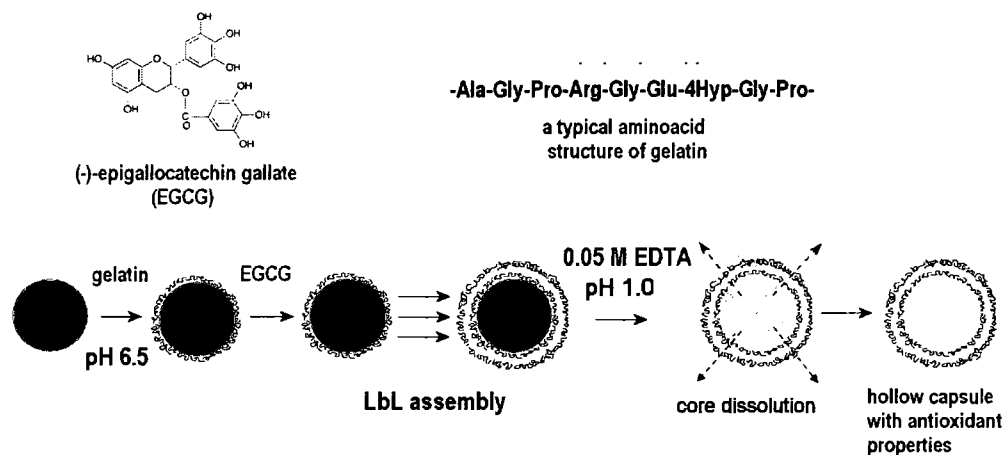


Figure 2.1 Scheme of Gela/EGCG hollow capsule preparation [26].

We used gelatins that contain many glycine, proline and 4-hydroxyproline residues [22] as the protein components of the assemblies. The two types of gelatin depend on whether they have been treated with an acid or alkaline base. Acid pretreatment produces gelatin with an isoelectric point in the range of 7 to 9 (Type A gelatin), whereas an alkaline treatment gives samples with $pI = 4.7-5.4$ (Type B gelatin) [22]. The regularities in layer formation and the stability of the forming structures are affected by the properties of these gelatins.

Polyphenols are useful in protecting against free radical species in oxidizing media and hence their incorporation in LbL fabrications helps in introducing additional antioxidant properties to the assemblies [23, 24], further prolonging their life-time and enhancing the effectiveness of the encapsulated substances.

Materials and Methods

(-)-Epigallocatechin gallate from green tea (EGCG), gelatin, type A from porcine skin (GelA, ~300 Bloom), gelatin, type B from bovine skin (GelB, 225 bloom), sodium chloride, hydrochloric acid, sodium hydroxide, potassium persulphate ($K_2S_2O_8$), 2,2'-azinobis(3-ethylbenzothiazoline-6-sulfonic acid) diammonium salt (ABTS), tetramethylrodamine-5-isothiocyanate (TRITC) and fluorescein isothiocyanate (FITC) were purchased from Sigma-Aldrich and used as received.

Fluorescently labeled gelatins, GelA -FITC and GelB-TRITC, were prepared as in [53, 54], and the labeled proteins were separated using *Amersham Bioscience* PD-10 desalting columns.

Film Fabrication

0.9 x 1.8 x 0.09 cm³ quartz slides were sequentially dipped into 3.0 mg/mL aqueous solutions of a gelatin (GelA or GelB) and EGCG at pH 6.5 for 15 min per layer to obtain (GelA/EGCG)_n and (GelB/EGCG)_n (n=0.5-10) assembled films. The time of adsorption was 15 min per layer with three intermediate washings in deionized (DI) water [26].

We used a USI-System, Japan Quartz Crystal Microbalance (QCM) to estimate the thickness of the deposited gelatin/EGCG multilayers by monitoring the changes in frequency with an accuracy of ± 1 Hz. The frequency values were then converted into thickness using experimental scaling with the Sauerbrey equation: ΔD (nm) = - 0.016 ΔF (Hz). Further, the frequency decrease was used to recalculate the mass of the deposited material using the following equation: Δm (ng) = -0.84 ΔF (Hz). All the resonators were rinsed with DI water and dried under a stream of nitrogen. Gelatin was adsorbed on the

resonators as a precursor layer before fabricating layers using polyphenols. After adsorption of each layer, the resonators were washed in an excess amount of DI water and dried under a stream of nitrogen. For each experiment involving gelatin A, four resonators were used in sets of two. To check if the solution that is repeatedly used for the alternations of the assembly layers affects the amount of material deposited on the resonators, the adsorption on one of the resonators was started after 10 adsorption cycles (five bilayers) had been done for another resonator. We ran two independent sets of adsorption for GelB/EGCG multilayers.

(Gelatin/EGCG)₄ Shell Preparation

MnCO₃ cores were used as scaffolds and layers of GelA or GelB were sequentially deposited in alternation with EGCG on the cores using the standard procedure previously used to produce polyelectrolyte capsules [43]. A bath sonicator was used to disperse the MnCO₃ microcores with a diameter of 4.0 μm (~ 0.2 g). The particles were rinsed twice with DI water at 3500 rpm to precipitate the particles. It was not necessary to fabricate a precursor polyelectrolyte layer on the microparticles. Gelatin formed the first layer in the assembly process. Finally, the microparticles were suspended in 1.0 mL and the assembly process was started by adding 0.5 mL of a 3 mg/mL gelatin solution to the 1.0 mL solution at pH 6.5 for 15 min. After the adsorption cycle was over, the particles were separated from the supernatant and rinsed three times with DI water. Similarly, an EGCG layer was formed by adding 0.5 mL of a 3 mg/mL EGCG solution per 1.0 mL of the suspension of gelatin-coated microparticles. The time of adsorption for all the adsorption cycles was fifteen minutes. The microparticles were separated by centrifugation and rinsed with DI water. A Brookhaven ZetaPlus Micro-Electrophoretic

Instrument was used to monitor the assembly by measuring the surface potential (ζ -potential). Sample preparation for the measurements involved using 20 μL of sample solution and re-dispersing them in 2 mL of DI water.

In order to obtain GelA/EGCG empty capsules that had four bilayers on them, 0.25 mL of microcores with GelA/EGCG shells was mixed with 0.75 mL of a 0.05 M EDTA for 3 days. On the fourth day, the pH was adjusted to 1.0 for 30 min. The core dissolution can be confirmed visually and the supernatant was replaced with 1 mL of fresh 0.05 M EDTA. The pH of the suspension was adjusted to 9.0 for 1 min, and then the (GelA/EGCG)₄ capsules were separated by centrifugation and washed three times with DI water to remove soluble salts. It was crucial to use 0.05 M EDTA solution and also adjust the pH to obtain the desired hollow microcapsules. Adjusting the pH with 0.1 M HCl solution without using EDTA to dissolve the carbonate cores did not produce the capsules free of core traces. All the dissolution methods were tried with (GelB/EGCG)₄ capsules but none of them gave stable (GelB/EGCG)₄ capsules [26].

A *Q-ScopeTM 250 Quesant* instrument was used in an intermittent-contact mode to obtain Atomic force microscopy (AFM) images of dried capsules on mica and films on silicon supports. Confocal Laser Scanning Microscopy (*Leica DMI RE2*) was used to visualize the structure of Gel/EGCG shells on cores and microcapsules after core dissolution. SEM images were taken on a *Hitachi S-4800* Scanning Electron Microscope equipped with an energy dispersive x-ray analysis (EDAX) accessory. All the sample surfaces were sputtered with a 2 nm layer of Iridium to enhance image quality.

Capsule Permeability Test

We used Fluorescein isothiocyanate (FITC) and FITC-labeled dextrans (1 mg/mL, Sigma) with the molecular weights of 4,400, 77,000, and 2,000,000 for permeability testing experiments. 20 μ L of capsule solution was mixed with 20 μ L of dextran solution at pH 6.6. This sample was placed on a glass slide in the confocal microscope slide holder. The intensities of the light emitted by a capsule interior (I_{int}) and by the surrounding solution (I_{ext}) were measured 10 minutes after the dextran solution was added to the capsule solution. An average value was noted, after the measurements were completed, for 20-25 unbroken capsules [26].

ABTS⁺ Assay

A stock solution of cation-radicals of ABTS (ABTS⁺) was prepared as in [55]. 88 μ L of a 0.14 M K₂S₂O₈ was added to 5 mL of a 7·10⁻³ M ABTS aqueous solution and left overnight at room temperature. The obtained stock solution of intensive blue-green color was kept protected from light at +2⁰C. The stock solution was diluted with DI water (pH 6.5) immediately before use in such a way that the absorbance at 734 nm (A) was equal to 1.35 ± 0.05 ($l = 1.0$ cm, $\epsilon = 1.4 \cdot 10^4$ M⁻¹ cm⁻¹ [55]). It was made sure that the difference of A_0 in various series was not higher than ± 0.05 [26].

To evaluate antioxidant properties of free EGCG, GelA, or GelB, 10-250 μ L of 0.3-3.0 mg/mL solution of the components were added to 2.0 mL of the aqueous ABTS⁺ solution (pH 6.5) as above under constant stirring. Absorbance of the mixture at 734 nm (A_t) was tracked in time for 60 min with readings taken at intervals of 10 s using an *Agilent 8453* spectrometer. The influence of gelatin on EGCG determination with the ABTS⁺ assay was also evaluated and found to be moderate [26].

Quartz slides with (GelA/EGCG) n or (GelB/EGCG) n layers on them were placed into 2.0 mL of the ABTS⁺ solution under stirring and changes of A_t were followed in time. The moment of slide immersion into the solution was taken as t_0 . To evaluate the background change due to quartz slide immersion, the empty wet supports were placed into the ABTS⁺ solution under experimental conditions and the A_{734} drop, typically 0.14 ± 0.05 a.u., was taken into account in further calculations.

Results and Discussion

Layer-by-Layer Assembly on QCM Resonators

A steady pattern was observed with the deposition of the gelatin/EGCG multilayers for each layer adsorbed on the resonators (Figure 2.2). The first two bilayers were 5.0-7.0 nm and then the thickness of the GelA/EGCG bilayer increased up to 10 nm per layer for four deposition cycles. There was a sharp increase in the thickness from the fifth cycle onwards, with a step higher than 30 nm (Figure 2.3). It is possible that the sharp increase is due to the high concentration of the protein/ gelatin multilayer. The results were consistent for all the runs [26].

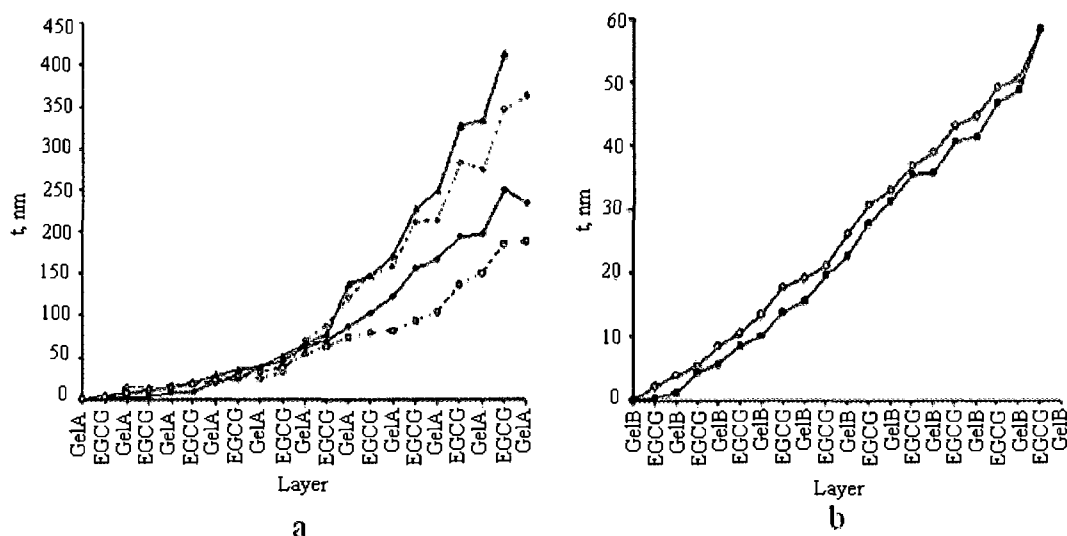


Figure 2.2 QCM assembly of GelA (a) and GelB (b) in alternation with EGCG. The results of independent experiments are presented.

Solution contamination or deterioration in the assembly process as a result of bulk film formation was not an issue since the adsorption of GelA/EGCG layers on one of the resonators was started after five bilayers had been already adsorbed on another from the same solution.

The total thickness of the GelA/EGCG multilayers is higher than that of GelB/EGCG films having the same number of bilayers. It was seen that the GelB/EGCG bilayer thickness increased with sequential deposition of layers but the increase was not so prominent as compared to the GelA/EGCG films. The first GelB/EGCG bilayers had a thickness of 2-4 nm and increased to 6-8 nm for further layers (Figure 2.3).

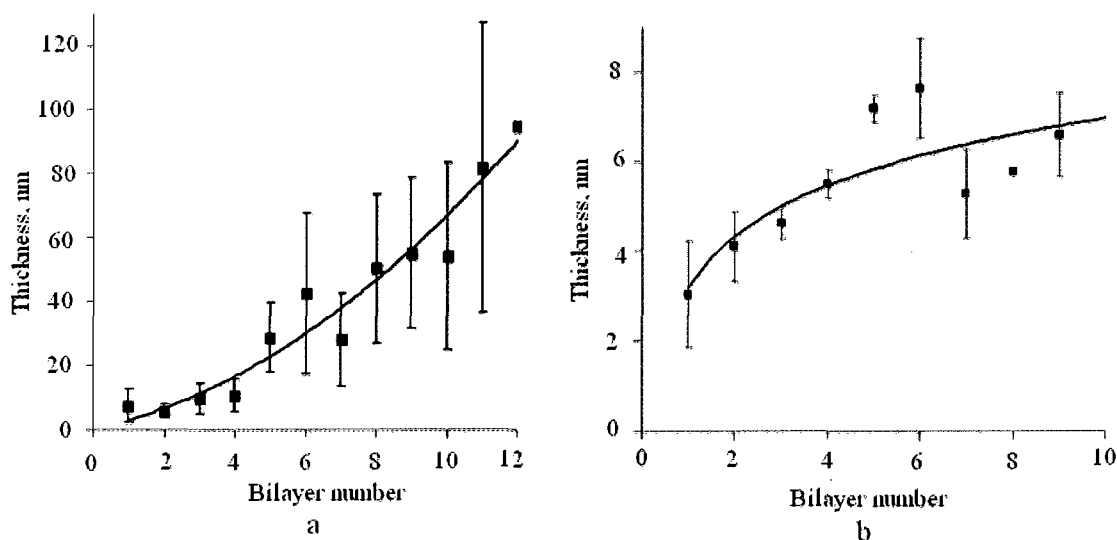


Figure 2.3 Thickness of GelA/EGCG (a) and GelB/EGCG bilayers (b) as a function of bilayer number, $n=3$.

It has been established that polyphenol/protein binding is based mainly on hydrogen bonding between hydrophobic aminoacid residues of proteins and phenol ring of polyphenols [1, 36, 37, 39-42], but is also affected by protein charge [50, 51]. Our study was based on the assumption that hydrophobic forces are mainly involved in the formation of Gelatin/EGCG layers, since EGCG does not form stable LbL assemblies with polycations, unlike tannic acid [21]. The physical chemical properties of the gelatin (varying charge density and Bloom numbers) that we used for our study were responsible for the GelA/EGCG bilayers' thickness being higher than that of the EGCG/GelB bilayers. One probable cause of the exponential growth of the layers was the adsorption of more than one layer of EGCG or gelatin per deposition cycle [26]. Bulk films can usually be formed by a partial release of EGCG from previously adsorbed layers into protein solution and an extra adsorption of EGCG into already deposited gelatin layers from its solution. It has been shown that EGCG tends to form complexes of varying

stoichiometry with proteins [36, 37, 39-42], making the complexation of EGCG with hydrophobic proteins a multistage process.

Influence of Gelatin on EGCG **Determination with the ABTS⁺** **Assay**

To prepare a stock solution of cation-radicals of ABTS (ABTS⁺), 88 μL of a 0.14 M $\text{K}_2\text{S}_2\text{O}_8$ was added to 5 mL of a $7 \cdot 10^{-3}$ M ABTS aqueous solution and left overnight at room temperature [26]. The obtained solution of intensive blue-green color was kept protected from light at +2°C and was diluted with deionized (DI) water (pH 6.5) immediately before use in such a way that the absorbance at 734 nm (A_0) was equal to 1.35 ± 0.05 ($l = 1.0 \text{ cm}$, $\epsilon = 1.4 \cdot 10^4 \text{ M}^{-1} \text{ cm}^{-1}$). The variation of A_0 in different series was not higher than ± 0.05 .

To evaluate antioxidant properties of free EGCG, GelA, or GelB, 10-250 μL of a 0.3-3.0 mg/mL solution of the components were added to 2.0 mL of the ABTS⁺ solution (pH 6.5) as above under constant stirring. Absorbance of the mixture at 734 nm (A_t) was followed in time for 60 min with readings taken at 10 s intervals using an Agilent 8453 spectrometer.

Interaction of ABTS⁺ with EGCG **in Solution**

Interaction of EGCG with ABTS⁺ happens in a two step process. The first step happens within the first 20 s after adding EGCG to an ABTS⁺ solution and is followed by a long slow scavenging stage (Figure 2.4) [26].

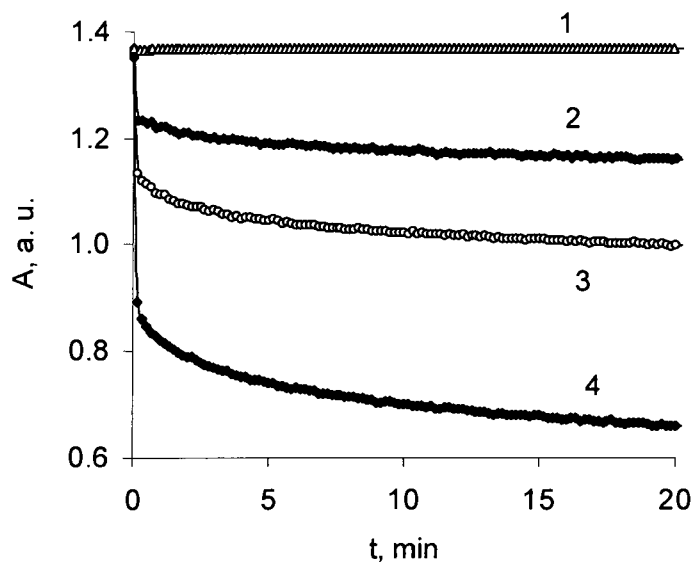


Figure 2.4 $A_{734 \text{ nm}}$ changes after addition of EGCG to an $\text{ABTS}^{+\bullet}$ solution. Concentration of EGCG 10^6 , M: 1-0, 2-1.1, and 3-2.2, 4-6.4.

This property has been attributed to biphasic kinetics that are observed for the $\text{ABTS}^{+\bullet}$ reaction with several other antioxidants and complex flavonoid compounds due to scavenging by polyphenol oxidation products formed in the early stages of the reaction [56-60]. The estimated radical scavenging activity (RSA) for EGCG, which indicates how many $\text{ABTS}^{+\bullet}$ radicals react with one inhibitor molecule, reaches 11.5 ± 1.9 after 20 min. For several other polypeptides, including trolox and gallic acid, it has been shown that 1.92 ABTS cation-radicals can react with one $-\text{OH}$ group [59]. Since one molecule of EGCG has eight $-\text{OH}$ groups, we could estimate that the reaction is completed to about 75% after 20 min. The RSA value reaches 13.8 ± 0.7 (Figure 2.5) after 24 h. It can be seen from (Figure 2.6) that the presence of 0.03-1.9 mg of gelatin per 1 mg of EGCG has only a small influence on the EGCG determination in solution with the $\text{ABTS}^{+\bullet}$ assay after 20 min of reaction.

To evaluate the influence of gelatin on the EGCG determination using the ABTS^{•+} assay, 0-0.75 mg/mL of a 3 mg/mL GelA solution was mixed with 0.4 mL of a 0.5 mg/mL EGCG solution and left overnight. Then the mixture was sonicated for 1 min and 10 μ L of the mixture was added to 2 mL of the ABTS^{•+}, as above and mixed. The absorbance of the mixture at 734 nm (A) was determined at 6 min, 20 min, 1.5 h, and 24 h after the mixing [26].

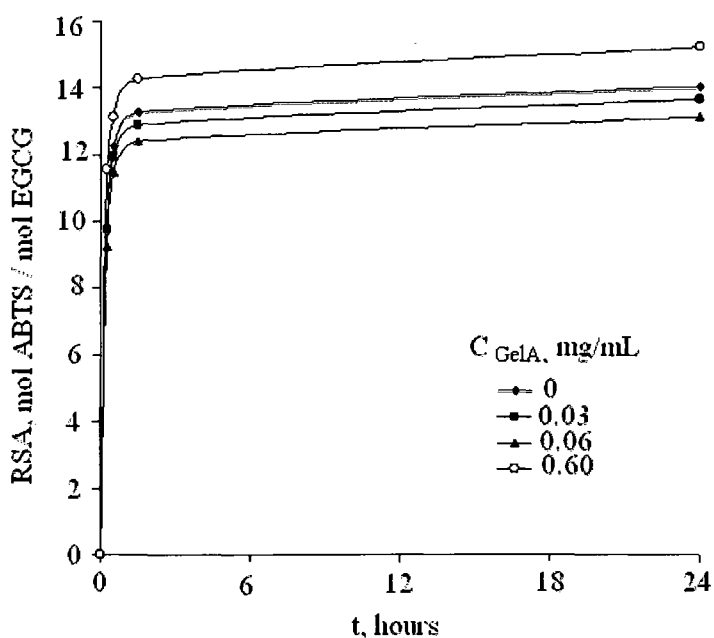


Figure 2.5 RSA parameter of EGCG in time in the presence of different amounts of GelA. $C_{EGCG} = 0.5$ mg/ml.

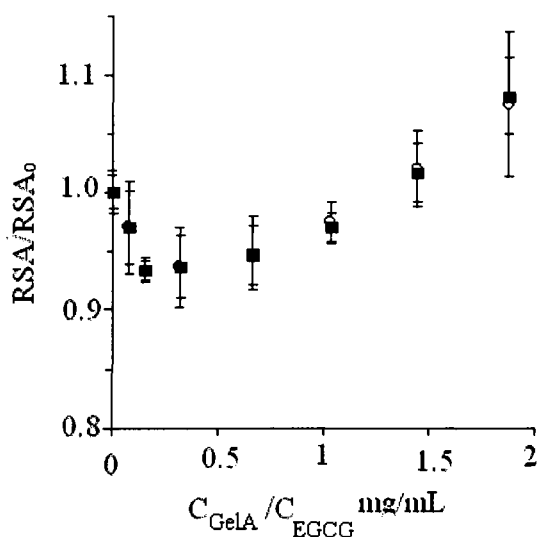


Figure 2.6 RSA/RSA₀ as a function of gelatin concentration. $C_{\text{EGCG}} = 0.5$ mg/mL. Time: 20 min (○) and 24 h (■).

The ratio of an EGCG concentration determined in the presence of gelatin to that in the solution without the protein is between 0.93-1.07. This influence was neglected for our study. GelA and GelB had less than 0.2 mmol -OH groups per 1g, which is at least two hundred times less than EGCG [26]. The amount of ABTS^{•+} that reacted with gelatin in the EGCG/GelB mixtures and films could be neglected in our calculation.

Interaction of ABTS^{•+} with Gelatin/EGCG Multilayers

The reaction of EGCG with the ABTS cation-radicals retains biphasic characteristics for Gel/EGCG films (Figure 2.7a) [26]. It was found that the initial ABTS^{•+} scavenging rate (W) for films (Figure 2.7) is several times lower than that in a solution ($W_{\text{sol}} \sim 10^{-5}$ - 10^{-4} M/s). One probable reason for such a phenomenon could be the inhibition of the ABTS^{•+} reaction with EGCG by the strong complexes formed by gelatin with the compound in the initial stages [1]. The reaction of EGCG with ABTS^{•+} for

Gelatin/EGCG films was not completed even after 60 min; a further slow decrease of cation-radical absorbance was always observed.

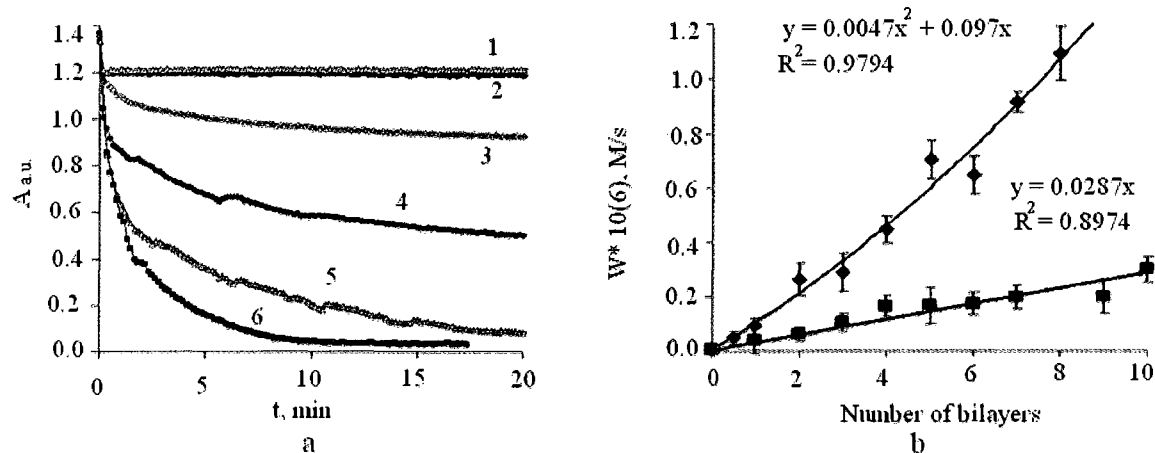


Figure 2.7 a) Kinetic curves of ABTS cation-radical decay on GelA/EGCG films with different number of bilayers (1-6), b) initial rate of ABTS^{+•} consumption over the time period of 30 s as a function of number of bilayers, $n=3$.

An average value of EGCG adsorbed in the EGCG/Gelatin films was evaluated from the change in absorbance of an ABTS^{+•} solution after the corresponding films were immersed in the solution for 20 min. [26]. We assumed that the RSA in the films was equal to that in solution. The EGCG content was shown to be about 272 and 89 ng/cm² per layer for multilayers of Gelatin A and Gelatin B, respectively. GelA-based layers had a higher amount of EGCG that was correlated with the formation of thick GelA/EGCG bilayers and this was consistent with our QCM data. QCM data was used to calculate the percentage of EGCG in the multilayer films. The estimated value for GelA/EGCG was about 30 % w/w for EGCG and higher than 28% w/w for GelB/EGCG layers.

It was seen that the value of W increases with increasing number of bilayers in the film and no plateau is observed on the graph (Figure 2.7b) for Gelatin/EGCG films, unlike that for tannic acid/polyallylamine hydrochloride multilayers [23, 24]. This can be

explained by an exponential growth of Gelatin/EGCG layers, which was also observed by QCM along with an imperfect structure of the film.

The AFM data (Figure 2.8 a) showed that the surface of a dried (Gela/EGCG)_{8.5} film was very rough, with numerous aggregates of 300-500 nm in diameter. Figure 2.8b shows that at a higher resolution, smaller complexes of Gela and EGCG with a size less than 100 nm are observed in the structure of the bigger aggregates.

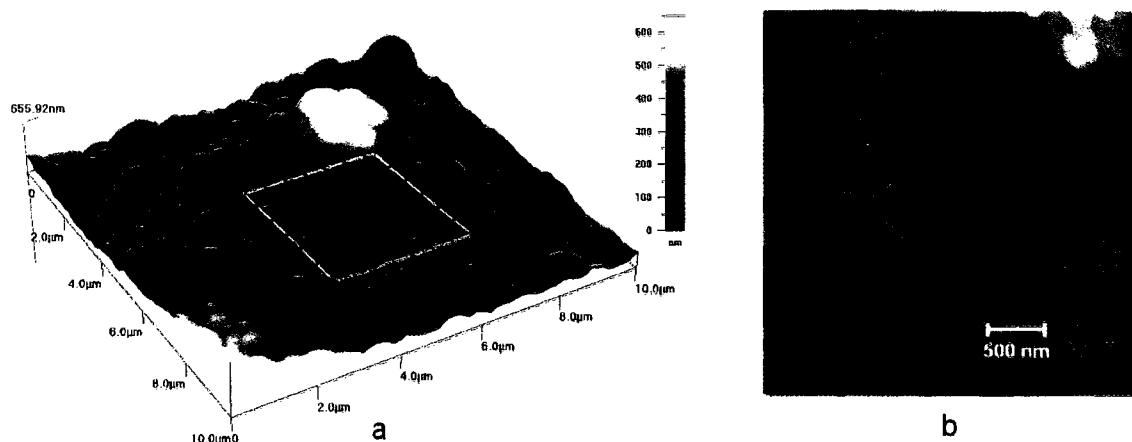


Figure 2.8 AFM image of the surface of a dried (Gela/EGCG)_{8.5} film (a) and magnified surface image (b).

We found similar patterns for GelB/EGCG multilayers but they were less rough. This is characteristic for films both with EGCG and gelatin outermost layers. The hydrophobic complexes are formed in the course of the LbL assembly of gelatin and EGCG but their size and shape is affected by film collapse during drying. We assume that the parent wet Gelatin/EGCG multilayers have a porous structure with plenty of isolated islands of hydrophobic material. This facilitates the diffusion of the ABTS⁺ reagent in the film structures [26].

Gelatin/EGCG Assembly on Cores

We show that flat quartz supports can be used as scaffolds to fabricate both EGCG/GelA and EGCG/GelB layers. We then tried to form shells consisting of gelatins and EGCG over MnCO_3 microparticles. Gelatin always formed the first layer for the microparticles. The ζ -potential values for GelA were positive and were negative for GelB coated microparticles. This could be explained with the isoelectric points of the gelatins (Figure 2.9) [26].

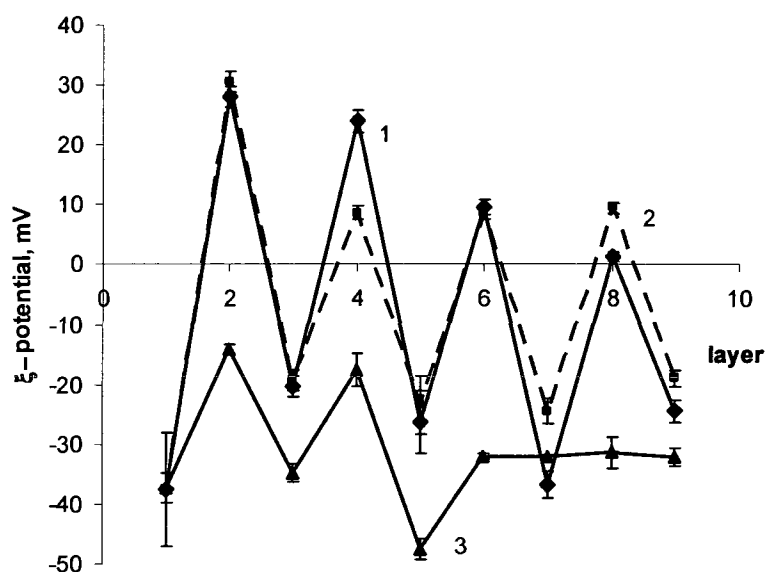


Figure 2.9 ζ -potential changes during the LbL assembly of GelA (1), GelA-FITC (2), or GelB (3) and EGCG on MnCO_3 cores at pH 6.5, $n=2$.

There was good alternation of charges for the GelA/EGCG shell; the microparticle surface charge had a positive value for microparticles with GelA as the external layer and a negative value for those coated with EGCG (Figure 2.9).

For the EGCG/GelB assembly, there was not much variation in the negative value at pH 6.5 (experimental conditions). A negative surface charge of the nanoparticles coated with EGCG as the outermost layer was consistent with the direct measurements of

the electrophoretic potential of an EGCG solution, indicating the polyphenols have an apparent pKa value between 3 and 4 [61]. The negative surface charge of EGCG-coated nanoparticles could also be related with values obtained using tannic acid [23], since it has similar structural elements. Figure 2.10 shows confocal images of Gelatin/EGCG shells coated around MnCO_3 . GelA was preliminary labeled with FITC, and GelB with TRITC to enhance the contrast of the fluorescence images.

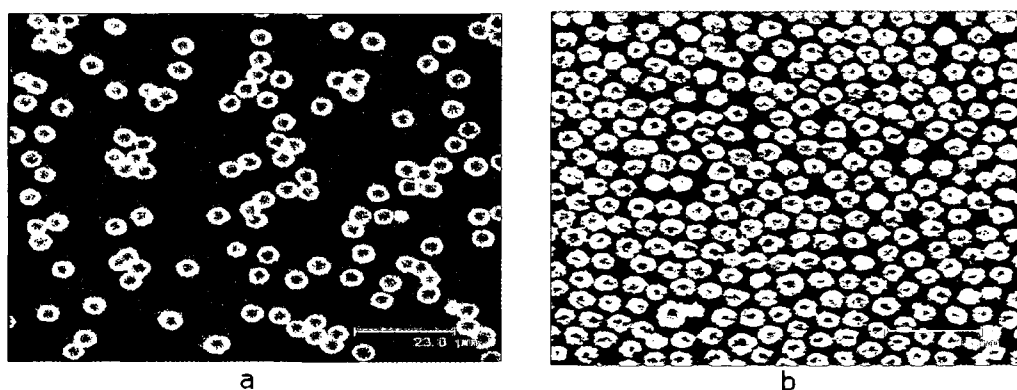


Figure 2.10 $(\text{GelA-FITC/EGCG})_4$ (a) and $(\text{GelB-TRITC/EGCG})_4$ (b) shells on MnCO_3 cores.

When compared, the $(\text{GelA-FITC/EGCG})_4$ shells appear to be rather uniform, forming rings with equally distributed fluorescence and, therefore, with equally distributed components around the cores as compared to a non-uniform distribution of TRITC-labeled GelB for $(\text{GelB-TRITC/EGCG})_4$. The non-uniform distribution for GelB-TRITC/EGCG shells is indicative of the formation of a net of hydrophobic GelB/EGCG complexes around the cores. We tried adsorbing a positively charged layer of GelA as the first layer to exclude the possibility of the bad attachment of GelB to a negatively charged core surface. After depositing a uniform layer of GelA, a shell of $\text{EGCG}/(\text{GelB/EGCG})_3$ was formed around it. There was no change in the uneven

distribution of TRITC fluorescence. We were able to fabricate shells around the cores using both GelA and GelB and this was in good agreement with the data obtained by QCM [26].

(GelA/EGCG)₄ Capsules

The (GelA/EGCG)₄ capsules obtained after core dissolution had a tendency to attach to each other or to an unwetted portion of a glass slide when a droplet was used for sample characterization [26]. The capsules were very light and extremely hydrophobic. The average diameter of (GelA/EGCG)₄ capsules was observed to be close to the size of the initial cores. Figure 2.11 shows that the majority of the capsules are slightly deformed. A probable explanation would be the high hydrophobicity of the wall material (up to ca. 20 % of capsules were collapsed, broken, or had holes). We were not able to prepare free-standing GelB/EGCG capsules using any of the techniques that we tested. We speculate here that the properties of the gelatins used influence the formation of stable, uniform, defect-free protein/polyphenol shells around cores and free-standing capsules in aqueous media.

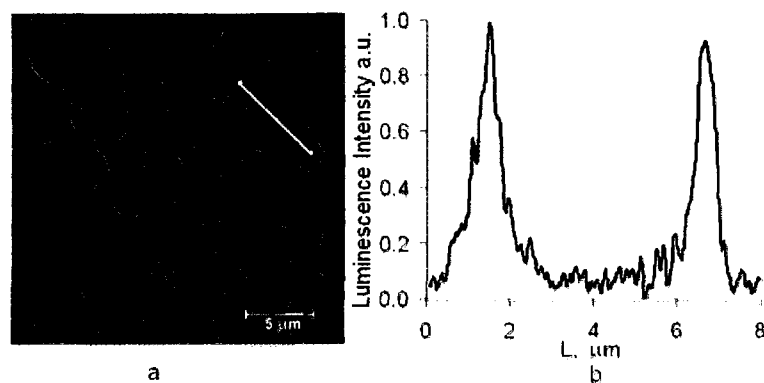


Figure 2.11 Confocal image of (GelA/EGCG)₄ capsules (a) and intensity profile (b) along the indicated cross-section.

Such coatings or microcapsules cannot be obtained if the major type of interaction between polyphenol and protein components in a system is hydrogen bonding. Electrostatic forces are essential to make the systems stable in an aqueous media.

The atomic ratio of elements in the capsule material was found to be 94.19:5.70:0.11 (C:O:Mn) according to EDAX analysis [26]. The Mn signal could be compared to the background noise, and the capsule material could be considered to be practically having no traces of the core material.

The diameter of the (Gelatin/EGCG)₄ capsules after drying is about 4-5 microns, as shown in SEM and AFM images (Figure 2.12) [26]. The drying causes the Gelatin/EGCG capsules to collapse with the formation of typical folds on capsule walls. AFM was used to determine the thickness of the samples. The diameter of the capsule walls consisting of Gelatin/EGCG aggregates was 50-300 nm and had a height of 5-7 nm. The thickness of two folded walls of a four bilayer GelA/EGCG capsule was 28-30 nm and corresponded to a Gelatin/EGCG bilayer thickness of approximately 3.7 nm. This value was found to be lower than that found for GelA/EGCG bilayers by QCM (8.5 ±4.3 nm per layer, averaged for four first bilayers). The inconsistency can be explained by the different experimental conditions for the assemblies; the films on the quartz resonators were dried after each adsorbed layer, while capsule walls were assembled in “wet” conditions, with only rinsing steps involved in between the alternate adsorption [26].

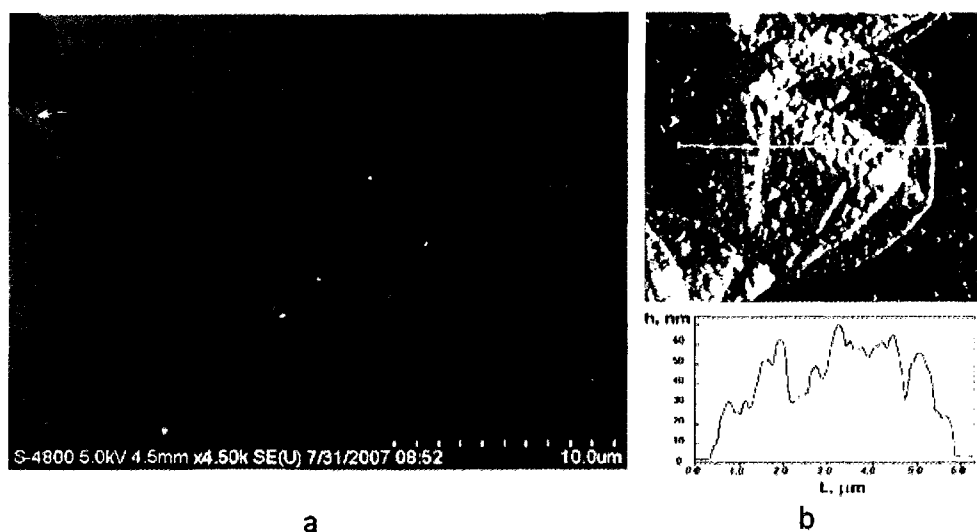


Figure 2.12 SEM (a) and AFM (b) images of dried (GelA/EGCG)₄ capsules. The graph presents the AFM height profile along the indicated cross-section.

Figure 2.12 shows that a small fraction of nanoparticles separated from the capsules was observed both in SEM and AFM images of (GelA/EGCG)₄ capsules. The EGCG/Gelatin aggregates appear to be probably due to slow partial dissolution of the capsule material. Protein/polyphenol binding is principally a reversible process, and a slow dissolution of protein/polyphenol complexes occurs while the conditions are changed [26, 36, 37, 39-42].

We tested the permeability of (GelA/EGCG)₄ capsule walls for FITC-labeled dextrans of different molecular weight at pH 6.5 in water. The unbroken unfolded capsules were counted and it was seen that the ratio of fluorescence intensities in the inner volume of the capsules and in the surrounding solution decreased with the increasing of dextran's MW, as shown in Figure 2.13. A delayed interior fluorescence was observed for dextrans of all molecular weights tested as well as for low molecular weight FITC. Similar results have been previously observed only for tannic acid/chitosan microcapsules at pH 6.5 [43].

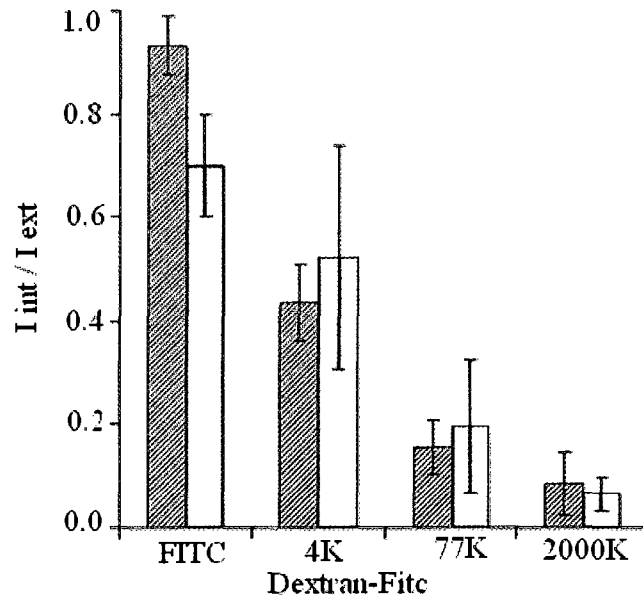


Figure 2.13 Permeability of (GelA/EGCG)₄ (shaded) and (GelA-FITC/EGCG)₄ (grey) capsules for FITC- labeled dextrans of different molecular weights at pH 6.5, time=10 min, n=3.

Several other types of capsules, including those of tannic acid/polyelectrolyte [21] and polyallylamine hydrochloride/polystyrene sulfonate [26, 45, 46], are completely permeable at all pH levels for substances with molecular weight lower than several thousands. Only tannic acid/poly(diallyldimethylammonium chloride) capsules showed slightly delayed interior fluorescence in the case of dextran with molecular weight of 4000 at pH 6.5 [21]. The GelA/EGCG shells formed directly on the surface of a compacted drug or combined with template polyelectrolyte microcapsules can be used to control the release of encapsulated compounds over a wide range of pH and molecular weights due to their size selective permeability and also introduce additional antioxidant properties due to polyphenols adsorption onto the capsule walls.

CHAPTER 3

LAYER-BY-LAYER COATED GELATIN NANOPARTICLES AS A VEHICLE FOR DELIVERY OF NATURAL POLYPHENOLS

Overview

This chapter is based on my contribution to the publication titled ‘Layer-by-Layer coated gelatin nanoparticles as vehicle for delivery of natural polyphenols,’ *ACS Nano*, 2009 [62]. Natural polyphenols, like epigallocatechin gallate (EGCG) and epicatechin gallate, have been recently demonstrated to be effective cancer chemopreventive agents in animal studies, and recent data from human clinical trials suggest that tea polyphenols can slow the progression of prostate cancer or lower the biological activities of proteins promoting cancer progression [63, 64]. Several other polyphenols, such as curcumin [63], luteolin [65], and resveratrol, are under intensive investigation as possible anticancer agents [64]. Plant phytochemicals can be used as chemopreventive and anti-cancer agents in humans; a large body of preclinical research and epidemiological data support this hypothesis.

Low bioavailability and short half-life are the two major problems of using polyphenols to treat cancer [62]. A solution to this problem would be to use polyphenol-loaded nanoparticles [27-29] instead of free compounds. The structures of the compounds, however, vary widely and are moderately soluble and oxidize quickly under

basic conditions [1-3, 41, 66-69]. This creates additional challenges for encapsulation. There is published literature that shows formation of nanocomplexes via polyphenol/protein binding [41, 66-69], alternated LbL assembly of polyphenols as films on planar support, or shells on microcores [21, 43] that have been used to produce micro- and nano-particles that contain the target substances. It has been observed that in several cases, it is difficult to control size, colloidal stability, and solubility of the nanoparticles and to design nanoparticles with a high concentration of the target polyphenol followed by its release in a controlled manner [62].

(-)-Epigallocatechin gallate (EGCG), which is a flavonoid, originates from the plant *Camelia sinensis* and is the major component of green tea extract and is highly soluble in aqueous buffers and several organic solvents. These properties make several commonly used methods of encapsulation unfeasible [62]. Several attempts to encapsulate EGCG in nanoparticles have been limited to a PGLA nanoparticulate formulation used for *in vivo* evaluation of antioxidant efficacy of EGCG in a rat model [70] and chitosan-tripolyphosphate nanoparticles for encapsulation of green tea catechin extracts [71].

We encased EGCG into Gelatin-based 200-300 nm sized particles that had a soft gel-like interior and fabricated a surrounding shell of polyelectrolytes (polystyrene sulfonate/polyallylamine hydrochloride (PSS/PAH), polyglutamic acid/poly-L-lysine (PGA/PLL), dextran sulfate/protamine sulfate (DexS/ProtS), carboxymethyl cellulose/Gelatin, type A (CMC/GelA) using the LbL technique [10, 72-76], as shown in Figure 3.1 [62]. It has been proven that Gelatin-based nanoparticles are relatively safe and are effective for non-viral gene delivery vehicles and have a prolonged *in vivo*

circulation time with high accumulation at the tumor side [77-79]. Modification of nanoparticle surfaces with polyelectrolyte LbL shells allows for modulating nanoparticle cell uptake rate and ratio, providing a template for their modification with tumor targeting agents, increasing nanoparticles colloidal stability and controlling loading/release characteristics [10, 73-76]. EGCG has a reversible reaction with hydrophobic moieties of proline rich peptides, thus providing loading/release characteristics in a pH dependent manner [37, 39, 43].

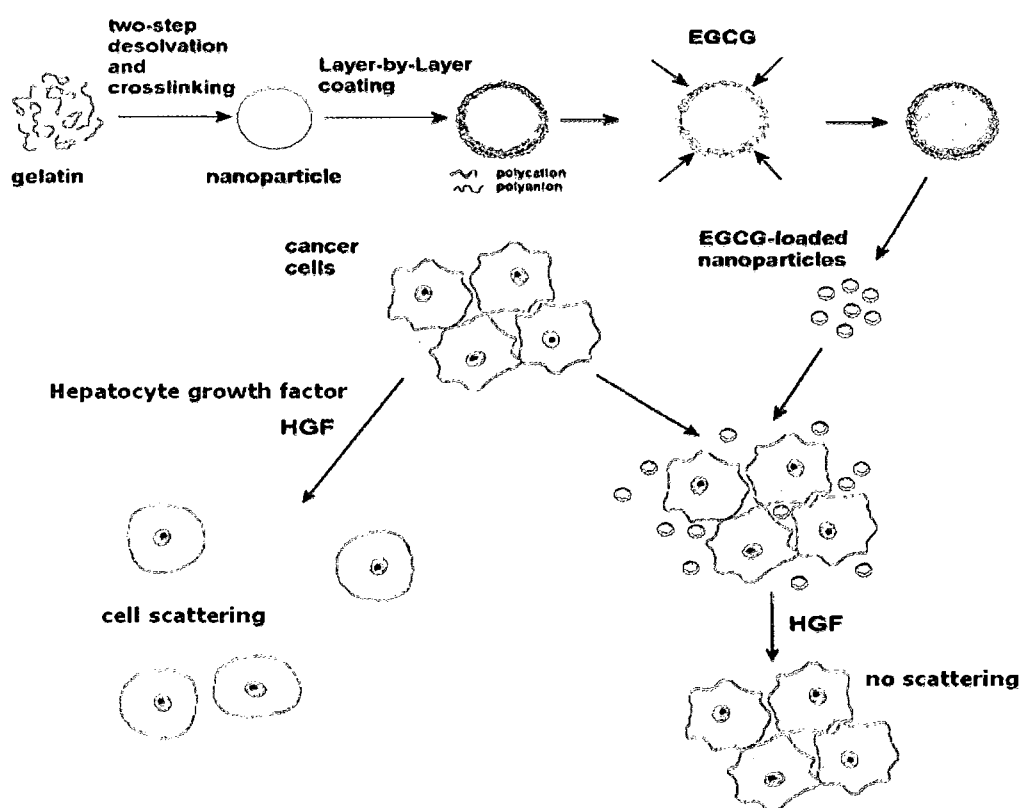


Figure 3.1 Schematic presentation of preparation of LbL-coated Gelatin nanoparticles containing EGCG and their effect on cancer cells [62].

Materials and Methods

Gelatin, type A from porcine skin (GelA, Sigma G1890, 300 Bloom) or Gelatin, type B from bovine skin (GelB, Sigma G9391, 225 bloom), glutaraldehyde (25% solution, Grad II, Sigma), acetone (Richard-Allan, Scientific Grade ACS), 2, 2'-azinobis(3-ethylbenzothiazoline-6-sulfonic acid) diammonium salt (ABTS), potassium persulfate ($K_2S_2O_8$) were used without additional purification.

Polyelectrolytes, polystyrene sulfonate (PSS), polyallylamine hydrochloride (PAH), poly-L-glutamic acid (PGA) and poly-L-lysine (PLL), dextran sulfate (DexS), protein protamine sulfate (ProtS), and polyphenols, curcumin, epigallocatechin gallate (EGCG), tannic acid (TA), and mixture of theaflavin and theaflavin gallate (TF) were purchased from Sigma-Aldrich.

Nanoparticles Preparation

Gelatin nanoparticles were prepared using a modified two-step desolvation method [62, 80-81]. 1.25 g of Gelatin was dissolved in 25 mL of DI water by gradually heating to 50 °C and then 25 mL of acetone was rapidly added to the solution. After two minutes, a white colored supernatant was formed. The gel-like precipitate was redissolved in 25 mL of water after gradually heating to 50 °C and pH was adjusted with HCl. The range of pH tested was between 1.5 and 5. Then 75 mL of acetone was slowly added under constant stirring at 40 °C for 15 min (less than 3 mL/min). The solution turns milky white after adding 55-60 mL of acetone into the mixture at pH 3.0. 0.2 mL of 25% glutaraldehyde was admixed to the stirring mixture immediately after addition of acetone. The sample was stirred for 1 hour, followed by overnight incubation at room temperature. The samples were then placed into plastic tubes and kept at +2 °C until further study.

Since the amount of glutaraldehyde used to crosslink the nanoparticles is very small, we assume that it completely reacts with the nanoparticles and it is therefore safe to assume that there is no free glutaraldehyde in the mixture [62].

The prepared suspension was divided into 2 mL aliquots, and Gelatin nanoparticles were separated from the supernatant by centrifugation at 6000-7000 rpm for 20 min and washed with 75% aqueous acetone three times. Finally, to concentrate the sample, the content of each tube was resuspended in 0.5 mL of 75% acetone and combined together. The concentration of solid material in the suspension was usually as high as 30-40 mg/mL and, if needed, was estimated for each batch separately. The nanoparticles, as a stable suspension of white or yellowish white color, were kept at +2 °C until used [62]. Nanoparticles prepared at pH 2.5-3.0 from the second desolvation stage were used for all further studies.

LbL Shell Assembly on Gelatin Nanoparticles

For polyelectrolyte encapsulation of Gelatin nanoparticles, 0.4 mL of a 3 mg/mL solution of polyanion (PSS, PGA, DexS), polycation (PAH, PLL) or protamine sulfate (PtS) at pH 6.0 were added sequentially to 1.5 mL of an aqueous suspension containing 15-20 mg/mL Gelatin A nanoparticles. After 30 min adsorption of each layer, the nanoparticles were washed with DI water three times. The corresponding polyanion was always deposited as the first layer on positive Gelatin nanocores. Deposition of each layer was monitored with ζ -potential measurements [62]. For SEM imaging, one layer of SiO₂ nanoparticles (7 nm) was deposited on top of Gelatin particles coated with a (DexS/PtS)₂ shell. The detailed procedure for formation of LbL shells on microcores that was followed has been demonstrated [10, 70, 71].

The adsorption of PSS was carried out on 10 mg/mL GelA nanoparticles from a 0.2 mg/mL PSS supernatant in a step-wise manner [62] and the amount of PSS remaining in solution was estimated using UV-Visible spectroscopy to estimate the amount of polyanion that can be adsorbed by the nanoparticles for one of the experiments.

Discoloration of ABTS^{•+} by Polyphenols in Solution

A stock solution of cation-radical ABTS (ABTS^{•+}) was prepared as described [55]. 88 μL of 0.14 M $\text{K}_2\text{S}_2\text{O}_8$ were added to 5 mL of $7 \cdot 10^{-3}$ M ABTS aqueous solution and left overnight at room temperature. The obtained stock solution of intensive blue-green color was kept protected from light and stored at $+2\text{ }^\circ\text{C}$. The stock solution was diluted with DI water (pH 6.5) immediately before use in such a way that the absorbance at 734 nm (A_0) was equal to 1.40 ± 0.05 ($l = 1.0\text{ cm}$, $\epsilon = 1.4 \cdot 10^4\text{ M}^{-1}\text{ cm}^{-1}$ [81]). The difference of A_0 in separate series was not higher than ± 0.05 .

To calibrate the ABTS^{•+} assay, that was initially designed to evaluate antioxidant properties of phenolic substances [55, 58-61], 10-250 μL of 0.1-3.0 mg/mL solution of different polyphenols (curcumin, EGCG, TA, TF) or Gelatin were added to 2.0 or 3.0 mL of an aqueous ABTS^{•+} solution (pH 6.5), as above, and thoroughly mixed [62]. Absorbance of the mixture at 734 nm (A_t) was read spectrophotometrically using an *Agilent 8453* spectrometer. To evaluate the effect of sample dilution on A_t , a series of blank experiments, where pure DI water was added in the place of a polyphenol containing sample, was carried out and the results were used to estimate A_t changes. In a separate series of experiments to determine the time interval necessary to complete the polyphenol reaction with ABTS^{•+}, absorbance of the mixture at 734 nm was followed in

time for 120 min with readings taken at 10 s intervals under constant stirring of the sample. The concentration of each polyphenol was evaluated from the absorbance change after 90 min using an experimentally obtained calibration coefficient.

Discoloration of ABTS^{•+} by Gelatin Nanoparticles Containing Polyphenols

To determine the amount of polyphenols loaded in Gelatin nanoparticles, 5-20 μL of EGCG-containing sample was added to 2.0-3.0 mL of the aqueous ABTS^{•+} solution (pH 6.5) as above and thoroughly mixed. The decrease of absorbance at 734 nm (A_t) after 90 min was converted into polyphenol concentration [62].

The effect of nanoparticles on the results of the EGCG determination with the ABTS^{•+} method was evaluated in an additional series of experiments. Solutions containing 0.5 mg/mL of EGCG and nanoparticles in the range of 0-0.75 mg/mL were prepared and tested. Due to spectral confounding, particles were separated from the reaction volume using a 0.2 μm filter before the addition of the ABTS reagent.

Loading of EGCG and other Polyphenols into Gelatin Nanoparticles

Loading of EGCG into uncoated particles by adsorption of the polyphenol from its concentrated aqueous solution was compared at different pH values [62]. Typically, 0.4 mL of 10.0 mg/mL EGCG was mixed with 0.4 mL water and the pH was adjusted to the value under investigation with HCl or NaOH. Then, 0.2 mL of nanoparticle suspension were added at room temperature and mixed. After 60 min, EGCG-loaded nanoparticles were separated from the supernatant by centrifugation at 6000-7000 rpm for 20 min, the supernatant was replaced with 2.0 mL of DI water (pH 6.5) and the

nanoparticles were resuspended; the washing procedure was repeated, and then the loaded nanoparticles were diluted in 0.25 mL of DI water. The concentration of EGCG in the sample was determined using the ABTS⁺ assay and the concentration of solid residue was calculated using QCM. EGCG was loaded into nanoparticles modified with different polyelectrolyte layers using the same procedure as above except that the nanoparticles were initially suspended in DI water. A blank sample with uncoated nanoparticles from the same original sample was used as a control in each experimental series. For extended release studies, the nanoparticles were encapsulated with a 3mg/mL PAH and PSS. Two layers were adsorbed onto the nanoparticles [62]. 300 µl of 5mg/mL EGCG was adsorbed onto 300µL of the coated nanoparticles for 48 hours at pH 6.8. Release studies were performed at pH 3 using the adsorbed sample by adding 100µL of the loaded sample to 5 mL DI under constant stirring (~200 rpm). 1 mL aliquots were taken over a period of 10 hours.

Tannic acid adsorption into gelatin nanoparticles followed the exact procedure for EGCG. The loading procedure was modified taking into account the solubility of other polyphenols. Theaflavin was loaded from a 1.6 mg/mL supernatant containing 25% of acetone. Curcumin was adsorbed from a 0.08 mg/mL supernatant containing 25% ethanol and 12.5% acetone. The polyphenols were in excess in all cases in relation to the particle concentration [62].

EGCG Release from Gelatin Particles

In a typical release experiment, 0.1-0.2 mL of EGCG-loaded sample, with known initial concentrations of EGCG and nanoparticles, was added to 5-10 mL of DI water with known pH and mixed. The samples were mixed immediately, and 0.2 mL aliquots

were taken with 10-60 min intervals with a syringe and the solution was passed through an *Anotop* or *Pall* syringe filter with 0.2 μm cutoff [62]. The filtrate was collected and tested for EGCG concentration. The total concentration of EGCG in the reaction mixture was determined after the release was complete for each experiment.

To evaluate the percentage of EGCG released as a function of particle concentration, a suspension of EGCG-loaded particles was added to different volumes of DI water and, after 20 min, the supernatant was separated by passing the sample through the 0.2 μm filter and the concentration of EGCG in it was determined using the ABTS⁺ assay.

Western Blotting

MDA-MB-231 cells were obtained from ATCC and grown in DMEM (Cellgro; Herndon, VA) and supplemented with 10% FBS (Gemini Bio-Products; West Sacramento, CA) and 1% penicillin/streptomycin (Cellgro) [62]. MDA-MB-231 cells were plated at 90% confluence in a 24 well plate. The following day, MDA-MB-231 cells were treated with either 5 μM free EGCG, 1 or 5 μM EGCG as coated nanoparticles or the equivalent volume at 5 μM of control nanoparticles for 30 minutes or 5 hours. The cells were pulsed with 30 ng/ml HGF (Hepatocyte Growth Factor, Calbiochem; 30 ng/ml) for 30 minutes immediately upon EGCG treatment or 30 minutes prior to the 5 hours time point [62]. Protein lysates were harvested in 125 μl boiling Laemmli sample buffer (125 mM Tris; 4% SDS; 0.01% bromophenol blue; 30% Sucrose; 5% β -mercaptoethanol). 10 μl of the lysates were run on a 10 % SDS-PAGE gel, transferred to PVDF membrane (Pall Corporation; Pensacola, FL), blocked with 5% milk in TBS-T (50 mM Tris-HCl, pH 7.5 150 mM NaCl, 0.1% Tween-20) for 1 hour and probed with

antibodies to the proteins listed below overnight at 4°C. The following day, the membranes were washed with TBS-T and probed with horseradish peroxidase conjugated secondary antibodies (GE Healthcare; Buckinghamshire, UK). The membranes were washed with TBS-T and the signal was detected with ECL Plus (GE Healthcare). Antibodies used included: phospho-Erk, phospho-Akt, phospho-c-Met (Cell Signaling Technology; Beverly, MA) and Tubulin (Neomarkers; Fremont, CA).

Characterization of Nanoparticles

The measurements of nanoparticle hydrodynamic diameter and ζ -potential were carried out on a ZetaPlus Potential Analyzer microelectrophoretic instrument in water. For the measurements, 0.1 mL of nanoparticle suspension was redispersed in 2 mL of water. To determine the isoelectric point of the Gelatin nanoparticles, the diluted solutions were used after 24 h for the measurements.

SEM images were taken on a *Hitachi S-4800* Scanning Electron Microscope. The samples for SEM imaging were typically prepared by applying 2-5 μ L of diluted particle suspension in water (GelA) or ethanol (GelB) on the surface of a Si template followed by overnight drying at room temperature. To enhance image quality, the sample surface was sputtered with a 2 nm layer of iridium [62].

AFM images were obtained using a *Q-ScopeTM 250 Quesant* instrument in intermittent-contact mode. Samples were prepared as above on freshly cleaved mica.

The concentration of solid residue in a Gelatin nanoparticle sample was estimated using the Quartz Crystal Microbalance (QCM) technique. Typically, 2-5 μ L of each sample was placed on one side of a pre-cleaned horizontally placed quartz resonator and the drop was dried at room temperature in air (~ 30 min). The frequency changes of the

resonator were monitored using a *USI-System*, Japan 9 MHz QCM instrument with an accuracy of ± 1 Hz. The mass of the deposited material was recalculated from the frequency shift according to the Sauerbrey equation: Δm (ng) = - 0.84 ΔF (Hz). The resonator was then replaced with a new one and the procedure was repeated. For each sample, two or four independent runs were done with different resonators and the results were averaged. Typical experimental deviation between different runs was less than 15 %. Dry Gelatin nanoparticles containing EGCG were obtained using a *Modulyo* freeze drier. The samples were frozen in liquid nitrogen [62].

Results and Discussion

Nanoparticles Preparation

We used gelatins with relatively higher Bloom numbers (300 Bloom for Gela and 225 Bloom for GelB), as compared with the original work of Coester [62, 79], in our study to increase the strength of the gel-like nanoparticles. The procedure for Gelatin nanoparticle preparation was slightly modified in order to obtain a stable suspension of the nanoparticles with a minimal diameter [62]. Parameters, such as the temperature for the first and second desolvation stages, the amounts of reagents that were added (acetone and gluteraldehyde), and the rates of their addition [80], were constant for all the experiments, while the pH value during the final stage of nanoparticle preparation was varied in range from 1.5 to 5. It was observed, that at pH 4 and higher, the method produced unstable large particles of 700-750 nm diameter [62], which tend to precipitate very quickly, as shown in (Figure 3.2).

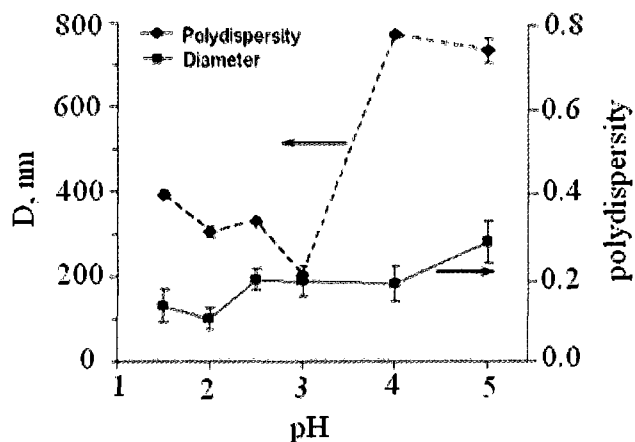


Figure 3.2 Gelatin A nanoparticles diameter and polydispersity as a function of pH on the second desolvation stage, $n=2$.

The suspensions of nanoparticles that we obtained at pH 3.0 were small and extremely stable. The diameter of the Gela nanoparticles was around 200 nm and was reproducible. With further decrease in the pH value, the diameter of the nanoparticle increased to 300 nm and eventually to 400 nm. It was observed that the nanoparticles prepared at these low pH values retained their stability at least for four weeks [62]. Polydispersity readings checked for the variation in the size of the particles. Our results were in good agreement with those established by several other researchers [80, 81], where the pH range of 2.3-3.8 was recommended for the second desolvation stage. This could explain the sharp decrease in viscosity of gelatin aqueous solutions below pH 3 as being due to protonation of aspartic and glutamic aminoacid residues [82]. However, the observed minimum nanoparticle diameter has not been previously reported and was probably related to the higher Bloom numbers for the Gelatin used. The hydrodynamic diameter of nanoparticles prepared from GelB and measured using a Zeta potentiometer at pH 3.0 was 127 nm. We used nanoparticles of Gela prepared at pH 2.5-3.0 and GelB obtained at pH 3.0 for our study [62].

Characterization of Gelatin Nanoparticles

It can be seen from Figure 3.4 that both GelA and GelB particles have isoelectric points between pH 6 and pH 7 [62]. It was seen that the hydrodynamic diameter of the gelled nanoparticles slightly increased with increasing pH. This increase was 3.7 nm and 6.5 nm per one pH unit for GelA and GelB, respectively, and no large swelling or partial particles dissolution was observed, even at pH 10. This indicated the formation of relatively inflexible cross-linked chain net in the nanoparticles' interior [62].

From our AFM results, the effective diameter of dried GelB nanoparticles, as prepared from 75% acetone, was 120-150 nm (Figure 3.3 a). These values corresponded to the hydrodynamic diameter scattering of the nanoparticles (Figure 3.2) [62]. When the 300 nm GelA nanoparticles were deposited from aqueous suspension and dried on a mica support, their average diameter appeared to be 367 ± 15 nm (Figure 3.3 b, d) with a height of 58 ± 8 nm. The nanoparticles collapse and slightly deform after they are dried. If we consider the shape of a dried nanoparticle as a cone and assume that the density of the material is 1.1 g/cm^3 [76], the mass of one GelA nanoparticle is $2.3 \cdot 10^{-15}$ g. If the nanoparticle's actual size is assumed to be equal to its hydrodynamic diameter, the Gelatin nanoparticles consist of 15% of solid Gelatin, while the remaining 85% is water. [62] The dry Gelatin material in our study is referred to as solid material of a suspension, always keeping in mind that the nanoparticles actual volume is about 5.7 times higher.

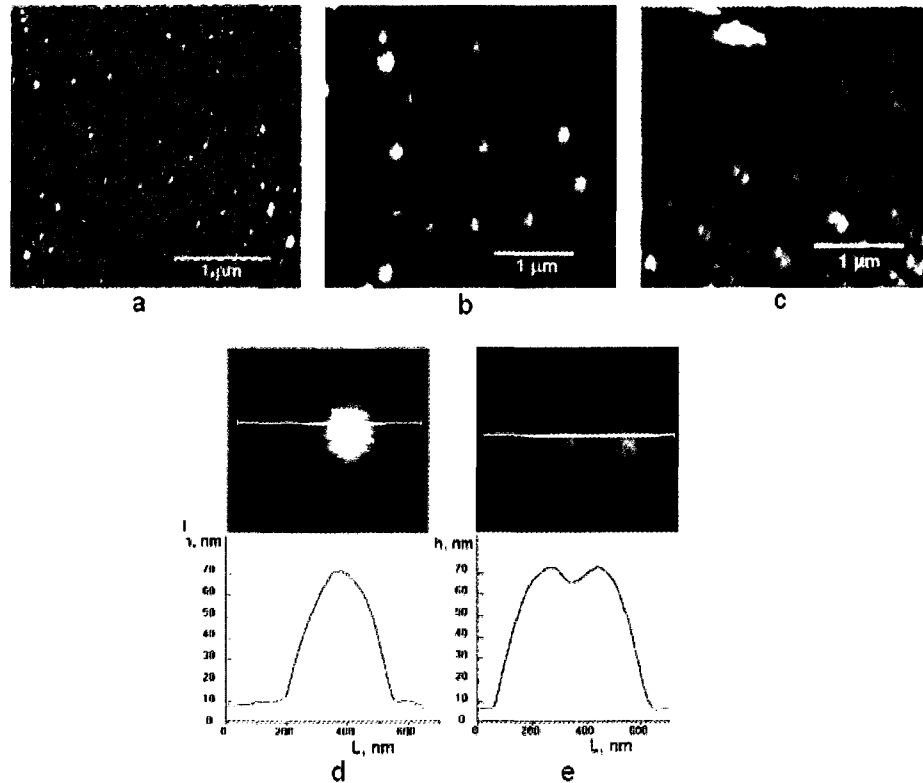


Figure 3.3 AFM images of 120 nm Gelatin B (a, sample from 75 % acetone) and 300 nm Gelatin A (b - e, from water) uncoated (b, d) and coated with (PGA/PLL)₂ (c) and (PGA/PLL)₄ (e) shells. The corresponding profiles show sample elevation across the indicated lines.

LbL Assembly of Polyelectrolytes on Gelatin Nanoparticles

We used two combinations of polyanion/polycation pairs, PSS/PAH (strong polyanion/weak polycation) as synthetic polymers and PGA/PLL (weak polyanion/strong polycation) as biocompatible polymers to encapsulate gelatin nanoparticles that were around 300 nm in diameter, as well as two combinations of polyanion/protein, DexS/ProtS (strong polyanion/strongly positively charged polypeptide), and CMC/GelA (weak polyanion/weak positively charged protein) [10, 72] that were both biocompatible. It was found that the surface of uncoated nanoparticles is positive with a surface charge of + 20 mV at pH 6.0, (Figure 3.4). The assembly was confirmed by the adsorption of a

polyanion that resulted in changing the value of the surface charge to a negative one. Surface charge alternation with sequential deposition of polycation and polyanion layers was observed for all combinations used except CMC/GelA, where the ζ -potential of nanoparticles with a GelA outermost layer was slightly negative (Figure 3.4) [62].

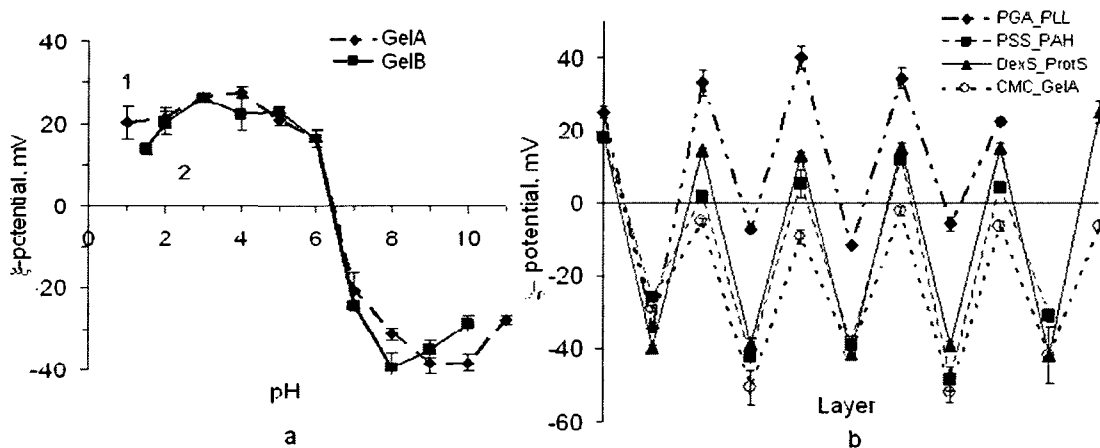


Figure 3.4 Surface charge of Gelatin nanoparticles as functions of a) pH (1- GelA, 2- GelB) and b) outermost polyelectrolyte layer (GelA, pH 6.0), $n=2$.

It was confirmed that the assembly took place on the surface of the nanoparticles. Although the weak polyelectrolytes or proteins were highly charged in a solution of pH 6.0 [10, 72], the surface charge values for the corresponding layer was only slightly positive or slightly negative. We observed that there was aggregation of the nanoparticles that had a weak polyelectrolyte as the outermost layer and the effective diameter and polydispersity of the particles was also increased. The aggregation of the particles was decreased by fabricating a layer of a strong polyelectrolyte as the next layer [62].

It can be seen from the AFM and SEM images of coated nanoparticles (Figure 3.3 c,e, and 3.5b) that the deposition of polyelectrolyte layers does not change the size or shape of the nanoparticles. The thickness for a four bilayer shell wall was estimated to be

20 nm based on QCM monitoring of the PGA/PLL multilayer assembly on a QCM electrode.

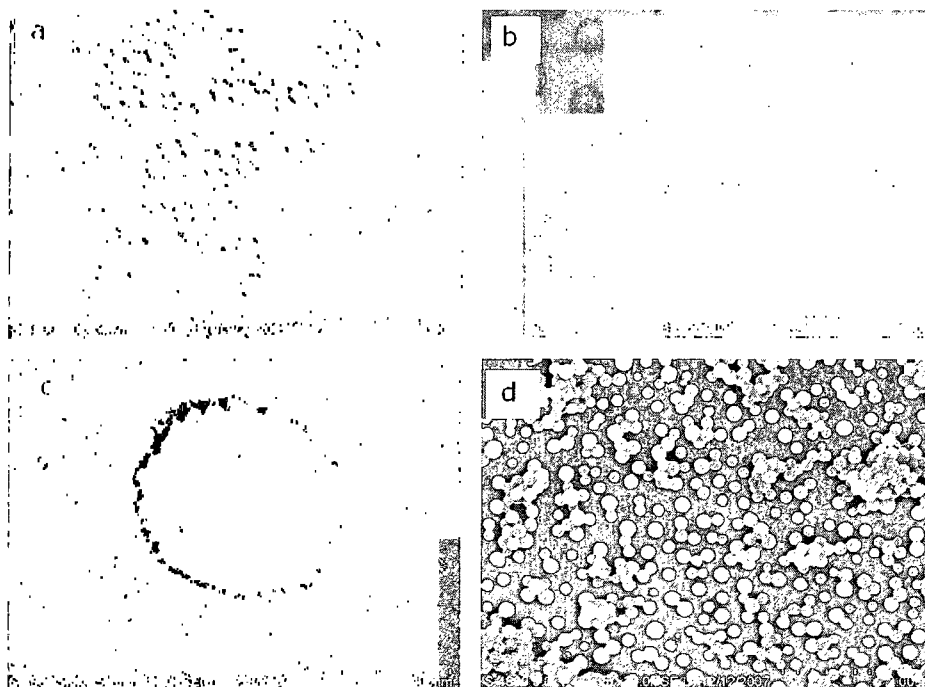


Figure 3.5 SEM images of 200 nm (a) and 300 nm (b-d) GelA nanoparticles: a) uncoated, b) coated with $(\text{PGA/PLL})_2$ shells, c) one nanoparticle coated with $(\text{DexS/PtS})_2\text{SiO}_2$ shell, and d) uncoated nanoparticles after loading EGCG.

The estimated mass of nanoparticles coated with $(\text{PGA/PLL})_2$ or $(\text{PGA/PLL})_4$ layers was almost the same as that of the initial nanoparticles. SEM imaging (Figure 3.5c) confirmed that the interior of the gelatin nanoparticles that had an outermost layer of silica for $(\text{DexS/PtS})_2/\text{SiO}_2$ composition remained gel-like and collapsed after drying leaving the upper layer of silica nanoparticles intact [62]. From our data, using different characterization methods, we proved that the adsorbed polyelectrolytes form a thin shell around the nanoparticles with minimal penetration of the coating polyelectrolytes inside the nanoparticles. In fact, about 0.13 g of PSS per 1 g of nanoparticles is necessary to saturate the first layer polyanion adsorption. This amount corresponds to about ca. 1 nm

PSS layer thickness, if a high effective surface area of Gelatin nanoparticles and the formation of a single polyanion layer are assumed [62]. Our observations were in agreement with the results showing internal layering of the LbL film with only 30-40% intermixing by height between adjacent layers, as found by neutron reflectivity [83, 84].

Polyphenol Adsorption into Nanoparticles

We loaded four different polyphenols *viz.* curcumin, EGCG, TA, and TF by adsorption into the Gelatin nanoparticles in order to evaluate nanoparticle loading efficiency (Figure 3.6) [62]. The polyphenols that had higher molecular weights and a large number of phenolic –OH groups adsorbed better than the others. It was demonstrated that the amount of theaflavin, the polyphenol with the highest molecular weight among those investigated, could reach up to 70% of the mass of the nanoparticle solid material [62]. The loading efficiency of tannic acid and EGCG was relatively lower, and it was almost negligible for curcumin. The regularities of polyphenol adsorption correspond to the general features of polyphenol-protein interaction and binding [3, 37, 39, 41, 43, 66-69]. Most of the naturally occurring polyphenols, such as tannic acid, EGCG, gallic acid, catechins etc., are well known for their ability to precipitate salivary rich proteins (albumin, gelatin, casein) from aqueous solutions, although the binding strength varies highly and depends on the combination of the protein/polyphenol pair.

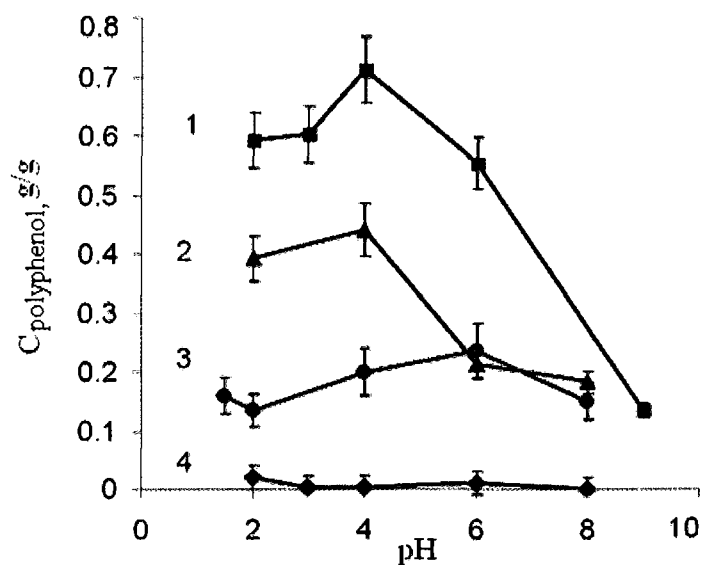


Figure 3.6 Total $C_{\text{polyphenol}}$ in suspension after loading theaflavins (1), tannic acid (2), EGCG (3), and curcumin (4) in 200 nm GelA particles, $n=3$.

The interaction and binding of gelatins with polyphenols is based mainly on hydrogen bonding between the hydrophobic amino acid, mostly proline residues of the gelatins and phenol rings of the polyphenols [62]. The presence of additional galloyl ester group(s) increases its binding [9]. The interaction between polyphenols and proteins is a reversible and multistage process which can not be attributed to a single interaction reaction, as the complexes may redissolve with changing conditions, eg. pH [37, 39]. We assumed that the hydrophobic character of the EGCG-Gelatin interaction played a major role in the manufactured nanoparticles, since we used glutaraldehyde for crosslinking that used free amine groups of Gelatin.

The amount of polyphenols adsorbed in the nanoparticles decreases when the pH of loading is increased [62]. This is probably due to the higher solubility of the phenolate forms of the compounds [37, 39, 41, 43, 66-69] and the change in the charge of the nanoparticle's interior. It was also seen that at pH higher than 8, all the polyphenols

became less stable and easily oxidized, making it difficult to test their adsorption under strongly basic conditions [62].

We demonstrated that the loading of all polyphenols into GelA nanoparticles was higher than that for GelB nanoparticles. Different amino acid content of the Gelatins can result in tailored hydrophobicity of the nanoparticles, affecting adsorption. We could exclude any influence of nanoparticle diameter on the value of EGCG loading in our experiments because such influence was found to be almost negligible for GelA nanoparticles of different diameters (Figure 3.7) which is within the range of experimental error [62].

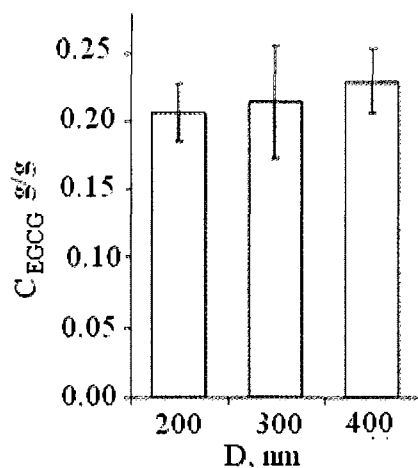


Figure 3.7 Concentration of EGCG in uncoated GelA nanoparticles of different diameters, n=5.

The diameter of EGCG-loaded nanoparticles was typically less than 200 nm (Figure 3.5d) and was in agreement with their initial diameter as estimated by SEM and ζ -potential measurements.

The EGCG concentration in the samples (Figure 3.8) was not influenced by the polyelectrolyte layers, and long 20-30 hours adsorption gives similar loadings [62].

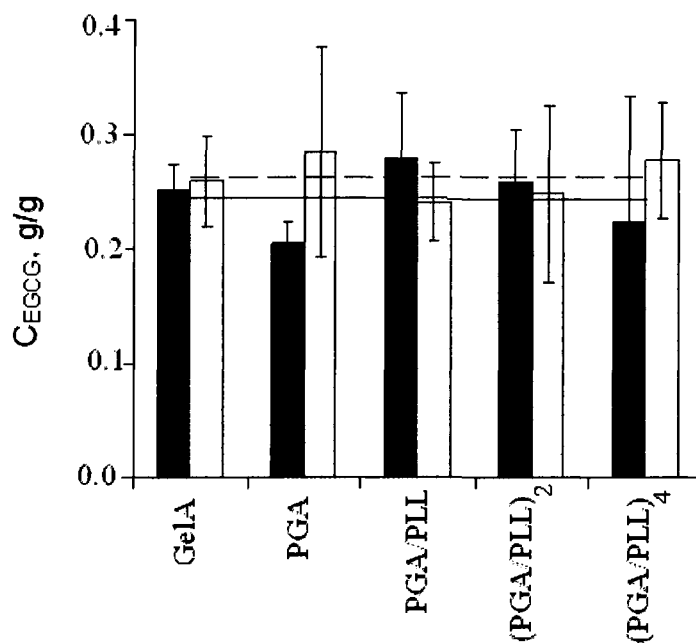


Figure 3.8 Concentration of EGCG in nanoparticles coated with different number of PGA/PLL bilayers, dark and shaded bars indicate independent data, n=3 for each.

EGCG Release from Nanoparticles

We observed that the release of EGCG from uncoated GelA nanoparticles was very fast at all pH values and was primarily dependent on the loading and release conditions. While the pH of EGCG loading was close to the pH value used for release experiments, a steady-state concentration of EGCG in solution was reached almost immediately, but only a part of EGCG appeared to be in the solution [62]. When EGCG was adsorbed into nanoparticles at pH 4.0 and released at pH 7.5, the maximum concentration of EGCG was found 1 min after the addition of the nanoparticles. The further decrease of EGCG concentration indicates a slow system relaxation to a new equilibrium. It should be noted that the total EGCG concentration released after 3 h remains on the level of 90-95% of the initial samples; the loss could be attributed to the adsorption of the nanoparticles on the vial walls [62]. A similar release, up to the level of

40-60% of encapsulated substance, was previously observed for chitosan-tripolyphosphate nanoparticles containing tea extract and attributed to covalent binding of catechins to the matrix [71].

It was shown that if the nanoparticles are recollected and redispersed in water again, additional EGCG is released [62] and a new concentration equilibrium is reached, as shown in Figure 3.9).

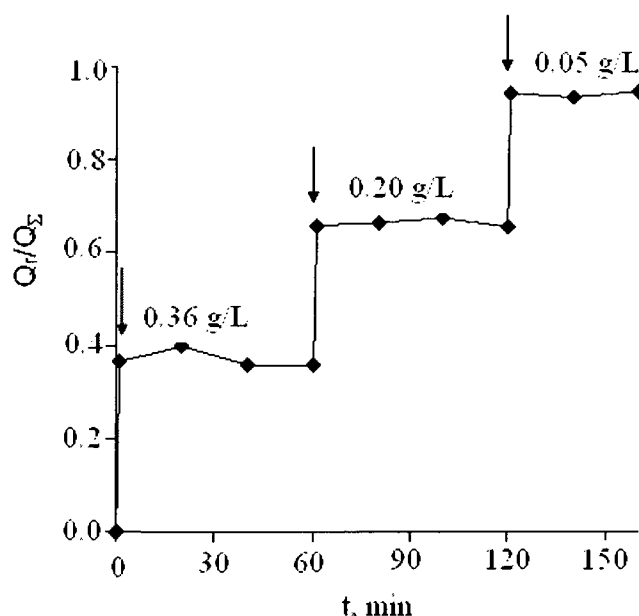


Figure 3.9 Three-stage release of EGCG from gelatin nanoparticles at pH 6.0.

In the above figure, arrows indicate the moments when the nanoparticles were redispersed in a new portion of DI water. The values above the curves show nanoparticles concentration on each release stage. Concentration of EGCG is 0.17 g/g. The release data are given in parts released per gram of nanoparticles. It took three steps to release almost 100% of EGCG indicating that the EGCG-Gelatin nanoparticles interaction is reversible and that there is minimal covalent binding of EGCG with the gelatin matrix [62].

The ratio of EGCG concentration in supernatant (C) and its total concentration in the sample (C_{Σ}) does not linearly depend [62] on the nanoparticle concentration (C_{NP}) (Figure 3.10).

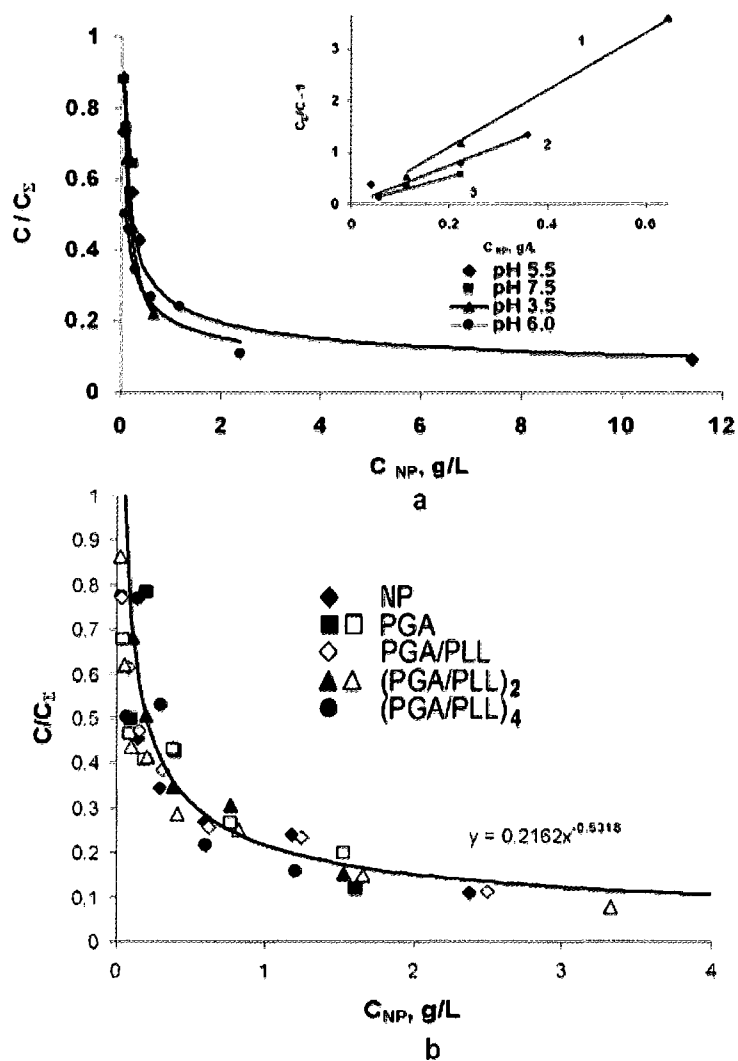


Figure 3.10 C/C_{Σ} as a function of nanoparticles concentration. a) uncoated nanoparticles, b) PGA/PLL coated nanoparticles. The insert in a) shows the curves in $C_{\Sigma}/C - 1$ vs. C_{NP} coordinates.

In a solution with a high concentration of nanoparticles, EGCG is mostly in the nanoparticle's volume while, after addition of water, it is immediately released until new

steady-state conditions are reached. At a given pH, the data fit into a linear correlation $(C_{\Sigma}-C)/C = K_d \cdot C_{NP}$, where K_d is the distribution (partition) coefficient (Figure 3.10a insert). The calculated values of K_d range from 2.6 to 5.9 for the different pH values used for loading and release (Table 3.1). A higher K_d value corresponds to a higher amount of EGCG remaining in the nanoparticles [62]. One can calculate that, at pH 5.5 ($K_d=3.6$) for uncoated Gelatin nanoparticles with a total EGCG loading of 0.2 g per 1 g of nanoparticles in a suspension with $C_{NP} = 2.5$ g/L, up to 90% of EGCG is adsorbed in nanoparticle volume, while the total volume of the nanoparticles in the solution is only around 1.5 %.

Table 3.1 K_d as a function of pH and nanoparticles coating [62].

Sample	pH of loading	pH of release	K_d
Uncoated 200 nm	4	3.5	5.5, 4.1
		5.5	3.7
		7.5	2.6
	8	8	5.9
Uncoated 300 nm	4	5.5	3.6 ± 0.2
		8	3.0
Coated with PGA	4	5.5	3.3 ± 0.1
PGA/PLL	4	5.5	3.1 ± 0.1
(PGA/PLL) ₂	4	5.5	3.6 ± 0.1
(PGA/PLL) ₄	4	5.5	4.4 ± 0.3
(CMC/GelA) ₄	4	5.5	1.9 ± 0.3
(CMC/GelA) _{4.5} dry	4	5.5	1.9
(CMC/GelA) ₅	4	5.5	1.4
(CMC/GelA) ₅ dry	4	5.5	1.5
(DexS/PtS) ₄	8	5.5	5.8
(DexS/PtS) ₅	8	8	3.8
(DexS/PtS) ₅	4	8	3.1

Sustained Release of EGCG from LbL Coated Nanoparticles

Gelatin nanoparticles with PSS/PAH bilayer loaded with 2.5 mg/mL EGCG demonstrate sustained release. This PSS/PAH shell, consisting of only one polyanion/polycation bilayer, cannot itself represent a dense diffusion barrier shell on the nanoparticle surface [62]. This indicates that the diffusion barrier structure involves a deeper interaction of the polyelectrolytes with the Gelatin core, similar to the LbL protective barrier formation on soft PEG-assisted microcapsules for insulin delivery [85]. We obtained slow release, as compared with almost immediate 15 min EGCG release from uncoated Gelatin nanoparticles. The maximum concentration of EGCG in solution was reached at 8 hours. Figure 3.11 shows an averaged data over two different samples. The time interval is comparable to that observed for chitosan-tripolyphosphate nanoparticles [71].

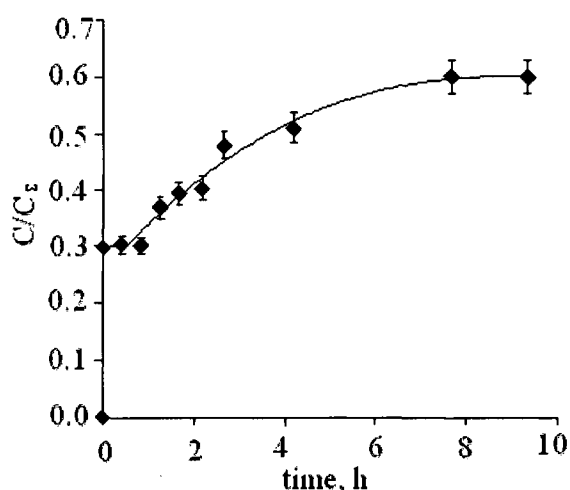


Figure 3.11 EGCG release from 275 nm GelA nanoparticles coated with PSS/PAH shells. CNP = 0.22 g/L. pH of loading 6.8, pH of release 3.0. Time of loading is 48 h, n=3.

A baseline concentration is observed at the first two points, since the particles are stored in excess EGCG. Concentration equilibrium is reached because of the nanoparticles contained in the release volume. A similar release profile was also obtained by using a biocompatible LbL shell of anionic dextran sulfate and cationic protamine sulfate, but was relatively less efficient in slowing the release [62].

Biological Activities of LbL Coated Nanoparticles Containing EGCG

In order to consider EGCG-nanoparticles to be a viable therapeutic option, it was necessary to ensure that EGCG-nanoparticles function similar to free EGCG in a cell-culture model system [62]. It has previously been shown that EGCG is capable of inhibiting numerous cell-signaling pathways, including the c-Met/HGF pathways. The secreted growth factor, HGF, activates the cell-membrane receptor, c-Met, leading to an increase in intracellular signaling and culminating in HGF induced cell scattering, motility, and invasion. Invasion is one of the necessary steps leading to tumor metastasis; a lethal event in most cancer patients [62]. It has been demonstrated that free EGCG blocks HGF-induced scattering and activation of the c-Met receptor in a variety of tumor cell-lines [85]. In order to determine if the biological activity of EGCG loaded into the nanoparticles was maintained after nanoparticle processing, similar to free EGCG, the breast carcinoma cell line, MDA-MB-231, was pre-treated for varying times and concentrations with Gelatin nanoparticles without EGCG, nanoparticles with EGCG, and free EGCG [62]. HGF was added and lysates were prepared 30 minutes later. Western blot analysis was performed using antibodies to detect phosphorylated c-Met and the downstream signaling molecules Akt and Erk, which are key molecules allowing signaling through the PI 3-kinase and map kinase pathways, respectively. Figure 3.12

illustrates that HGF induced a major increase in the phosphorylation of c-Met, Akt and Erk. Free EGCG (5 micromolar), at early timepoints was able to inhibit HGF induced c-Met, Akt, and Erk activation, as observed previously, while coated nanoparticles with and without EGCG were unable to inhibit HGF induced signaling with short preincubation times [62].

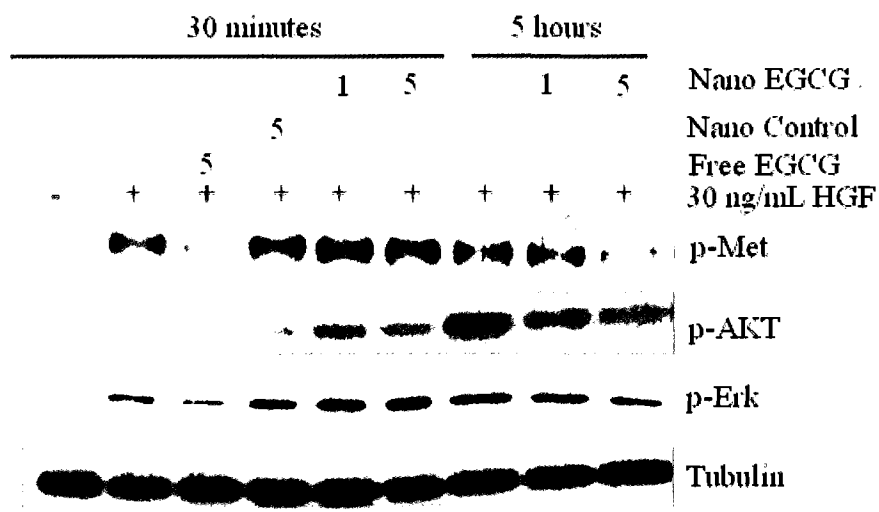


Figure 3.12 Western Blot Analysis to measure c-Met activation, 1 and 5 indicate concentration of EGCG (μM) [62].

However, the EGCG containing nanoparticles were capable of blocking HGF induced signaling with longer preincubation times, thus demonstrating that the EGCG released from the nanoparticles maintained its biological activity, and that EGCG is being slowly released from the nanoparticles in concordance with the rate of EGCG release measured in Figure 3.11 [62].

CHAPTER 4

LBL NANOENCAPSULATION OF MICROBES FOR CELL SURFACE MODIFICATION AND INVESTIGATION OF CELLULAR UPTAKE

Overview

This chapter is based on my contribution to the publication titled ‘Layer-by-layer nanoencapsulation of microbes: controlled cell surface modification and investigation of substrate uptake in bacteria,’ *Macromolecular Bioscience*, 2009 [86]. LbL nano-assembly has been used for a wide range of biomedical applications [27]. Charged templates have been used for self-assembly of oppositely charged polyions with precise thickness that can incorporate components that are of special interest to researchers [7, 87-91]. Few microbiological templates have been explored, as compared to a wide variety of inorganic and organic templates for assembly. It has been shown that latex, lipid microtubules, blood platelets, erythrocytes and stem cells have been used successfully as templates for fabricating polyion shells [13, 88, 92-96]. *Escherichia coli* and other bacteria of different genera have been used for encapsulation using LbL and some cellular activity of the modified cells has been demonstrated for *E.coli* [89-97]. We have shown that bacterial spores can be successfully used for fabricating nanoorganized polyelectrolyte cells [98]. We made a successful attempt, by using LbL, to answer questions in microbiology by constructing cell surfaces with a defined architecture on

cells that were alive and metabolically active [86]. The encapsulation of the entire cell gave colloidal stability and the choice of polyions helped in varying the surface charge and controlling the hydrophilicity or hydrophobicity [99]. This is an innovative technique that helps in the investigation of uptake and release of substrates and products in bacteria and adhesion of bacteria to their substrates or hosts. Another application would be in the food industry, where a protective coating of bacteria would help to extend the shelf life of the products. However, the focus of the research has so far been only on demonstrating the encapsulation of bacteria using LbL self-assembly. A concrete application of the method on a defined microbiological problem has not been shown until now. Our experiments were designed to address this issue [86].

We have used two different independent approaches of the LbL technique for the investigation of the microbial surface. One was the investigation of changes in the electrochemical potential of the cell surface by coating the cells with nanoshells consisting of, at the most, three or less layers and the other one was the investigation of the influence of building a physical barrier around the cell by creating shells of four or more layers [86]. We also explored other possibilities in investigating the effect of defined changes in the surface characteristics by using various synthetic and biocompatible polymers for electrostatic nanoassembly. It has been demonstrated that different proteins can be incorporated in the fabricated shells and their release can be controlled as desired [100].

We investigated the uptake of elemental sulfur in encapsulated cells of the phototrophic purple sulfur bacterium *Alc. Vinosum* as an example for organic as well as inorganic substrate uptake in the whole group of gram-negative bacteria [86]. We chose

Alc. Vinosum for this purpose because it essentially needs reduced sulfur compounds under photolithoautotrophic growth conditions, allows the use of soluble and insoluble substrates, and the substrate uptake is easily detectable [86]. *Alc. Vinosum* uses reduced sulfur compounds like sulfide, thiosulfate and elemental sulfur as electron donors for anoxygenic photosynthesis. Sulphur globules start accumulating inside the cells when the reduced organic sulphur compounds are being oxidized to sulphate (final product) [101, 102]. Much remains to be explored about the uptake of sulfide and elemental sulfur in a cell. Although sulphide diffusion might be assumed for the small soluble substrate, there has to be an active mechanism for the uptake of insoluble elemental sulphur, because a close contact between the cell surface and elemental sulfur is necessary [103]. This mechanism of cell-sulfur contact during uptake of elemental sulfur has not yet been understood [86]. It has been demonstrated that hydrophobic interactions establish contact between the cell surface and elemental sulfur for the case of chemotrophic sulfur bacterium *Acidithiobacillus ferrooxidans* [104]. We used LbL assembly of various polyions to construct defined cell surfaces with different charge and hydrophobicity, and to build a physical barrier surrounding the cell to study the cell uptake in *Alc. Vinosum*. Furthermore, in comparison with elemental sulfur, the uptake of the soluble substrate sulfide was investigated [86].

Materials and Methods

Bacterial Strains, Medium and Growth Conditions

For encapsulation, cells of *Alc. Vinosum* DSMZ 180T (formerly *Chromatium Vinosum*) were grown photoorganoheterotrophically on malate [86]. After finishing the

encapsulation process, *Alc. Vinosum* was cultivated photolithoautotrophically in batch culture at room temperature under anaerobic conditions in 50 mL culture bottles containing modified Pfennig's medium (0 medium without sulfide) [105]. Solid elemental sulfur (S_0 ; 25 or 50 mM) or sulfide (1 or 5 mM) were added as the sole sulfur sources to the cultures. To maintain pH 7.0 ± 0.1 , sterile HCl and Na_2CO_3 solutions were added. Cultures grown with elemental sulfur were stirred. Elemental sulfur was purchased and used as received from Riedel-de Haen, sulfide 1 M stock solution was prepared using sodium sulfide (Sigma-Aldrich).

Polyelectrolytes for Bacteria Encapsulation

Different combinations of the anionic polyelectrolytes, sodium poly(styrene sulfonate) (PSS, MW 70000), poly(acrylic acid) (PAA, MW 5000), poly(glutamic acid) (PGA, MW 40000) and the cationic polyelectrolytes poly(allylamine)hydrochloride (PAH, MW.70000) and poly(diallyldimethylammonium chloride) (PDDA, MW 70000) were purchased from Sigma-Aldrich and used for nano-coating of the *Alc. Vinosum* cells.

LbL Shell Assembly on Microbes

50 mL cultures of *Alc. Vinosum* were centrifuged at 7000 rpm for 5 min and washed once with deionized water. ζ -potential were carried out on a ZetaPlus Potential Analyzer microelectrophoretic instrument in water. For the measurements, 0.2 mL of culture was redispersed in 2 mL of water. The cultures were adsorbed with positively charged polymer solution for 10 min. The polymer solution was removed from the cells by washing them two times with deionized water. ζ -potential was determined and the cells were then adsorbed with negatively charged polymer solution for another 10 min.

The washing step followed after every step of adsorption and the assembly of the polymers was repeated until the desired number of layers was assembled onto the cells [86].

Confocal Microscopy

Fluorescein isothiocyanate (FITC) labeled PAH was used to label negatively charged cells. 1 mL of encapsulated cells was incubated with FITC for 10 min; afterwards the cells were washed ten times for 5 min at 8000 r.p.m with deionized water. These samples were observed under a Leica DMI RE2 confocal laser scanning microscope with a 65x oil immersion objective lens [86].

Scanning Electron Microscopy

1 mL of encapsulated cells was washed three times at 8000 r.p.m for 5 min. 0.1 mL of this sample was used for SEM studies. The sample was allowed to air dry and was not heated while an iridium layer was deposited via sputtering (3 nm thickness). The samples were observed with a *Hitachi S-4800* Scanning Electron Microscope [86].

Intracellular Sulfur, Protein and Sulfate Determination in the Cultures

Intracellular sulfur concentration and protein concentration were determined as described by Hensen, et al. [105]. Sulfate was determined using the method of Sörbo [106].

Results and Discussion

LbL self assembly has been used in studies demonstrating the possibility of encapsulating living bacterial cells, but has not been applied for solving other microbiological problems. In our study, we investigated the effects of *Alc. Vinosum* cell

encapsulation with polyelectrolytes on the uptake of the soluble substrate sulfide and the insoluble substrate elemental sulfur [86]. We successfully demonstrated the use of LbL for substrate uptake studies in gram-negative bacteria in order to show the eligibility of the technique for further applications. We had two different approaches to prove that LbL coated cells behave differently for sulphide and sulphur uptake. For the first approach, we fabricated three and four layers on the cell surface. We were able to obtain a thin, permeable shell, which helps in changing the electrochemical properties of the cell surface. Furthermore, different polyelectrolytes, when used as the outermost layer, helped us in attributing more hydrophobic or hydrophilic properties to the surface. For the second approach, a physical barrier was created by the assembly of five and six layers to the cell surface [86]. Table 4.1 shows all the polyelectrolyte combinations that we used for our study and their growth conditions [86].

Table 4.1 Encapsulation and growth conditions for *Alc. Vinosum* [86].

Polymer combination/culture	Number of layers	Surface charge	Electron donor	
			Sulfide (mM)	Elemental Sulfur (mM)
<i>Alc. Vinosum</i>	-	-	5	50
Control with 4 layers	-	-	5	50
Control with 6 layers	-	-	5	50
PDDA/PGA	3	+	5	50
PDDA/PGA	4	-	5	50
PAH/PAA	3	+	5	50
PAH/PAA	4	-	5	50
PAH/PSS	3	+	2	25
PAH/PSS	4	-	2	25
PDDA/PSS	3	+	1	25
PDDA/PSS	4	-	1	25
PDDA/PAA	3	+	0.5	25
PDDA/PAA	4	-	0.5	25
PAH/PSS	5	+	5	50
PAH/PSS	6	-	5	50
PDDA/PSS	5	+	5	50
PDDA/PSS	6	-	5	50

Electrochemical Changes of the Cell Surface

Five different combinations of polymers were used to investigate the effect of changes in the surface charge on oxidation of sulfide and uptake of elemental sulfur. One pair was a mixture of synthetic and biocompatible polymers (PDDA/ PGA), while all the other pairs of polymers were synthetic ones. Figure 4.1a and b show Zeta potentiometer readings for cell encapsulation with PDDA/ PGA and PAH/ PSS, respectively. *Alc. Vinosum* cells were negatively charged before encapsulation (-20.4 mV and -25.1 mV, respectively) and further encapsulation steps show reversal between negative and positive charges for each assembly step indicating successful shell formation [86].

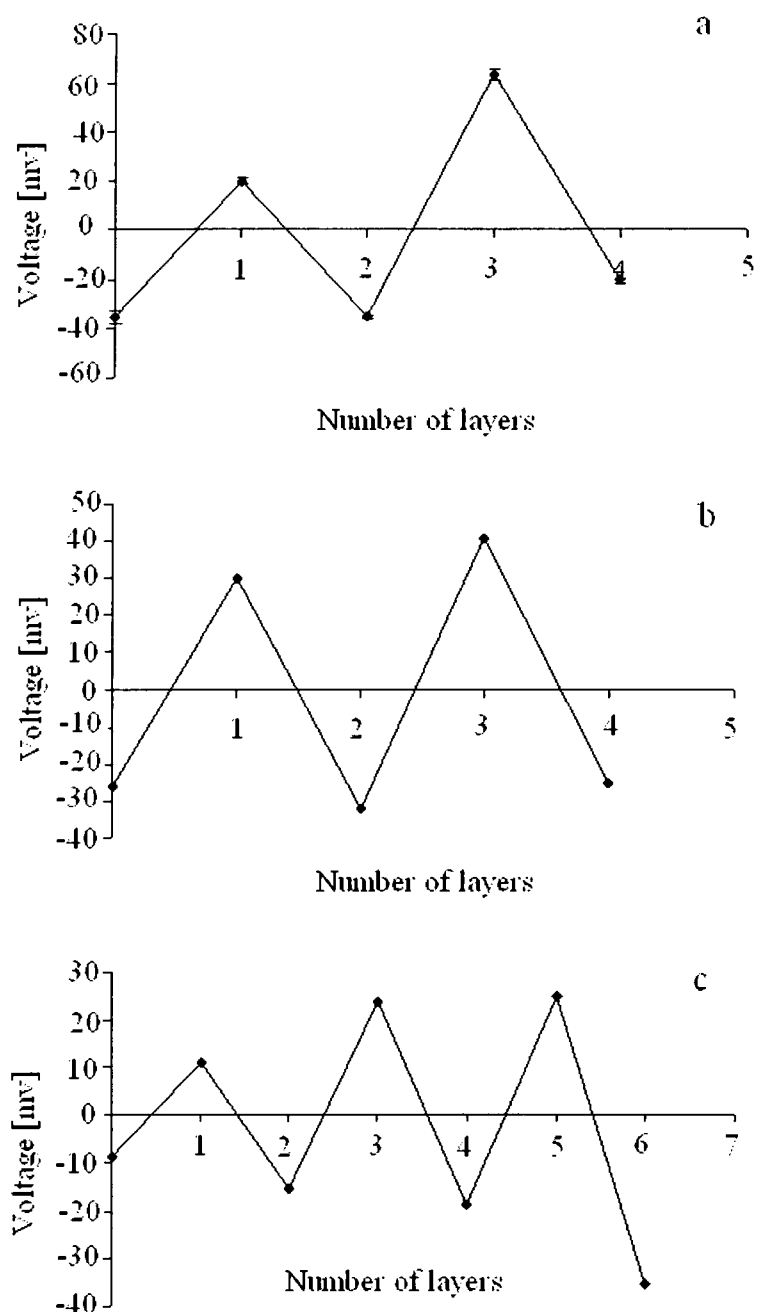


Figure 4.1 Zeta potentiometer readings during the encapsulation of *Alc. Vinosum* with PDDA/PGA (a) and PAH/PAA (b) with 3 and 4 layers, respectively, and PAH/PSS (c) with 5 and 6 layers.

Similar results were obtained for combinations of PDDA/PSS, PAH/PAA and PDDA/ PAA [86]. For each pair of polymers, one culture was prepared with three layers

yielding a positively charged surface and one culture had a negative surface charge, like the original *Alc. Vinosum* cells, due to the four layers assembled on the cells. The shell formation was also confirmed with confocal microscopy and FESEM imaging.

Alc. Vinosum cells were transferred into the modified Pfenning's medium after the encapsulation process. Elemental sulfur or sulphide was added as the single sulfur source in different concentrations. The cultures containing this substrate were stirred during growth in order to facilitate dispersion of elemental sulfur. The control cells were treated exactly like the cells being encapsulated as the cells are exposed to oxygen and deionized water during the encapsulation process. Deionized water was used without polymers for the control set of samples. It was observed that the control cultures slightly changed color from red to a more brownish red, but they did not show differences in oxidation of sulfide and uptake of elemental sulfur as compared to the *Alc. Vinosum* cells, which were directly transferred from photoheteroorganic growth to photolithoautotrophic growth [86] on reduced sulfur compounds (Figures 4.2 and 4.3).

We demonstrated that during the growth of cells with sulfide, the formation of intracellular sulfur, which is the first detectable product of sulfide uptake and oxidation, was similar in both the cultures (Figure 4.2a). It was also seen that the formation of sulfate (Figure 4.2b) and protein concentration showed slight growth of the cultures (Figure 4.2c). With the addition of elemental sulfur to the cultures as the sulfur source, it was not possible to separate sulfur globule containing cells from the surrounding elemental sulfur [86]. In this case only the protein and sulfate concentration were determined to show growth of the cultures. Detection of sulfate, which is the end product of elemental sulfur oxidation in the cultures, indicated the uptake of elemental sulfur.

Protein concentration of the control cells, that were also exposed to oxygen and deionized water, indicates cell growth and sulfate formation indicates a comparable uptake and further oxidation of elemental sulfur (Figure 4.3a, b). This helped to demonstrate that the encapsulation process does not affect the metabolic activity of the cells. However, encapsulation of cells with different combinations of polymers did not give any differences in oxidation of sulfide and uptake of elemental sulfur when all the cells were grown with 5 mM sulfide and 50 mM elemental sulfur, respectively [86]. The change was not observed for the negatively or for the positively charged cells (Figure 4.2a, b, c and Figure 4.3a, b). For the case of cells that were fed with sulfide, the concentrations of 5 mM negatively charged sulfide indicated the saturation of the positively charged cell surface allowing further sulfide to be absorbed into the polymeric shell. For this reason, sulfide concentrations in the cultures were decreased to 2, 1 and 0.5 mM (Figure 4.2a, b, c). A difference in sulfur globule formation between the positively and negatively charged cells was still not observed [86]. A decrease of elemental sulfur concentration to 0.25 mM also did not produce an effect on the uptake of the substrate (Figure 4.3a, b). These results point towards the fact that the surface charge of the cells does not play a vital role in the formation of cell-sulfur contact and, therefore, in the uptake of elemental sulfur in *Alc. Vinosum*. Similar observations have been made for the case of the chemotrophic sulfur bacterium, *Ath. Ferrooxidans* [104]. In column chromatography experiments with strongly acidic and strongly basic ion exchangers, sulfur grown *Ath. ferrooxidans* cells do not attach on both columns, but instead, the cells attach to hydrophobic columns [104]. We used PSS as the outermost layer in one set of experiments, which is a stronger polyanion than PAA, making the surface even more

hydrophobic [99], but this did not yield any distinct differences in the uptake of elemental sulfur. It was assumed that the differences in hydrophobicity between PSS and PAA are not large enough to cause a clear difference in adhesion of elemental sulfur to the cell and, therefore, in the uptake of the substrate [86]. Furthermore, uptake and oxidation of sulfide were also not affected by a change of the electrochemical potential of the cells, although the substrate is oppositely charged than the cells coated with three layers.

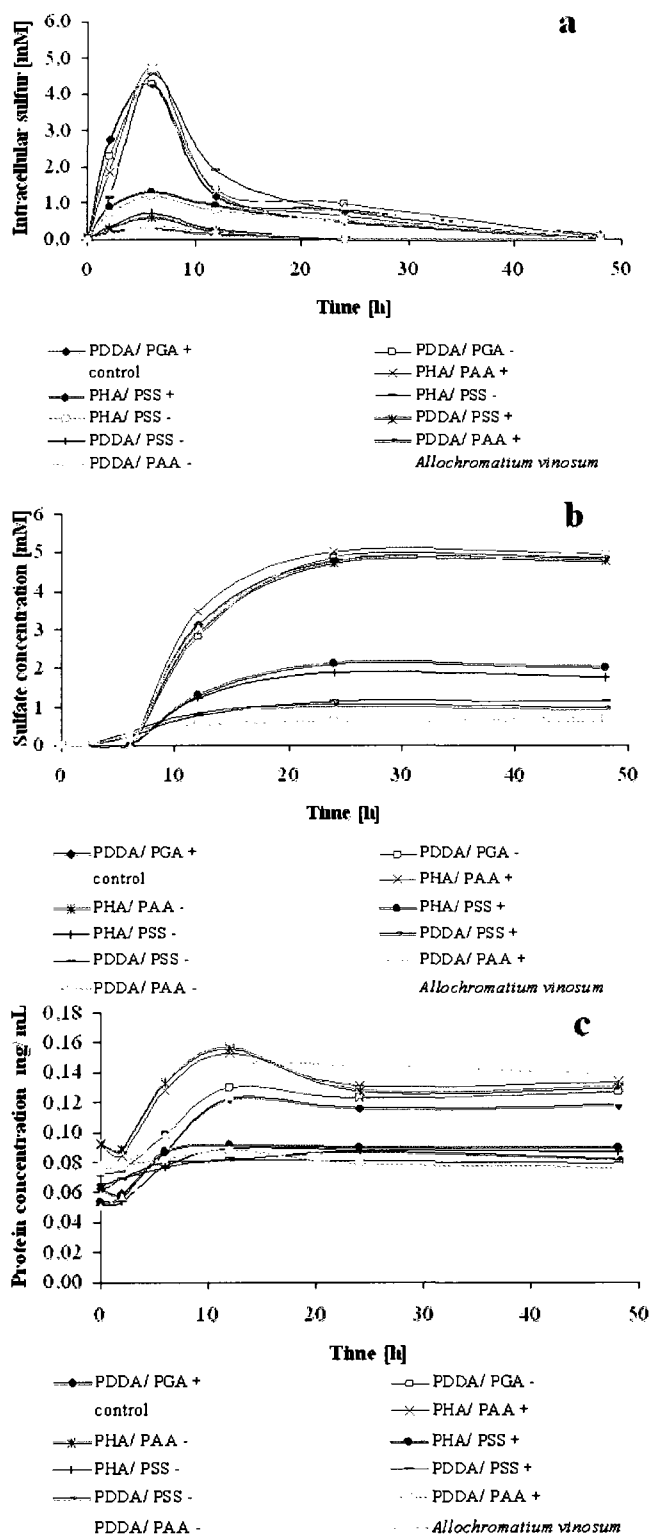


Figure 4.2 Formation of intracellular sulfur (a), sulfate (b) and protein concentration (c) with 3 and 4 layers encapsulated *Alc. Vinosum* during cell growth with sulphide [86].

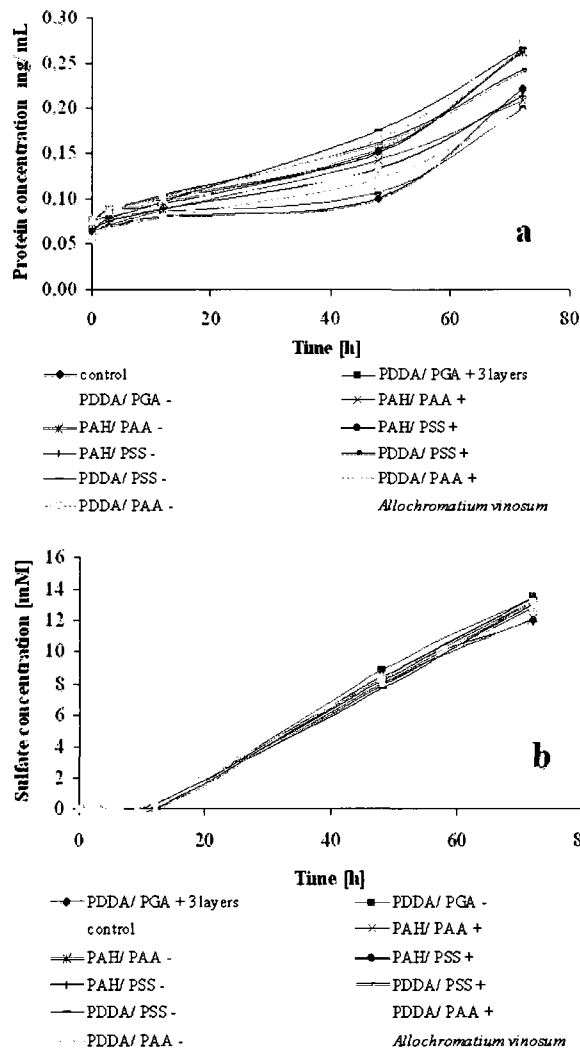


Figure 4.3 Protein concentration (a), formation of sulfate (b) with 3 and 4 layers encapsulated *Alc. Vinosum* during cell growth with elemental sulphur [86].

Physical Barrier by Nanoshell

For this purpose, *Alc. Vinosum* cells were encapsulated with five and six layers using two different pairs of polymers. Figure 4.1 shows the Zeta potentiometer readings during the encapsulation process with PAH/PSS. Starting with the negatively charged *Alc. Vinosum* cells, there was charge reversal with every step of encapsulation, again indicating shell formation. Similar results were obtained by using PDDA/PSS (data not shown). In order to observe the effects of surface charge at that shell thickness, again

positively (five layers) and negatively (six layers) charged cells were obtained. [86]. Furthermore, shell formation was confirmed by confocal microscopy (Figure 4.4) and FE-SEM imaging (Figure 4.5). The cell surface appears rough in the SEM image because it had been coated with the polymers.

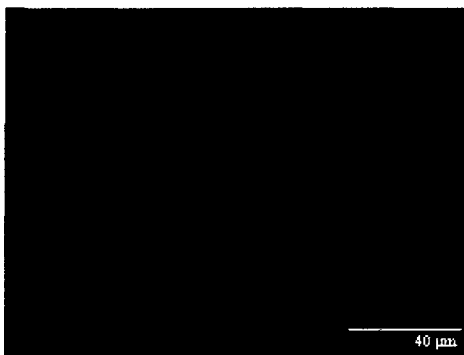


Figure 4.4 Confocal microscopy image of *Alc. Vinosum* encapsulated with PAH/PAA cells during growth with elemental sulfur.



Figure 4.5 FE-SEM image of *Alc. Vinosum* encapsulated with PAH/PAA during growth with elemental sulfur.

For confocal microscopy, an additional layer of PAH labeled with the fluorescent dye FITC was adsorbed on the positively charged cells as the outermost layer, making it possible to visualize a green ring around the cells, indicating encapsulation. A few dye molecules diffused into the cells and stained the periplasmic sulfur globules [86]. Figure

4.4 shows a green ring for PAH/PSS encapsulated cells that were fed with elemental sulfur, indicating encapsulation of the cell. The green structures inside the cells indicate the uptake of elemental sulfur. FESEM images, like the one in Figure 4.5 for the same culture, showed that there is no change in the surface profile of the encapsulated cells.

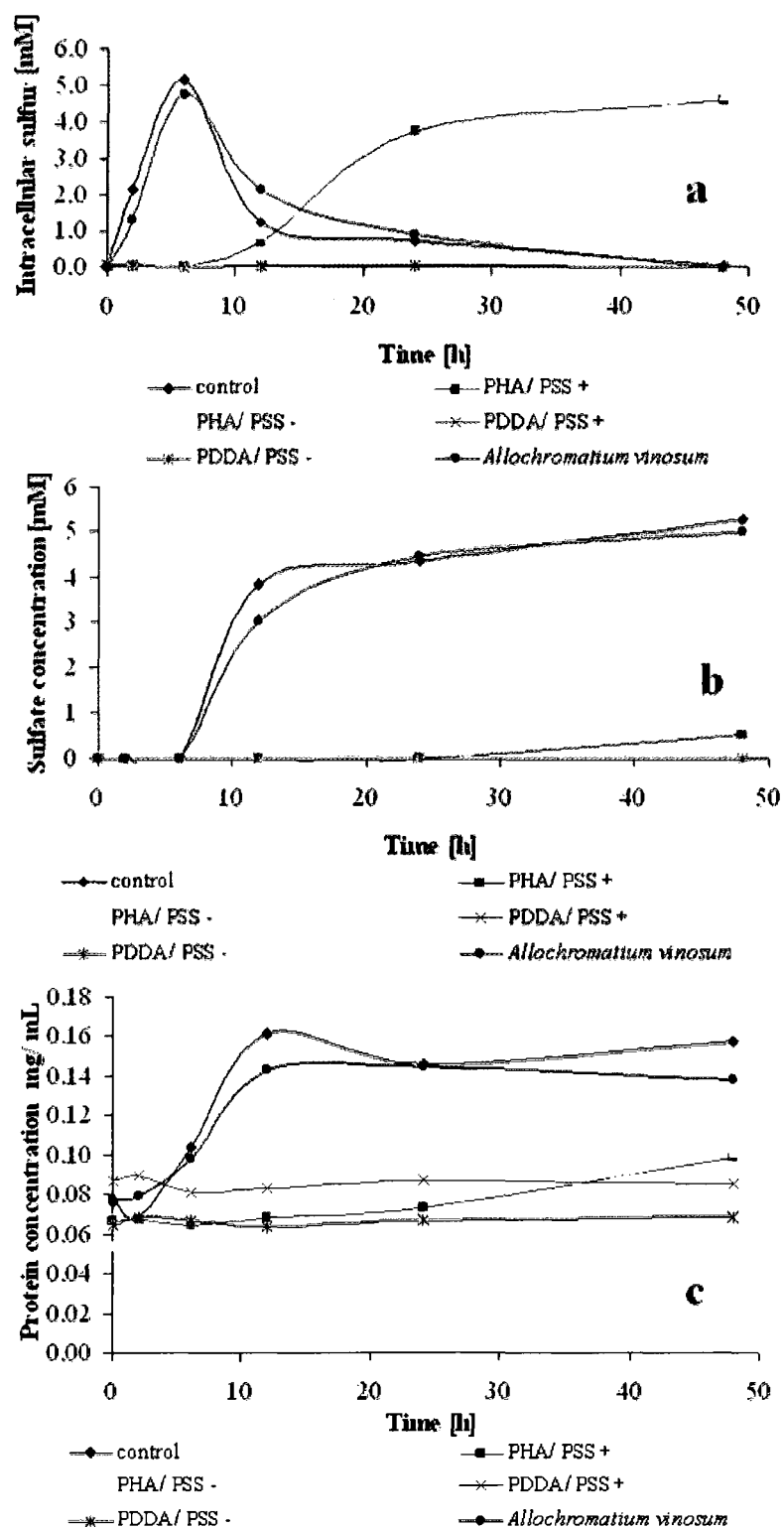


Figure 4.6 Formation of intracellular sulfur (a), sulfate (b) and protein concentration (c) with 5 and 6 layers encapsulated *Alc. Vinosum* during cell growth with sulphide [86].

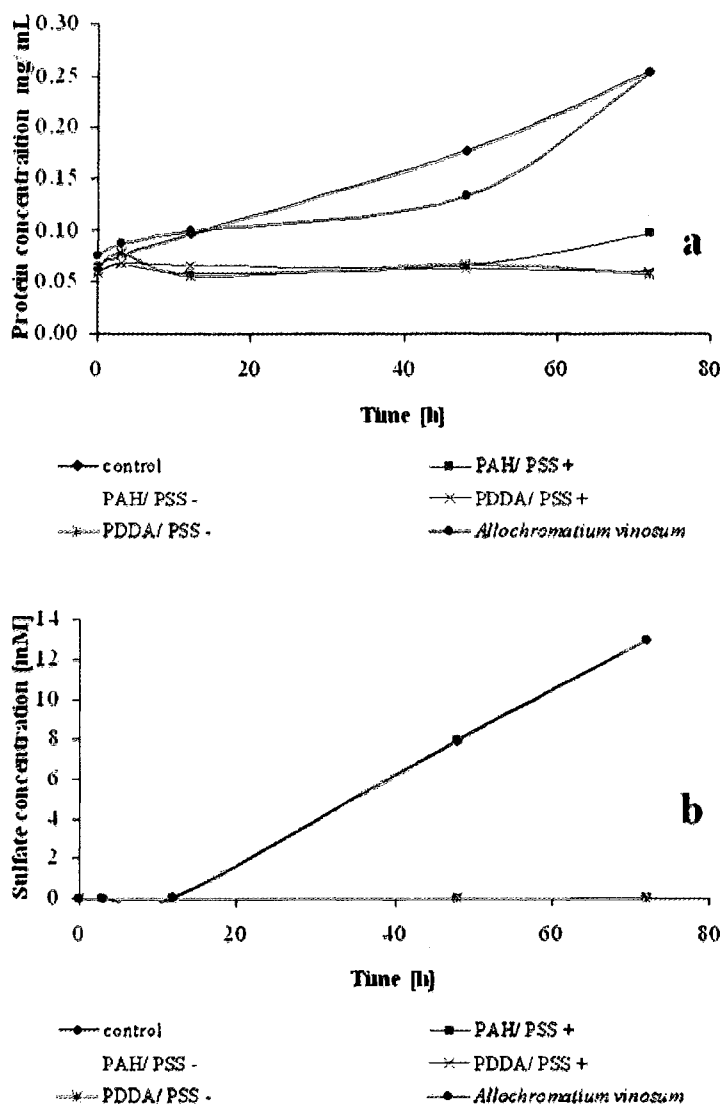


Figure 4.7 Protein concentration (a) and formation of sulfate (b) with 5 and 6 layers encapsulated *Alc. Vinosum* during cell growth with elemental sulphur [86].

After encapsulation, cells were cultivated as described above. We had a set of control samples that were treated exactly like the encapsulated samples, but without any polymers. This was done to make sure that the control samples and the encapsulated samples are exposed to oxygen for the same amount of time. It was seen that the control cells showed similar growth to *Alc. Vinosum* cells, which were directly transferred from photoheteroorganic growth on malate to photolithoautotrophic growth with reduced

sulfur compounds (Figures 4.6 and 4.7), indicating that the extended coating process did not affect the metabolic activity of the cells [86]. The positively as well as the negatively charged cells took up sulfide and elemental sulfur slower than the control cells when the cells were encapsulated with five or six layers of PAH and PSS. It was seen that sulfide and elemental sulfur were not taken up during 72 h when PDDA and PSS were used (Figure 4.6a, b, c and Figure 4.7a, b). When the cells were fed with sulfide, intracellular sulfur and sulfate formation were strongly slowed, compared to the control cells, when PAH and PSS were used for coating indicating slower uptake. There was no formation of intracellular sulfur and sulfate when PDDA and PSS were used for encapsulation [86]. The determination of protein concentration showed little growth for PAH/PSS encapsulated cells and a nearly constant protein concentration for 72 h indicated that the cultures did not grow at all when PDDA and PSS were used for coating. These results indicate that the surface charge does not have an effect on oxidation of sulfide and uptake of elemental sulfur, but also indicates that an increase in the number of layers provides a more compact shell which acts as a physical barrier against diffusion of the substrate through the shell [86]. It has been established that anionic and cationic polyelectrolyte layers interact and penetrate each other which leads to differences in the architecture of the shell, when different polymers are used for encapsulation [5]. This helps in explaining why shells obtained using PDDA/PSS completely inhibit uptake of elemental sulfur and sulfide while shells of PAH/PSS only slow this process, although the number of layers assembled in both the cases is the same. We were able to demonstrate that nanoassembly of a larger number of polymers to bacterial cells allows the formation of a physical barrier between the cell and the surrounding medium inhibiting uptake of substrates. This

function can be used to protect the cell from environmental factors. The results also indicate the possibility to influence the structure of the physical barrier by the choice of the polyelectrolytes used for the coating process [86].

CHAPTER 5

ENCAPSULATION OF BACTERIAL SPORES IN NANOORGANIZED POLYELECTROLYTE SHELLS

Overview

This chapter is based on my contribution to the publication titled ‘Encapsulation of bacterial spores in nanoorganized polyelectrolyte shells,’ *Langmuir*, 2009 [107]. The modification of surface architecture of biological cells while retaining the internal working properties of the native system, is a great challenge. Directly using or mimicking the processes of a biological cell in miniaturized devices will revolutionize system design; however, synthesizing the intricacies of biology is problematic [108]. In order to make such modification, one has to work in the submicron regime and use benign reaction conditions that do not denature the properties of the biological materials [107]. Cells require functional organic/inorganic interfaces, special fluidic support and nutrition delivery. Moreover, the final 3D architectures must provide a compatible construction that does not disturb the crucial elements of the cells [109]. Some previous work explored immobilization of mammalian cells in silica pores using chemical vapor deposition methods. The sol-gel matrices incorporate the cells within a scaffold intended to control multicellular organization. The approach may allow material to circumvent the host immune reactions and support the cell proliferation for tissue regeneration, but none of the approaches provided a bio/nano interface for 3D spatial control of biological cells

[110]. Rubner, et al. have fabricated polyelectrolyte multilayer patches on cells and have explored the surface functionalization of living cells. This technique is related to their earlier “Janus” technology of asymmetrical functionalization of microparticles [111-113]. Modification of bacteria or bacterial spores bring additional challenges because they are much smaller (typically ca. 1 micrometer) and have a more fluid cell wall. The starting point of the current research was to reproduce some of the spore shell features using *in vitro* self-assembly methods.

The shell formation was based on LbL electrostatic assembly via alternate adsorption of cationic and anionic species [6, 7, 47, 92, 94, 114]. This mild nanoassembly method does not involve any covalent binding and is based on cooperative electrostatic attraction of sequentially adsorbed polycations and polyanions. Every deposited polymer bilayer gives an approximately 2-5 nm thickness increment [107]. Multilayers of 4-5 polyelectrolyte bilayers are permeable to low molecular weight molecules but cannot be penetrated by large macromolecules and proteins. Nanoorganized polyelectrolyte shells have already found applications for drug microencapsulation, due to the tunable properties of the polyelectrolyte coatings [12, 115]. Different numbers of polyelectrolyte layers in the shells and their different compositions have allowed for controlled release of drugs from such LbL capsules [12]. Researchers have successfully extended an LbL approach to three dimensional microparticles [62]. Therefore, nutrition can be delivered to the cell in a controllable manner through the polyelectrolyte shells and an additional protection of the cell interior may be provided [107]. Furthermore, polyelectrolyte coating may protect cells from immune attacks, protect them in harsh conditions, and even decompose external harmful agents through active border defense, as was

demonstrated in [47] for catalase assisted hydrogen peroxide decomposition in LbL multilayers. The modification of whole cells can guide them to selected tissues or organs, as was demonstrated for the targeting of platelets containing an antibody within the outer layer of the deposited LbL shell [26].

This technique has been used to encapsulate blood cells (erythrocytes and platelets), yeast cells, and mesenchymal stem cells [26, 95, 103-119]. Synthetic polyelectrolytes, anionic sodium poly(styrene sulfonate) and cationic poly(allylamine) hydrochloride were used to form nano-organized shells on single cells. The shell formation was confirmed with fluorescent laser confocal microscopy, AFM, and small-angle neutron scattering. LbL assembly of natural polyelectrolytes (chitosan, alginate, and hyaluronic acid) also allowed encapsulation of *Escherichia coli* cells, and experiments using a second generation of *E. coli* cells demonstrated that cell activity was sustained in the presence of the polyelectrolyte shell [118]. The same LbL technology allowed the introduction of enzymatic activity onto yeast cell shells in order to promote the conversion of lactate into pyruvate [119]. If one can modify bacterial pathogenesis as a means of delivery, it may also have future applications for drug and gene delivery [107].

Although researchers have tried various encapsulation techniques for bacteria (spray drying, extrusion, emulsion and phase separation), not much has been done in the field on spore encapsulation to explore the temporal and spatial control of spore germination [107]. In the present work, we demonstrate the engineered coating of bacterial spores with thin multilayers of various polyelectrolytes, proteins and nanoparticles using LbL deposition (Figure 5.1). Following assembly, the coat

morphology was characterized using fluorescent laser confocal microscopy and scanning electron microscopy. Spore viability and germination kinetics were monitored by quantifying the release of dipicolinic acid, which occurs at the onset of spore germination [107].

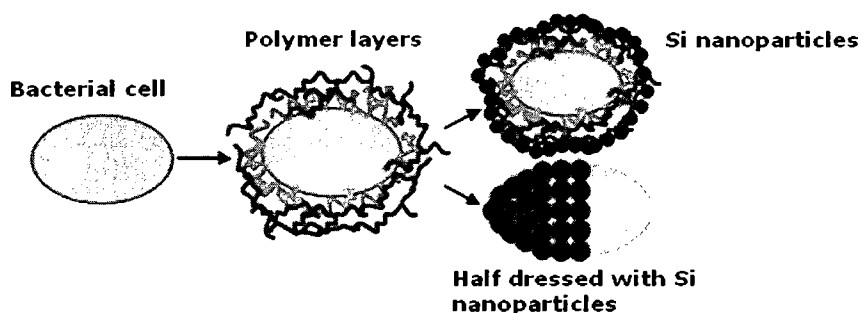


Figure 5.1 Scheme for coating bacterial spores with polyelectrolyte multilayers and nanoparticles using LbL [107].

Methods and Materials

Bacillus Subtilis strain 168 was obtained from the American Type Culture Collection (ATCC 23857). Synthetic sodium poly (styrene sulphonate) (PSS, Mw 100 kDa), poly(dimethyldiallyl ammonium chloride) (PDDA, Mw 100 kDa), and biocompatible polyelectrolytes polyglutamic acid (PGA, Mw 50 kDa), polylysine (PLL, Mw 50 kDa), GelA, and proteins albumin and lysozyme were all obtained from Sigma Aldrich. For fluorescent confocal microscopy measurements, rhodamine isothiocyanate (RITC) labeled polyallylamine hydrochloride and polylysine were used. RITC was obtained from Sigma Aldrich. Silica nanoparticles (Ludox TM -40 colloidal silica, 40 wt. % suspension in water) were also obtained from Sigma Aldrich. 2, 6-pyridine dicarboxylic acid (DPA, 99%) and terbium chloride hexahydrate (TbCl₃, 99.9%) were also purchased from Sigma Aldrich. L-alanine (L-Ala, ≥99.5%) was purchased from

Fluka. All other reagents were purchased from Sigma-Aldrich and were of the highest purity available.

Spore Preparation and Isolation

B. Subtilis was grown overnight in nutrient media and spread onto sporulation agar plates [120]. After the plates were incubated for 3 to 5 days at 37°C, sterile water was added to each plate and the cellular material was collected by scraping with a bent glass rod and decanting the slurry into a sterile centrifuge tube. The cell slurry was centrifuged at 15,000 × g for 10 min. The cells were lysed by re-suspending the pellet in equal volume of SDS solution (0.5%) and then centrifuged to collect spores (15000 × g, 10 min); the supernatant containing cell debris was discarded. The spore pellet was suspended and collected 2 additional times using the SDS treatment and then five times with sterile water to remove trace amounts of SDS [107]. The purity of the spore preparations was confirmed by microscopic inspection and malachite green spore stain procedure [99]. Spores were re-suspended in sterile water and transferred to glass ampules (108 to 109 spore ampule⁻¹), lyophilized, and sealed in the tubes under vacuum. The samples were stored at -20° C until used.

Shell LbL Assembly

All treatment and layering steps were done at 25° (except where noted) and contained in 1.5 ml polypropylene centrifuge tubes [107]. The bacterial spore samples were re-suspended in 1 mL of ultra pure water (DI) before use in LbL assembly. The sample was then centrifuged at a speed of ~ 9000 rpm and the supernatant was replaced with pure water. The spore sample was washed three times to make sure that it was free of the medium. The cells were further suspended in 0.75 mL of water and were ready for

assembly. The concentration of aqueous polyelectrolytes was 2 mg/mL (pH 6.8). All polymer samples were treated briefly in a sonicating bath and then vortexed before use in the assembly. GelA solution was heated at 45° C for 5 minutes prior to the layering steps. Polyelectrolytes (0.5 mL) were added to 0.75 mL spore dispersion and kept for 15 min for adsorption completion. Polycations and polyanions were adsorbed sequentially and washed with 1 mL DI water between steps and centrifuged to obtain spore separation from the supernatants. The spore samples were briefly sonicated after each washing step to prevent aggregation [107]. Conditions of the polycation/polyanion sequential adsorption and bilayer thickness optimization were elaborated using the QCM (Quartz Crystal Microbalance, 9 MHz, silver plated electrodes of 0.16 cm², USI-System Co, Japan). We used the Sauerbrey's equation based formula $L \text{ (nm)} = -0.017 \Delta F \text{ (Hz)}$ for determining the thickness of the films (L) with coefficient based on SEM scaling of one of the samples as described in [6].

Zeta Potentiometer Measurements

An electrical surface ζ -potential of the bacterial spores and of the polyelectrolytes shells on the spores was measured using a ZetaPlus Potential Analyzer with six measurements taken for each sample to ensure data reliability [107].

Confocal Microscopy

Encapsulated bacterial spores were coated with a final layer of cationic polymer labeled with rhodamine isothiocyanate (RITC). The samples were then washed three times by centrifuging and re-suspending the cells in ultrapure water. 10 μ L of the sample was sufficient to visualize the capsules under the *Leica DMI RE2* confocal laser scanning microscopy. A 63x oil immersion objective lens was used to image the encapsulated cells [107].

Scanning Electron Microscopy

A *Hitachi S-4800* Scanning Electron Microscope was used to image uncoated and encapsulated spores. In order to enhance image clarity, preformed silica nanoparticles were coated onto spore shell surface prior to SEM analysis [107]. The positive surface charge on the PAH-encapsulated spores allowed a reasonably strong ionic interaction with silica, which is negative. Silica nanoparticles (22 nm and 72 nm diameters) were diluted in water (final concentration 1mg/mL). The initial charge of the 22 nm and 72 nm particles was -48 mV and -55 mV respectively. 0.5 mL of the silica nanoparticles dispersion was added to ~ 0.1 mL PAH-RITC labeled encapsulated bacterial spore solution and incubated for 30 minutes for adsorption completion. The sample was then rinsed with water and centrifuged at 9,000 rpm to remove the excess silica. Finally the sample is suspended in 1 mL of water; 0.1 mL of this sample was used for SEM studies. The sample was allowed to air dry and was not heated while an iridium layer was deposited via sputtering (3 nm thickness) [107].

Spore Germination Kinetic Assays

Spore viability was measured using a spore germination assay, as previously described [122]. The assay is based upon dipicolinic acid (DPA) release following germination induction by L-alanine exposure. DPA release is monitored over time by measuring the fluorescence emission of DPA when bound to terbium ions [107]. Spore preparations were resuspended in ultrapure water to final concentrations on the order of 10^6 and 10^8 viable spores mL^{-1} . Viable spore counts were measured by plating serial dilutions of the spore preparations onto solid nutrient media and enumerating the colonies. Spore preparations and serial dilutions were vigorously vortexed before plating to disrupt aggregated spores [107]. To activate spores before germination, spore

preparations were incubated at 70°C for 30 min. After incubation, spore solutions were diluted 1:10 into germination buffer (1.1 mM L-alanine, 10 µM TbCl₃, 0.45% NaCl, 0.25mM sodium acetate, pH 5.6) and incubated in a microtiter plate at 37°C. DPA release during germination was monitored in situ by measuring the Tb-DPA emission spectrum over time in the microtiter plate. The % DPA released is calculated by first measuring the basal level of DPA in spore preparations and also the total DPA content in the spores [107]. To measure the total DPA content in the spore suspensions (100% DPA release), the original spore preparation was diluted 1:10 into 0.653 mM dodecylamine and incubated at 60°C for 10 min in order to extract the available DPA [123]. After extraction, the spore solution was diluted 1:10 into germination buffer and immediately measured to determine the concentration of the Tb-DPA complex. The basal level of the DPA in the spore preparations (0% DPA release) was found by treating the activated spore solutions as described above except the germinant L-alanine, was omitted [107]. For each assay measurement, the relative fluorescence intensity was normalized to the fluorescence intensity of the buffer solution without spores and then to the basal DPA concentration and total DPA in the spore preparations according to the following formula: $(F_x - F_0\%) / (F_{100\%} - F_0\%)$, where F_x = fluorescence intensity of the sample, $F_{100\%}$ = fluorescence from the total DPA in the spore preparation and $F_0\%$ = fluorescence intensity of the basal DPA concentration. Each germination assay was completed in triplicate for native spores and each layering method [107].

Fluorimetry

Fluorometric analysis was completed using a microplate compatible fluorometer (Synergy HT) with time resolved fluorescence capability and Gen5 version 1.02.8 software (*BioTek Instruments Inc.*, Winooski, VT). Samples were analyzed in UV-

transparent plastic 96-well microtiter plates from Corning Inc. (Product # 3635, Acton, MA). The excitation wavelength was 275 nm and the emission wavelength was 545 nm with a bandwidth of 10 nm and 40 nm, respectively. The optics were positioned to read from the bottom of the microtiter plate and sensitivity was set at 180. The time delay before reading after excitation was 0.1 msec, the duration of the read was 9.9 msec and 10 reads were completed per well [107].

Results and Discussion

The ζ -potential measurements indicated that the surface potential of washed *B. Subtilis* spores is -22 ± 2 mV (Figure 5.2). Therefore, the LbL assembly processes were started with adsorption of cationic polymers. Adsorption of positively charged PDDA converted the spore surface charge to a modestly positive polarity [107].

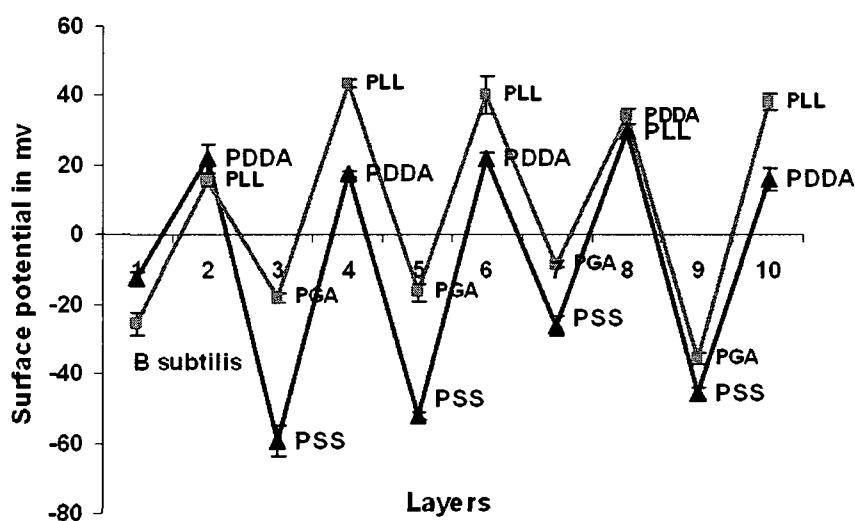


Figure 5.2 ζ -potential of *B. Subtilis* spore in DI water at pH 6.8, n=2.

The first shell assembly process proceeded with alternate adsorption of synthetic PDDA and PSS, which resulted in symmetric changes of the spore potential to positive

and negative, which is characteristic of LbL process. After deposition of four bilayers of PDDA/PSS, the ζ -potential was -50 mV after the PSS adsorption step and $+20$ mV at the final PDDA coat (tenth step in Figure 5.2). Therefore, the treatment can strongly influence spore surface charge, reversing polarity to strongly positive or greatly enhancing the negative charge as compared to the initial non-coated spores. The PSS outermost layer was more negatively charged than the PDDA outermost layer, but this tendency was changed for polyglutamic acid (PGA) alternated with polylysine (PLL). The PDDA/PSS encapsulated spores could be stably dispersed in aqueous solvents and did not aggregate due to the strong surface charge [107]. Using this process, one can stop the assembly at the polyanion adsorption stage to have spores with negative surface charge, or add one more polycation layer to have spores with a positive outermost layer.

At the next stage of the work, we used the biocompatible polyelectrolytes poly (lysine) (PLL) and poly (glutamic acid) (PGA) as the coating substrates [107]. PLL is positively charged and PGA is negatively charged at pH 6.5-7 due to amine and acid ionized groups, correspondingly. Again, deposition of the first layer of polylysine led to a positive ζ -surface potential ($+16$ mV). Deposition of the following anionic PGA layer decreased the ζ -potential to a negative -18 mV. The subsequent LbL PDDA/PGA deposition steps enhanced the surface ζ -potential and showed almost reproducible electrical potential reversal between $+45$ mV after PLL adsorption to -35 mV for PGA adsorption after four bilayer shell formations (Figure 5.2).

The QCM measurements indicated a difference in the thickness of deposited polyelectrolyte multilayers. The assembly of the PSS/PDDA multilayer provided an increment of 2.2 ± 0.2 nm for each bilayer, and the PLL/PGA multilayer processes

showed 3.5 ± 0.4 nm for each bilayer, when in a dry state [107]. QCM assembly monitoring was performed on a standard QCM electrode surface and results were transferred to spore shell thickness as an estimation, not taking into account specificity of the spore surface. In the hydrated state, the thickness of the multilayer wall will be two times larger [6, 114]. Accordingly, the thickness of the (PLL/PGA)₄ shell may be estimated as 28 ± 5 nm.

The surfaces of the LbL-coated spores were decorated with nanomaterials of known composition and size in order to image the surface topology because conventional staining methods will not selectively modify the polyelectrolyte layers compared to the spore coat. We obtained spores that were evenly coated with the nanoparticles thus providing them with an inert and mechanically stable layer [107]. This also helped us in studying the changes in the surface architectures. Negatively charged silica nanoparticles were deposited on the shell outermost layer (after polycations) and provided visualization using scanning electron microscopy. The ζ -potential of the (PLL/PGA)₄-modified spores that were subsequently coated with + PLL/silica decreased to -30 mV due to the adsorption of the negative silica outermost layer (not shown in Figure 5.2). After careful washing, the samples were studied with a scanning electron microscope and compared to uncoated spores (Figure 5.3).

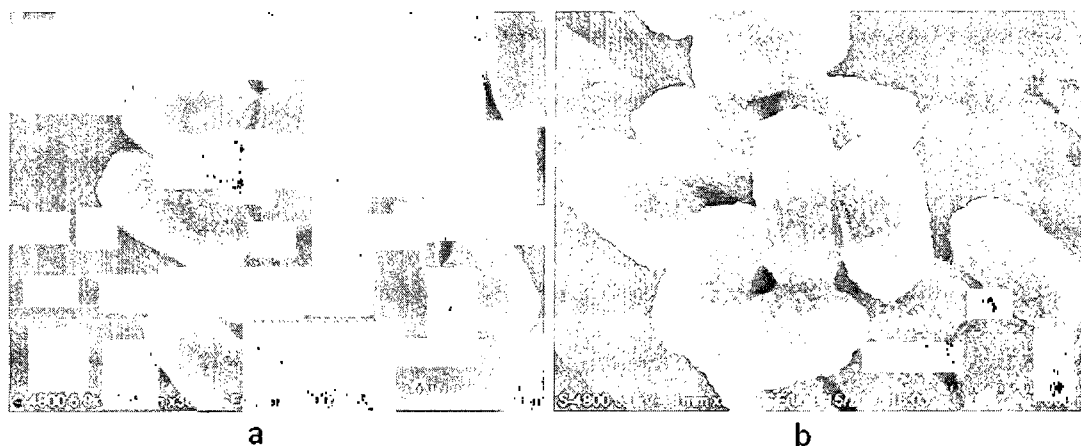


Figure 5.3 SEM images of *B. Subtilis* spores (a- control) and of (b) *B. Subtilis* coated with $(\text{PLL}/\text{PGA})_4 + \text{PLL} + 22 \text{ nm}$ silica nanoparticles.

It appears that a layer of the 22 nm diameter silica particles adsorbed onto the entire cell surface of the polycation treated spores, providing a uniform coating [107]. Formation of the shell with larger 72 nm diameter silica was also possible, as demonstrated in Figure 5.4(a) but together with well coated spores, some of the spores came out “half-dressed”.

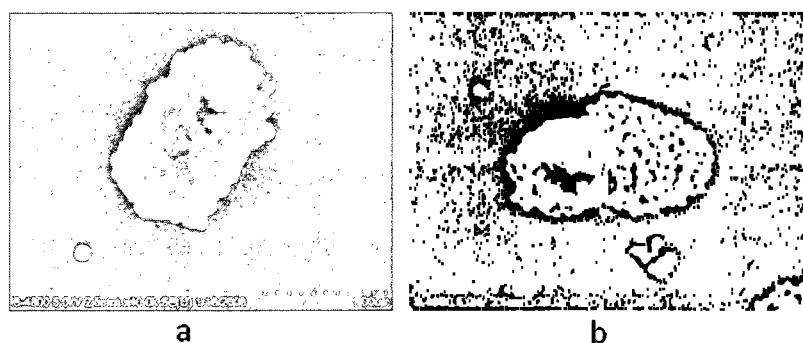


Figure 5.4 SEM images of *B. Subtilis* spores coated with $(\text{PLL}/\text{PGA})_4 + \text{PLL} + 72 \text{ nm}$ silica nanoparticles (a and b are two different spores).

Surveys of multiple fields during SEM analysis revealed that 10-15% of the treated spores were coated with 72-nm silica spheres [107]. The incompletely coated

nanoparticle may be related to the surface properties of certain parts of the coated spore surface. The differences may result when repulsive forces between the larger silica nanospheres were stronger than the attraction by the PLL coating, or possibly some of the surface may have poorly adsorbed the polymer and led to part of the layer breaking off from the surface [107].

Fluorescent confocal microscopy using rhodamine isothiocyanate (RITC) labeled PLL is presented in Figure 5.5. In the initial experiments, we found evidence that the RITC could penetrate the spore coats that were modified with 4 bilayers of PLL/PGA. This result may suggest that the preceding LbL process was somehow imperfect and that the PLL-RITC crossed the previous synthetic bilayers and then breached the spore surface. An alternative explanation would be that non-covalently bound RITC is released from the layer and penetrates to the spore surface [107].

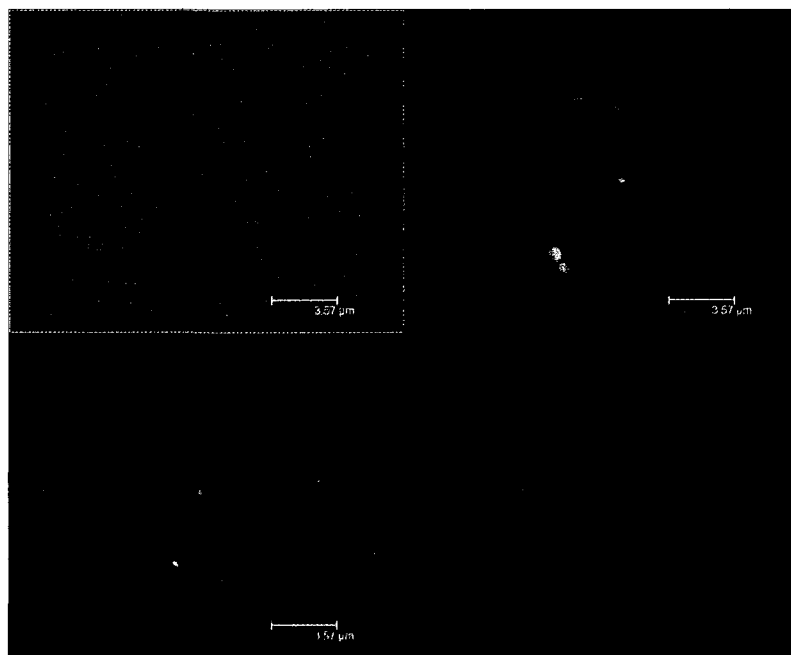


Figure 5.5 Confocal image of *B. Subtilis* with shell of (PLL/PGA)₄ labeled with PLL-RITC, immediately after the shell assembly (first day).

The phenomenon was overcome in subsequent modifications of the synthetic shell composition. The addition of a penultimate layer of GelA blocked the dye from crossing the synthetic coating or spore coat [107]. The green auto fluorescence from the spore interior is evident from the images obtained using a 530 nm filter; identical response is found with unlabeled spores under confocal imaging (not shown). Subsequent fluorescent images in transmission mode show that all the spores present in the field are coated with the shell containing the RITC. A well defined red layer evenly coated the spore surface, indicating that the structural morphology of the spore was retained (Figures 5.5 and 5.6). The image does not represent the actual polyelectrolyte shell wall since the limit for confocal microscopy resolution is approximately 200 nm while the actual shell thickness is likely to be no greater than 30 nm. The LbL shell provided a robust surface coating. After 15 days of storage at 4° C, the shell remained intact on the non germinated spore surfaces (Figure 5.6 b).

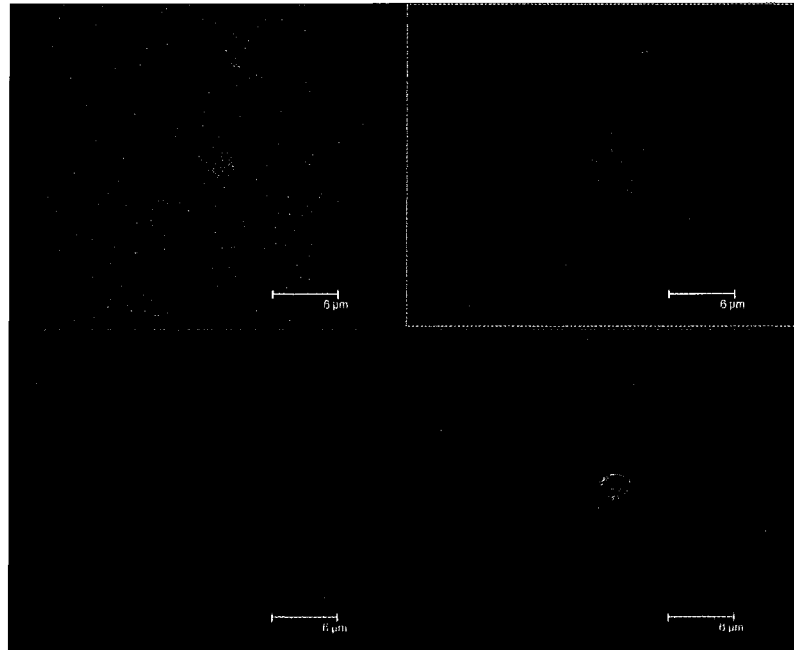


Figure 5.6 Confocal image of *B. Subtilis* with shell of (PLL/PGA)₄ - Gelatin labeled with PLL-RITC (fifteenth day).

The Effect of Coatings on Spore Viability and Germination.

Measurements of spore germination using the DPA release assay distinguished the rate and extent of the germination of the various spore preparations. In all cases, the spores retained viability; this was clear from simple cultivation showing that vegetative cells grew out from the spore inoculum and was clearly evident in the DPA assay results [107]. The assay measured the apparent germination kinetics and variation in the onset of germination within the population. Following the addition of a soluble germinant, the fluorescent DPA-terbium complex was detected almost immediately, showing insignificant differences in the onset of germination compared to the uncoated controls (Figure 5.7). This result suggests that the synthetic layers were permeated by the germinant; however, the initial rate of DPA release differed [107]. As one would expect, the coating reduces the coat permeability, which was reflected by the reduced rate of

initial DPA release. The extent of DPA release differed amongst the modified spores as compared to the controls. The cells coated with PGA/PLL bilayers showed only a 50% apparent germination compared to the control sample. All other shells reached a plateau of about 70% of the chemically lysed samples. The controls showed approximately 90% germination over a period of 80 minutes [107]. The difference in the total DPA release compared to the control may be due to a portion of the spores that are present being unable to germinate normally during the assay.

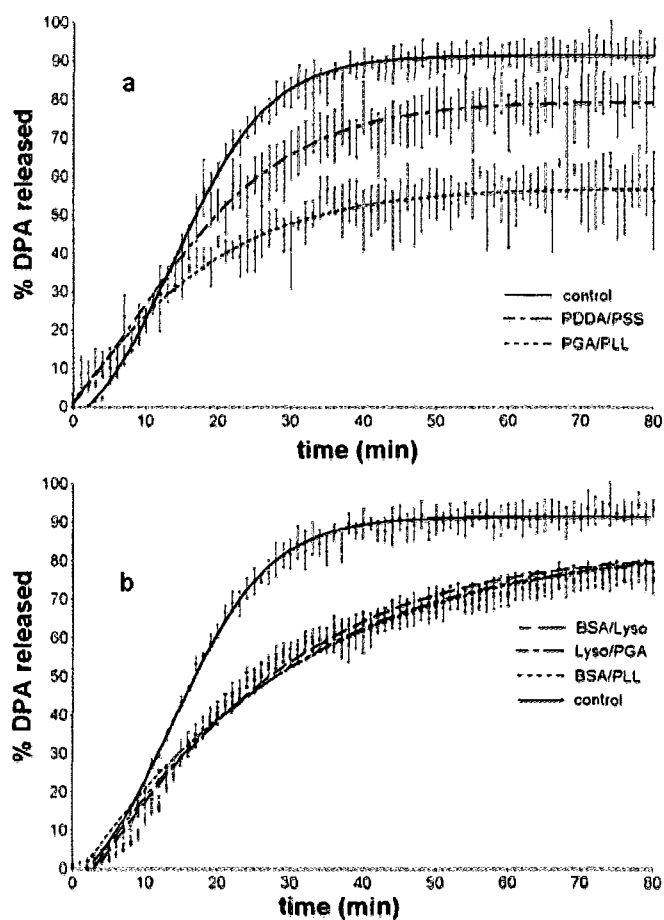


Figure 5.7 (a-b) Kinetics of apparent spore germination monitored by release of dipicolinic acid (DPA), $n=3$.

CHAPTER 6

CONCLUSION AND FUTURE WORK

We demonstrated a successful LbL assembly of a natural polyphenol, (-)-epigallocatechin gallate, in alternation with proline-rich proteins, and Gelatins. It was shown that both type A and type B Gelatins, that have different isoelectric points and are charged differently under experimental conditions, formed relatively bulky multilayers in alternation with EGCG suggesting that the interaction between the components is mainly hydrophobic. It was also established that electrostatic forces play an important role in the interaction between components in order to obtain a stable defect-free protein/polyphenol coating around microcores or free-standing microcapsules in aqueous media, as it occurs for the GelA/EGCG system. We proved that the EGCG content in the Gelatin/polyphenol film material was as high as 30 % w/w. Encapsulation of EGCG in LbL assembled films and microcapsules can be a prospective way to obtain new formulations of this cancer chemopreventive polyphenol for drug delivery applications.

We showed that natural polyphenols, with anti-cancer potential including EGCG, tannic acid, curcumin, and theaflavin, can be encapsulated into Gelatin-based 200-nm nanoparticles coated with organized 5-20 nm thick shells of polyelectrolytes (of different composition - from synthetic polyions to natural and biodegradable types) using the LbL technique. We demonstrated that the polyphenol loading was from 20 to 70 wt %. Factors affecting their release from the nanocapsules were investigated and, in the case of EGCG,

the release time reached 8 hours, as compared to a release time of a few minutes for non-encapsulated nanoparticles. We also showed that the nanoparticle-encapsulated EGCG retains its biological activity as both nanoparticles containing EGCG and free EGCG blocked HGF-induced intracellular signaling in the breast cancer cell-line MBA-MD-231. This work will help in developing nanoparticles that will target tumor cells to release EGCG and other chemotherapeutic or targeted anti-cancer agents. This work helped in initiating animal studies to measure the half-life of the nanoparticles and released EGCG. Further work needs to be done that will address the therapeutic potential of slow release EGCG-particles in a mouse tumor model. The size of the particles has to be reduced to 100 nm or lower, which is still a challenge.

For our Biomimetic applications, we showed that *Alc. Vinosum* can be encapsulated with different numbers of polyelectrolyte layers using electrostatic self-assembly without losing its metabolic activity. It was also demonstrated that the changes in the electrochemical potential of the cells do not play a role in the uptake of the soluble substrate sulfide or the uptake of the insoluble elemental sulfur. It was seen that an increase in the number of layers creates a physical barrier between the environment and the cell. The permeability of this barrier is highly dependent on the selected polyelectrolyte combination. We demonstrated that the LbL nano-assembly technique is a suitable tool for the investigation of substrate uptake in bacteria, for surface modification, and offers new possibilities in a wide variety of other microbiological applications. We showed that the LbL technique offers a great deal of flexibility for surface modifications using bacteria. Further studies will help in exploring the reasons for the change in the uptake mechanism for substrates. Encapsulation of bacterial cells can also exploit

numerous applications involving the protection of probiotic bacteria from the acidic conditions of the stomach, investigating the adhesion of bacteria to its substrates or hosts by incorporation of various proteins or other molecules in the shells.

We demonstrated that bacterial spores can be effectively encapsulated using LbL polyelectrolyte assembly methods. Individual bacterial spores were coated using synthetic and natural polyelectrolytes to form coatings as much as 30 nm thick on the surface of the spores with surface ζ -potential that could be adjusted between -30 and +40 mV. It was possible to further refine the coated structure with a finishing layer composed of silica nanoparticles. The finishing process adds to the toolbox available for nano-scale precision coatings and may impart further mechanical stability to the engineered architectures. Germination assays showed that the spores were viable even after encapsulation using various polyelectrolytes. The coatings appear to affect the diffusion rates of germinant influx into the spores and possibly the actual endospore germination. Customizing the coatings to control diffusion rates could be useful to specifically coordinate germination. For example, the number of layers or type of polymer might be adjusted to further affect response to the usual germinants. The effectiveness of the bio-derived polymers is also notable. The materials (simple amino acid-based polymers and proteins) may be more environmentally compatible, thus amenable to open applications, such as agricultural biopesticides.

REFERENCES

- [1] E. Haslam, "Natural polyphenols (vegetable tannins) as drugs: possible modes of action," *J Nat Prod*, vol. 59, pp. 205-15, 1996.
- [2] S. Quideau, K. S. Feldman, "Ellagitannin Chemistry," *Chem Rev*, vol. 96, pp. 475-504, 1996.
- [3] A. Bennick, "Interaction of plant polyphenols with salivary proteins," *Crit Rev Oral Biol Med*, vol. 13, pp. 184-96, 2002.
- [4] Y. M. Lvov, M. M. DeVilliers, *Nanotechnologies for Life Sciences* vol. 10. Berlin: *Wiley-VCH*, 2007.
- [5] G. Decher, Y. Lvov, H. Möhwald, "Assembly, structural characterization, and thermal behavior of Layer-by-Layer deposited ultrathin films of poly(vinyl sulfate) and poly(allylamine)," *Langmuir*, vol. 9, pp. 481-486, 1993.
- [6] K. Ariga, Y. Lvov, I. Ichinose, T. Kunitake, "Assembly of Multicomponent Protein Films by Means of Electrostatic Layer-by-Layer Adsorption," *J Am Chem Soc* vol. 117, pp. 6117-6123, 1995.
- [7] G. Decher, "Fuzzy Nanoassemblies: Toward Layered Polymeric Multicomposites " *Science*, vol. 277, pp. 1232-1237, 1997.
- [8] F. Caruso, Y. Lvov, "Bicollids with ordered urease multilayer shells as enzymatic reactors," *Anal Chem*, vol. 73, pp. 4212-4217, 2001.
- [9] F. Ackern, J.B. Tieke, L. Krasemann, A. Toutianoush, "Ultrathin Self-Assembled Polyelectrolyte Multilayer Membranes.," *Eur Phys J E*, vol. 5, pp. 29-39, 2001.
- [10] S. A. Jones, H. Ai, Y.M. Lvov, "Biomedical applications of electrostatic layer-by-Layer nano-assembly of polymers, enzymes, and nanoparticles," *Cell Biochem Biophys*, vol. 39, pp. 23-43, 2003.
- [11] R. K. Iler., "Multilayers of colloidal particles, " *J Coll Int Sci*, vol. 21, pp. 569-594, 1966.
- [12] S. A. Jones, H. Ai, M.M. DeVilliers, Y.M. Lvov, "Nano-encapsulation of furosemide microcrystals for controlled drug release," *J Control Rel*, vol. 86, pp. 59-68, 2003.
- [13] E. Donath, G.B. Sukhorukov, S. Davis, H. Lichtenfeld, F. Caruso, V.I. Popov, H. Möhwald, "Stepwise polyelectrolyte assembly on particle surfaces: a novel approach to colloid design," *Polym Adv Technol* vol. 9, pp. 759-767, 1998.

- [14] G. B. Sukhorukov, A. Alexei, A. Antipov, E. Donath, H. Möhwald, "Sustained release properties of polyelectrolyte multilayer capsules," *J Phys Chem B*, vol. 105, pp. 2281-2284, 2001.
- [15] I. Suzuki, H. Inoue, J. Anzai, "Modification of Polyelectrolyte Layered Assembly Using an Active Ester of Azobenzene Carboxylate," *Macromolecules*, vol. 35, pp. 6470-6474, 2002.
- [16] G. B. Sukhorukov, E. Donath, S. Moya, A. S. Susa, A. Voigt, J. Hartmann, and H. Mohwald, "Microencapsulation by means of step-wise adsorption of polyelectrolytes," *J Microencapsul*, vol. 17, pp. 177-85, 2000.
- [17] A. A. Antipov and G. B. Sukhorukov, "Polyelectrolyte multilayer capsules as vehicles with tunable permeability," *Adv Colloid Interface Sci*, vol. 111, pp. 49-61, 2004.
- [18] Y.M. Lvov, A. Alexei, A. Mamedov, H. Möhwald, G. Sukhorukov, "Urease Encapsulation in Nanoorganized Microshells," *NanoLett*, vol. 1, pp. 125-128, 2001.
- [19] T. Shutava, R. Ghan, A. Patel, V. John, Y.M. Lvov, "Enzyme-Catalyzed Polymerization of Phenols within Polyelectrolyte Microcapsules," *Macromolecules*, vol. 37, pp. 4519-4524, 2004.
- [20] Z. Zheng, T. Shutava, V. John, Y.M. Lvov, "Microcapsule Modification with Peroxidase-Catalyzed Phenol Polymerization," *Biomacromolecules*, vol. 5, pp. 914-921, 2004.
- [21] M. Prouty, T. Shutava, D. Kommirredy, Y. Lvov, "pH Responsive Decomposable Layer-by-Layer Nanofilms and Capsules on the Basis of Tannic Acid" *Macromolecules*, vol. 38, pp. 2850-2858, 2005.
- [22] R. Schrieber, H. Careis, *Gelatine Handbook: Theory and Industrial Practice*. Weinheim, Germany: Wiley-VCH Verlag GmbH & Co, 2007.
- [23] M. D. Prouty, T.G. Shutava, V.E. Agabekov, Y.M. Lvov, "Antioxidant Properties of Layer-by-Layer films on the Basis of Tannic Acid," *Chemistry Letters*, vol. 35, 2006.
- [24] T.G. Shutava, V. E. Agabekov, Y.M. Lvov, "Reaction of radical cations with multilayers of tannic acid and polyelectrolytes," *Russian Journal of General Chemistry*, vol. 77, pp. 1494-1501, 2007.
- [25] A. Hua, M. Fang, S. Jones, Y. Lvov, "Electrostatic Layer-by-Layer Nanoassembly on Biological Microtemplates: Platelets," *Biomacromolecules*, vol. 3, pp. 560-564, 2002.

- [26] T. G. Shutava, S. S. Balkundi, and Y. M. Lvov, "(-)-Epigallocatechin gallate/gelatin layer-by-layer assembled films and microcapsules," *J. Colloid Interface Sci.*, vol. 330, no. 2, pp. 276-283, 2009.
- [27] M. N. Ravi Kumar, R.A. Muzzarelli, C. Muzzarelli, H. Sashiwa, A.J Domb, "Chitosan Chemistry and Pharmaceutical Perspectives," *Chem Rev*, vol. 104, pp. 6017-6084, 2004.
- [28] S. V. Vinogradov, "Colloidal microgels in drug delivery applications," *Curr Pharm Des*, vol. 12, pp. 4703-4712, 2006.
- [29] Al-Tahami, J.Singh, Khaled "Polymer Based Delivery Systems for Peptides and Proteins," *Recent Patents on Drug Delivery & Formulation* vol. 1, pp. 65-71, 2007.
- [30] J. Y. Fang, W. R. Lee, S. C. Shen, and Y. L. Huang, "Effect of liposome encapsulation of tea catechins on their accumulation in basal cell carcinomas," *J Dermatol Sci*, vol. 42, pp. 101-109, 2006.
- [31] S. L. Kosaraju, D. Lynette, M. Emin, I. Konczak, and L. Lundin, "Delivering polyphenols for healthy ageing," *Nutrition Dietetics*, vol. 65, pp. S48-S52, 2008
- [32] S. L. Kosaraju, D. Lynette, A. Lawrence, "Preparation and characterisation of chitosan microspheres for antioxidant delivery" *Carbohydrate polymers*, vol. 64, pp. 163-167, 2006.
- [33] G. Shi, L., Rao, H. Yu, H. Xiang, G. Pen, S. Long, C. Yang, "Yeast-cell-based microencapsulation of chlorogenic acid as a water-soluble antioxidant" *Journal of Food Engineering*, vol. 80, pp. 1060-1067, 2007.
- [34] C. Lucas-Abellan, J. M. Fortea, J.A Gabaldon, E. Nunez-Delicado, "Complexation of resveratrol by native and modified cyclodextrins: Determination of complexation constant by enzymatic, solubility and fluorimetric assays" *Food Chemistry*, vol. 111, pp. 262-267, 2008.
- [35] G. Tan, C. D. Ford, T. Zheng, L. Liu, N. Sahiner, T.V. John, G.L. McPherson, V. Agarwal, A. Bose, J. He, "Encapsulation of phenolic and polyphenolic compounds in mesoporous silica to form novel structured phenolic silica composites.," *Polym Mater Sci Eng*, vol. 92, pp. 158-159, 2005.
- [36] J. A. Charlton, N. J. Baxter, M. L. Khan, A. J. Moir, E. Haslam, A. P. Davies and M. P. Williamson, "Polyphenol/Peptide Binding and Precipitation," *J Agric Food Chem*, vol. 50, pp. 1593-1601, 2002.
- [37] N. J. Baxter, T. H. Lilley, E. Haslam, and M. P. Williamson, "Multiple interactions between polyphenols and a salivary proline-rich protein repeat result in complexation and precipitation," *Biochemistry*, vol. 36, pp. 5566-77, May 6 1997.

- [38] N. W. Naurato, P. Lu, Y. Wroblewski, K.; Bennick, A., "Interaction of Tannin with Human Salivary Histatins," *J. Agric. Food Chem.*, vol. 47, 1999.
- [39] C. Pascal, C. Poncet-Legrand, A. Imberty, C. Gautier, P. Sarni-Manchado, V. Cheynier, and A. Vernhet, "Interactions between a non glycosylated human proline-rich protein and flavan-3-ols are affected by protein concentration and polyphenol/protein ratio," *J Agric Food Chem*, vol. 55, pp. 4895-901, 13 2007.
- [40] K. Ying, G. Cheng, F. Xing, "Gelatin/tannin complex nanospheres via molecular assembly," *J Appl Polymer Sci*, vol. 101, 2006.
- [41] E. Jöbstl, J. O'Connell, J.P.A. Fairclough, M.P. Williamson, "Molecular Model for Astringency Produced by Polyphenol/Protein Interactions" *Biomacromolecules*, vol. 5, 2004.
- [42] E. Jöbstl, J. R. Howse, P. A. Fairclough, M. P. Williamson, "Noncovalent Cross-Linking of Casein by Epigallocatechin Gallate Characterized by Single Molecule Force Microscopy" *J Agric Food Chem*, vol. 54, 2006.
- [43] T. G. Shutava, Y. M. Lvov, "Nano-engineered microcapsules of tannic acid and chitosan for protein encapsulation," *J Nanoscience nanotechnology*, vol. 6, pp. 1655-61, 2006.
- [44] Y. M. Lvov, H. Nalwa (Ed.), *Thin-film nanofabrication by alternate adsorption of polyions*, vol. 3. New York, 2001.
- [45] D. G. Shchukin, G. B. Sukhorukov, "Nanoparticle Synthesis in Engineered Organic Nanoscale Reactors," *Adv Mater*, vol. 16, pp. 671-682, 2004.
- [46] G. B. Sukhorukov, M. Brumen, E. Donath, H. Möhwald, "Hollow Polyelectrolyte Shells: Exclusion of Polymers and Donnan Equilibrium," *J Phys Chem B*, vol. 103, pp. 6434-6440, 1999.
- [47] T. G. Shutava, D. S. Kommireddy, Y. Lvov, "Layer-by-Layer Enzyme/Polyelectrolyte Films as a Functional Protective Barrier in Oxidizing Media," *J Am Chem Soc*, vol. 128, pp. 9926-9934, 2006.
- [48] J. I. Anzai, H. Takeshita, Y. Kobayashi, T. Osa, T. Hoshi, "Layer-by-Layer Construction of Enzyme Multilayers on an Electrode for the Preparation of Glucose and Lactate Sensors: Elimination of Ascorbate Interference by Means of an Ascorbate Oxidase Multilayer," *Anal Chem*, vol. 4, pp. 811-817, 1998.
- [49] I. Erel-Unal, S. A. Sukhishvili, "Hydrogen-Bonded Multilayers of a Neutral Polymer and a Polyphenol," *Macromolecules*, vol. 41, 2008.

- [50] X. Wang, H. Chi-Tang, Q. Huang, "Investigation of Adsorption Behavior of (-)-Epigallocatechin Gallate on Bovine Serum Albumin Surface Using Quartz Crystal Microbalance with Dissipation Monitoring," *J Agric Food Chem*, vol. 55, pp. 4987-4992, 2007.
- [51] M. Liu, Y. Zhang, Q. Yang, Q. Xie, and S. Yao, "Monitoring and estimation of the kinetics parameters in the binding process of tannic acid to bovine serum albumin with electrochemical quartz crystal impedance system," *J. Agric. Food Chem.*, vol. 54, no. 12, pp. 4087-4094, 2006.
- [52] M. Chitpan, X. Wang, C. T. Ho, and Q. Huang, "Monitoring the binding processes of black tea thearubigin to the bovine serum albumin surface using quartz crystal microbalance with dissipation monitoring," *J. Agric. Food Chem.*, vol. 55, no. 25, pp. 10110-10116, 2007.
- [53] T. E. Feltkamp and K. W. Pondman, "Comparative study of fluorescent labelled antibodies," *Dermatologica*, vol. 141, no. 6, p. 433, 1970.
- [54] J. W. Goding, "Conjugation of antibodies with fluorochromes: modifications to the standard methods," *J. Immunol. Methods*, vol. 13, no. 3-4, pp. 215-226, 1976.
- [55] R. Re, N. Pellegrini, A. Proteggente, A. Pannala, M. Yang, and C. Rice-Evans, "Antioxidant activity applying an improved ABTS radical cation decolorization assay," *Free Radic. Biol. Med.*, vol. 26, no. 9-10, pp. 1231-1237, 1999.
- [56] K. M. Riedl and A. E. Hagerman, "Tannin-protein complexes as radical scavengers and radical sinks," *J. Agric. Food Chem.*, vol. 49, no. 10, pp. 4917-4923, 2001.
- [57] A. M. Campos, C. P. Sotomayor, E. Pino, and E. Lissi, "A pyranine based procedure for evaluation of the total antioxidant potential (TRAP) of polyphenols. A comparison with closely related methodologies," *Biol. Res.*, vol. 37, no. 2, pp. 287-292, 2004.
- [58] D. D. Perez, F. Leighton, A. Aspee, C. Aliaga, and E. Lissi, "A comparison of methods employed to evaluate antioxidant capabilities," *Biol. Res.*, vol. 33, no. 2, pp. 71-77, 2000.
- [59] J. Takebayashi, A. Tai, and I. Yamamoto, "pH-dependent long-term radical scavenging activity of AA-2G and 6-Octa-AA-2G against 2,2'-azinobis(3-ethylbenzothiazoline-6-sulfonic acid) radical cation," *Biol. Pharm. Bull.*, vol. 26, no. 9, pp. 1368-1370, 2003.
- [60] K. S. Johnson, "Plant phenolics behave as radical scavengers in the context of insect (*Manduca sexta*) hemolymph and midgut fluid," *J. Agric. Food Chem.*, vol. 53, no. 26, pp. 10120-10126, 2005.

- [61] J. Y. Fang, C. F. Hung, T. L. Hwang, and W. W. Wong, "Transdermal delivery of tea catechins by electrically assisted methods," *Skin Pharmacol. Physiol*, vol. 19, no. 1, pp. 28-37, 2006.
- [62] T. G. Shutava, S. S. Balkundi, P. Vangala, J. J. Steffan, R. L. Bigelow, J. A. Cardelli, D. P. O'Neal, Y. M. Lvov, "Layer-by-Layer-Coated Gelatin Nanoparticles as a Vehicle for Delivery of Natural Polyphenols," *ACS Nano*, Epub., accepted in 2009
- [63] V. M. Adhami and H. Mukhtar, "Anti-oxidants from green tea and pomegranate for chemoprevention of prostate cancer," *Mol. Biotechnol.*, vol. 37, no. 1, pp. 52-57, 2007.
- [64] Y. J. Surh, "Cancer chemoprevention with dietary phytochemicals," *Nat. Rev. Cancer*, vol. 3, no. 10, pp. 768-780, 2003.
- [65] S. Bettuzzi, M. Barusi, F. Rizzi, G. Castagnetti, G. Peracchia, A. Corti, Chemoprevention of Human Prostate Cancer by Oral Administration of Green Tea Catechins in Volunteers with High-Grade Prostate Intraepithelial Neoplasia: a Preliminary Report from a One Year Proof of Principle Study. , " *Cancer Research* vol. 66, pp. 1234-1240, 2006.
- [66] P. Calderon, J. Van Buren, W.B. Robinson, "Factors Influencing the Formation of Precipitates and Hazes by Gelatin and Condensed and Hydrolyzable Tannins. ," *J Agric Food Chem*, vol. 16, pp. 479-482, 1968.
- [67] L. Gámiz-Gracia, M. D. Luques de Castro, "Development and Validation of a Flow-Injection Method for the Determination of Albumin Tannate, the Active Component of a Pharmaceutical Preparation. ," *J Pharm Biomed Anal*, vol. 15, pp. 447-452, 1997.
- [68] R. S. Osawa, T.P. Walsho, "Effects of Acidic and Alkaline Treatments on Tannic Acid and Its Binding Property to Protein.," *J Agric Food Chem*, vol. 41, pp. 704-707, 1999.
- [69] A. Barik, K. I. Priyadarsini, H. Mohan, "Photophysical studies on binding of curcumin to bovine serum albumins," *Photochem. Photobiol.*, vol. 77, no. 6, pp. 597-603, 2003.
- [70] J. Italia, P. Datta, D. D. Ankola, N. V. Ravi Kumar, "Nanoparticles Enhance Per Oral Bioavailability of Poorly Available Molecules: Epigallocatechin Gallate Nanoparticles Ameliorates Cyclosporine Induced Nephrotoxicity in Rats at Three Times Lower Dose Than Oral Solution. ," *J Biomed Nanotech*, vol. 4, pp. 304-312, 2008.
- [71] B. Hu, C. Pan, Y. Sun, Z. Hou, H., X. Zeng, "Optimization of Fabrication Parameters To Produce Chitosan-Tripolyphosphate Nanoparticles for Delivery of Tea Catechins. ," *J Agric Food Chem*, vol. 56, pp. 7451-7458, 2008.

- [72] M. McShane, Y. M. Lvov, *Layer-by-Layer Electrostatic Self-Assembly. In: Schwartz, J., Contescu, C. (Eds).*, New York: M. Dekker Publ.
- [73] A. S. Zahr and M. V. Pishko, "Encapsulation of paclitaxel in macromolecular nanoshells," *Biomacromolecules*, vol. 8, pp. 2004-10, 2007.
- [74] J. S. Zhou, L. Ma, C. Gao, J. Shen, "Polyelectrolyte Coated PLGA Nanoparticles: Templatation and Release Behavior.," *Macromol. Biosci.*, vol. 4, pp. 326-335, 2009.
- [75] H. Ai, J. J. Pink, X. Shuai, D. A. Boothman, J. Gao, "Interactions between self-assembled polyelectrolyte shells and tumor cells," *J Biomed Mater Research*, vol. 73A, pp. 303-312, 2005.
- [76] X. Qiu, S. Leporatti, E. D. Donath, H. Möhwald, "Studies on the Drug Release Properties of Polysaccharide Multilayers Encapsulated Ibuprofen Microparticles.," *Langmuir* vol. 17, pp. 5375-5380, 2001.
- [77] S. Kommareddy, M. Amiji, "Antiangiogenic Gene Therapy with Systemically Administered sFlt-1 Plasmid DNA in Engineered Gelatin-Based Nanovectors.," *Cancer Gene Therapy*, vol. 14, pp. 488-498, 2007.
- [78] G. Kaul, M. Amiji, "Tumor-Targeted Gene Delivery Using Poly(ethylene glycol)-Modified Gelatin Nanoparticles: *in vitro* and *in vivo* Studies.," *Pharm Res*, vol. 22, pp. 951-961, 2005.
- [79] S. Kommareddy, M. Amiji, "Biodistribution and Pharmacokinetic Analysis of Long-Circulating Thiolated Gelatin Nanoparticles Following Systemic Administration in Breast Cancer-Bearing Mice.," *J Pharm Sci*, vol. 96, pp. 397-407, 2007.
- [80] K. Zwiorek, J. Kloeckner, E. Wagner, and C. Coester, "Gelatin nanoparticles as a new and simple gene delivery system," *J. Pharm. Pharm. Sci.*, vol. 7, no. 4, pp. 22-28, 2005.
- [81] J. C. Zillies, K. Zwiorek, G. Winter, and C. Coester, "Method for quantifying the PEGylation of gelatin nanoparticle drug carrier systems using asymmetrical flow field-flow fractionation and refractive index detection," *Anal. Chem.*, vol. 79, no. 12, pp. 4574-4580, 2007.
- [82] C. W. Cumper, A. E. Alexander, "The viscosity and rigidity of gelatin in concentrated aqueous systems. I. Viscosity.," *Australian J. Sci. Res., Ser. A: Phys. Sci.*, vol. 5, pp. 146-152, 1952.
- [83] H. W. Jomaa, J. B. Schlenoff, "Salt-Induced Polyelectrolyte Interdiffusion in Multilayered Films: A Neutron Reflectivity Study.," *Macromolecules*, vol. 38, pp. 8473-8480, 2005.

- [84] E. Kharlampieva, V. Kozlovskaya, J. F. Ankner, S. A. Sukhishvili, "Hydrogen-Bonded Polymer Multilayers Probed by Neutron Reflectivity.," *Langmuir*, vol. 24, pp. 11346-11349, 2008.
- [85] R. L. Bigelow, J. A. Cardelli, "The Green Tea Catechins, (-)-Epigallocatechin-3-gallate (EGCG) and (-)-Epicatechin-3-gallate (ECG), Inhibit HGF/Met Signaling in Immortalized and Tumorigenic Breast Epithelial Cells.," *Oncogene* vol. 25, pp. 1922-1930, 2006.
- [86] B. Franz, S. Balkundi, C. Dahl, Y. Lvov, A. Prange, "Layer-by-Layer nano-encapsulation of microbes: Controlled cell surface modification and investigation of substrate uptake in bacteria," *Macromolecular Bioscience*, accepted in 2009
- [87] G. H. Decher, J.-D. Hong, "Buildup of ultrathin multilayer films by a self-assembly process: II. Consecutive adsorption of anionic and cationic bipolar amphiphiles and polyelectrolytes on charged surfaces.," *Ber Bunsen-Ges Phys Chem*, vol. 95, pp. 1430-1434, 1991.
- [88] Y. M. Lvov, B. Munge, O. Giraldo, I. Ichinose, S. L. Suib, J. F. Rusling, "Films of Manganese Oxide Nanoparticles with Polycations or Myoglobin from Alternate-Layer Adsorption," *Langmuir*, vol. 16, pp. 8850-8857, 2000.
- [89] V. V. Tsukruk, "Assembly of Supramolecular Polymers in Ultrathin Films," *Prog Polym Sci*, vol. 22, pp. 247-311, 1997.
- [90] J. B. Schlenoff, D. Laurento, H. Ly, J. Stepp, "Redox-active polyelectrolyte multilayers," *J Adv Mater*, vol. 10, pp. 347-349, 1998.
- [91] J. D. Mendelson, C. J. Barrett, V. V. Chan, A. J. Pal, A. M. Mayes, M. F. Rubner, "Fabrication of Microporous Thin Films from Polyelectrolyte Multilayers," *Langmuir*, vol. 16, pp. 5017-5023, 2000.
- [92] E. Donath, G. B. Sukhorukov, F. Caruso, S. Davis, S., H. Möhwald, "Novel hollow polymer shells by colloid-templated assembly of polyelectrolytes," *Angew Chem, Int. Ed.*, , vol. 37, pp. 2202-2205, 1998.
- [93] B. Neu, A. Voigt, R. Mitlöhner, S. Leporatti, C. Gao, E. Donath, H. Möhwald, H. Kiesewetter, H. J. Meiselman, H. Baumler, "Biological cells as templates for hollow microcapsules," *Journal of Microencapsulation*, vol. 18, pp. 385-395, 2001.
- [94] F. C. Caruso, R. A. Caruso, H. Möhwald, "Nanoengineering of inorganic and hybrid hollow spheres by colloidal templating," *Science*, vol. 282, pp. 1111-1114, 1998.
- [95] H. Möhwald, "From Langmuir-monolayers to nanocapsules," *Colloids Surf.*, vol. 171, pp. 25-31, 2000.

- [96] N. G. Veerabadran, P. L. Goli, S. S. Stewart-Clark, Y. M. Lvov, D. K. Mills, "Nanoencapsulation of Stem Cells within Polyelectrolyte Multilayer Shells," *Macromol. Biosci.*, vol. 7, pp. 877-882, 2007.
- [97] S. S. Balkundi, B. Franz, Y. M. Lvov, A. A. Prange, *Polym. Mater. Sci. and Engin.*, "Polyelectrolyte Nanoencapsulation of Bacteria through LbL Assembly," in *Polym Mater Sci and Engin, American Chemical Society Meeting*, Philadelphia, 2008, pp. 635-636.
- [98] S. S. Balkundi, N. G. Verrabadran; G. Johnson, G., M. Eby, Y M. Lvov, "Encapsulation of Bacterial Spores in Nanoorganized Polyelectrolyte Shells," *Langmuir*, 2009.
- [99] D. Yoo, S. S. Shiratori, M. F. Rubner, "Controlling Bilayer Composition and Surface Wettability of Sequentially Adsorbed Multilayers of Weak Polyelectrolytes," *Macromolecules*, vol. 31, pp. 4309-4318, 1998.
- [100] O. P. Tiourina, A. A. Antipov, G.B. Sukhorukov, N. L. Larionova, Y. M. Lvov, H. Möhwald, "Entrapment of alpha-chymotrypsin into hollow polyelectrolyte microcapsules," *Macromol. Biosci.*, vol. 1, pp. 209-214, 2001.
- [101] D. C. Brune, *In Anoxygenic photosynthetic bacteria; Blankenship, R. E.; Madigan, M. T.; Bauer, C. E., Eds.:* Kluwer Academic Publishers: Dordrecht, 1995.
- [102] C. Dahl, A. Prange, *Bacterial Inclusions:* Shively, J. M., Eds.; Springer, 2006.
- [103] B. Franz, H. Hormes, C. Dahl, A. Prange, "Utilization of solid 'elemental' sulfur by the phototrophic purple sulfur bacterium *Allochromatium vinosum*: a sulfur K-edge X-ray absorption spectroscopy study," *Microbiology-SGM*, vol. 153, pp. 1268-1274, 2007.
- [104] T. Gehrke, J. Thierry, D. Thierry, W. Sand, "Importance of Extracellular Polymeric Substances from *Thiobacillus ferrooxidans* for Bioleaching," *Appl Environ Microbiol*, vol. 64, pp. 2743-2747, 1998.
- [105] D. Hensen, D. Sperling, H. G. Trüper, D. C. Brune, C. Dahl, "Thiosulphate oxidation in the phototrophic sulphur bacterium *Allochromatium vinosum*," *Mol Microbiol.*, vol. 62, pp. 794-810, 2006.
- [106] B. Sörbo, "Sulfate: turbidimetric and nephelometric methods," *Meth Enzymol*, vol. 143, pp. 3-6, 1987.
- [107] S. S. Balkundi, N. G. Veerabadran, D. M. Eby, G. R. Johnson, Y. M. Lvov, "Encapsulation of Bacterial Spores in Nanoorganized Polyelectrolyte Shells (dagger)," *Langmuir*, Epub., accepted in 2009

- [108] H. A. Baca, A. Carlee, E. Carnes, D. Lopez, J. Flemming, D. Dunphy, S. Singh, G. Lopez, S. Brozik, M. Werner-Washburne, J. Brinker, "Cell-Directed Assembly of Lipid-Silica Nanostructures Providing Extended Cell Viability," *Science*, vol. 313, pp. 337-340, 2006.
- [109] S. Zhang, "Beyond the Petri dish," *Nat Biotechnology*, vol. 22, pp. 151-152, 2004.
- [110] M. M. Stevens, J.H. George, "Exploring and Engineering the Cell Surface Interface," *Science*, vol. 310, pp. 1135-1139, 2005.
- [111] A.J. Swiston, C. Cheng, S. H. Um, D. Irvine, R. Cohen, M. Rubner, "Surface functionalization of living cells with multilayer patches," *NanoLett*, vol. 8, pp. 4446-4453, 2008.
- [112] S. L. Yang, D. Lee, R. E. Cohen, M. Rubner, "Bioinert Solution-Cross-Linked Hydrogen-Bonded Multilayers on Colloidal Particles," *Langmuir*, vol. 20, pp. 5978-5981, 2004.
- [113] Z. Li, D. Lee, M. F. Rubner, R. E. Cohen, "Layer-by-Layer Assembled Janus Microcapsules," *Macromolecules*, vol. 38, pp. 7876-7879, 2005.
- [114] D. B. Shenoy, A. A. Antipov, G. B. Sukhorukov, H. Möhwald, "Layer-by-Layer Engineering of Biocompatible, Decomposable Core-Shell Structures," *Biomacromolecules*, vol. 4, pp. 265-272, 2003.
- [115] L. Richert, P. Lavallo, D. Vautier, B. Senger, J.F. Stolz, P. Schaaf, J. C. Voegel, C. Picart, "Cell Interactions with Polyelectrolyte Multilayer Films," *Biomacromolecules*, vol. 3, pp. 1170-1178, 2002.
- [116] A. Diaspro, D. Silvano, S. Krol, O. Cavalleri, A. Gliozzi, "Single Living Cell Encapsulation in Nano-organized Polyelectrolyte Shells," *Langmuir*, vol. 18, pp. 5047-5050, 2002.
- [117] M. Yu, A. Ivanesevic, "Encapsulated cells: an atomic force microscopy study " *Biomaterials*, vol. 25, pp. 3655-3662, 2004.
- [118] I. Estrela-Lopis, S. Leporatti, E. Typlt, D. Clemens, E. Donath, "Small Angle Neutron Scattering Investigations (SANS) of Polyelectrolyte Multilayer Capsules Templated on Human Red Blood Cells," *Langmuir*, vol. 23, pp. 7209-7215, 2007.
- [119] A. L. Hillberg, M. Tabrizian, "Biorecognition through Layer-by-Layer Polyelectrolyte Assembly: In-Situ Hybridization on Living Cells," *Biomacromolecules*, vol. 7, pp. 2742-2750, 2006.
- [120] P. Schaeffer, J. Millet, J. P. Aubert, "Catabolic repression of bacterial sporulation," *PNAS*, vol. 54, pp. 704-709, 1965.

- [121] A. B. Schaeffer, M. D. Fulton, "A simplified method of staining Endospores," *Science*, vol. 77, pp. 194-198, 1933.
- [122] A. A. Hindle, A. H. Halle, "Dipicolinic acid (DPA) assay revisited and appraised for spore detection," *Analyst*, vol. 124, pp. 1599-1605, 1999.
- [123] P. M. Pelegriano, N. F. Fell, J. B. Gillespie, "Enhanced spore detection using dipicolinate extraction techniques," *Anal Chim Acta*, vol. 455, pp. 167-172, 2002.